

Fig 7 A comparison between the variation in colony diameter length of HeLa cells of the control and 400ppm TiO₂-NPs treatment. The diameter lengths of the colonies in control group are larger than those treated by TiO₂-NPs

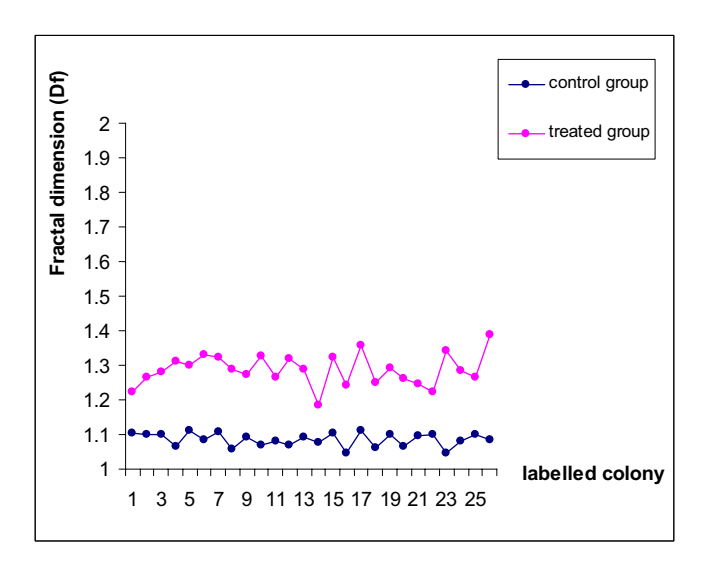


Fig. 8 Fractal dimensions of tumor boundaries at different conditions, namely control and TiO_2 treatment conditions. The data shows that the Df of the treated group (1.2870±0.0454) are systematically larger than those of control group(1.0852±0.0197). It also clearly illustrates that the shape treated samples is more diverse and rough on the surface

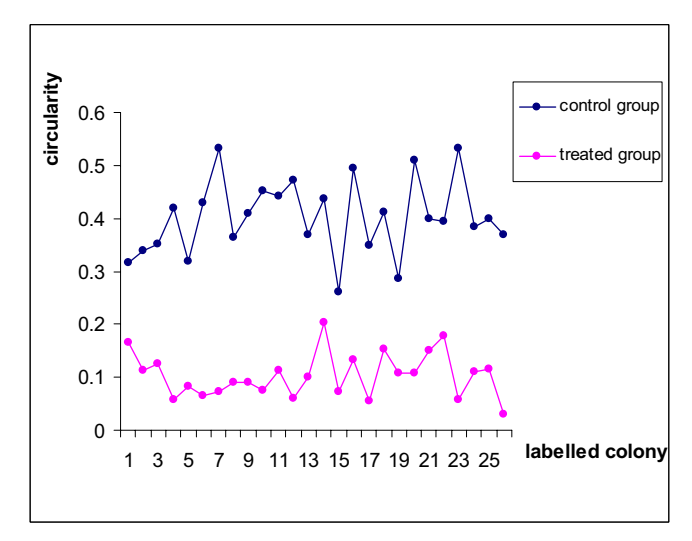


Fig. 9 A comparison between the variation in colony circularity of HeLa cells of the control and 400ppm TiO₂-NPs treatment. The circularities of the colonies in control group are larger than those treated by TiO₂-NPs

REFERENCES

- [1] Alivisatos A. Semiconductor Clusters, Nanocrystals and Quantum Dots Science of The Total Environment 271(5251): 933 937, 1996.
- Schwarzer H, Peukert W. Prediction of aggregation kinetics based on surface properties of nanoparticles. Chem Eng Sci 60:11-25, 2005.
- [3] Hunter R. Foundations of colloid Science University Press, Oxford, Great Britain. I, II
- [4] Waliszewski P. Complexity, dynamic cellular network, and tumourgenesis. Pol J Pathol 46:235-41,1997
- [5] Zhang A, Sun Y. Photocatalytic killing effect of TiO₂ nanoparticles on Ls-174-t human colon carcinoma cells. World J Gastroenterol. 10(21):3191-3193,2004
- [6] Hoffmann M, Martin ST, Choi WY, Bahnemann DW. Environmental Applications of Semiconductor Photocatalysis. Chem Rev 95:65.1995
- [7] Maness P. Snolinski S, Blake D, Wolfrum Z, Jacoby W. Solar Treatment as an Alternative for Water Disinfections. Appl Environ Microbiol 65:4094,1999
- [8] Heller A. Preparation of Ti-Si binary oxide thin film photocatalysts by the application of anionized cluster beam method. Acc. Chem. Res 28:503-508,1995
- [9] Ollis D, Pelizetti E, Serpone N. Environmintal Applications of Semiconductor Photocatalysis. Environ. Sci. Technol 25:1523-1529.1991
- [10] Sitkiewitz S, Heller A. Photocatalytic oxidiation of benzene and steatic on sol-gel derived TiO2 thin films attached to glass. New J. Chem 20:233-241,1996
- [11] Uchida H, Itoh S, Yoneyama H. Photocatalytic Decomposition of Propyzamide Using TiO2 Supported on Activated Carbon. Chem. Lett. 1995-1998, 1993.
- [12] Cai R, Hashimoto K, Itoh K, Kubota Y, Fujishima A. Photokilling of malignant cells with Ultrafine TiO2 powder. Bull. Chem. Soc. Jpn 64:1268-1273, 1991.
- [13] Ireland J, Klostermann P, Rice E, Clark R. Inactivation of Escherichia coli by titanium dioxide photocatalytic oxidation. Appl. Environ. Microbiol. 59:1668-1670, 1993.
- [14] Matsunaga T, Okochi M. TiO2. -mediated photochemical disinfection of. Escherichia coli using optical fibers. Environ. Sci. Technol 29:501-505, 1995.
- [15] Watts RJ, Kong S, Orr MP, Mille rGC, Henry BE. Photocatalytic Degradation of Toxins Secreted to Water by Cyanobateria and Unicellular Algae and Photocatalytic Degradation of The Cells of Selected Microorgantisms. Water Research 29:95-100. 1995.

- [16] Wei C, Lin W-Y, Zainal Z, Williams N, Zhu K, Kruzic A, Smith R, Rajeshwar K. Bactericidal Activity of TiO2 Photocatalysts in Aqueous Media: Towards a Solar-Assisted Water Disinfection System". Environ. Sci. Technol. 28:934-938, 1994.
- [17] Kikuchi Y, Sunada K, Iyoda T, Hashimoto K, Fujishima A. Photocatalytic bactericidal effect of TiO2 thin films: dynamic. view of the active oxygen species responsible for the effect. J. Photochem. Photobiol. A: Chem 106:51-56, 1997.
- [18] Minhua X, Jianamin M, Jianhua G, Zuhong L. Photocatalytic TiO2 nanoparticles damage to cellular membranes and genetic supramolecules, Suptamolecular. Science 5:511-513, 1998.
- [19] Mandelbrot B. How long is the coast of Britain? Statistical selfsimilarity and fractional dimension. Science 156:636-8, 1997.
- [20] BB. M. The fractal geometry of nature. Freeman, San Francisco. 1983.
- [21] Mach J, Mas F, Sagués F. Laplacian multifractality of growth probability distribution in electrodeposition. Europhys. Lett 25:271-27, 1994.
- [22] Shlesinger M, West B. Complex fractal dimension of the bronchial tree. Phys. Rev. Lett 67:2106-2108, 1991.
- [23] Burlando B. The fractal dimension of taxonomic systems. J. Theor. Biol 146:99-114, 1990.
- [24] Goldberger AGAN-ldfcCt, fractals, and complexity at the bedside. Lancet 347:1312-1314. Non-linear dynamics for clinicians: Chaos theory, fractals, and complexity at the bedside. Lancet 347:1312-1314, 1996
- [25] Churilla A, Gottschalke W, Liebovitch Lea. Membrane potential fluctuations of human T-lymphocytes have fractal characteristics of fractional Brownian motion. Ann Biomed Eng 24:99-108, 1996.
- [26] Family F, Masters B, Platt D. Fractal pattern formation in human retinal vessels. Physica D: Nonlinear Phenomena 38:98, 1989.
- [27] Fujikawa H, Matsushita M. Fractal growth of Bacillus subtilis on agar plates. J. Phys. Soc. Jpn 58:3875-3878, 1998.
- [28] Gitter J, Czerniecki M. Fractal analysis of the electromyographic interference pattern. J. Neurosci Methods 58:103-108, 1995.
- [29] Ito K, Gunji Y. Self-organization of living systems towards criticality at the edge of chaos. Biosystems 33:17-24, 1994.
- [30] Macheras P, Argyrakis P, Polymilis C. Fractal geometry, fractal kinetics and chaos en route to biopharmaceutical sciences. Eur J Drug Metab Pharmacokinet 21:77-86, 1996.
- [31] Mainster M. The fractal properties of retinal vessels: Embryological and clinical implications. Eye 4:235, 1990.
- [32] Ragazzi E. Hidden fractals in pharmacodynamics. Pharmazie 50:66-68 1995.
- [33] Smith TJ, Marks W, Lange Gea. A fractal analysis of cell images. J Neurosci Methods 27:173-180, 1998.
- [34] Turcott R, Teich M. Fractal character of the electrocardiogram: Distinguishing heart-failure and normal patients. Ann Biomed Eng 24:269-293, 1996.
- [35] Williams N. Fractal geometry gets the measure of life's scales. Science 276:34, 1997.
- [36] Bru A, Albertos S, Subiza J, Garcia-Asenjo JL, Bru I. The Universal Dynamics of Tumor Growth. Biophysic Journal 85:2948-2961, 2003.
- [37] Cross S. Fractals in Pathology. J. Pathol 182:1-8, 1997.
- [38] Laird A. Dynamics of tumor growth: comparison of Growth rates and extrapolation of growth curve to one cell. Br J Cancer 19:278-291, 1964.
- [39] Cai R, Kubota Y, Shuin T, Sakai H, Hashimot K, Fujishima A. Induction of cytotoxicity by photoexcited TiO2 particles. Cancer Res 52(8): 2346-8., 1992.
- [40] Kubota Y, Shuin T, Kawasaki C, Hosaka M, Kitamur H, Cai R, Sakai H, Hashimoto K, Fujishima A. Photokilling of T-24 human bladder cancer cells with titanium dioxide. Br. J. Cancer. Dec 70(6): 1107-11, 1994.

BIO-2747; No. of Pages 11

ARTICLE IN PRESS



Available online at www.sciencedirect.com



BioSystems xxx (2007) xxx-xxx



www.elsevier.com/locate/biosystems

The stochastic model of non-equilibrium mutagen-induced alterations of DNA: Implication to genetic instability in cancer

Darapond Triampo ^a, Wannapong Triampo ^{b,*}, I.-Ming Tang ^b, Yongwimon Lenbury ^c

a Department of Chemistry and Center for Vectors and Vector-Borne Diseases, Faculty of Science, and Institute for Innovation and Development of Learning Process, Mahidol University, Rama 6 Rd., Rajchataywee, Bangkok 10400, Thailand
 b R&D Group of Biological and Environmental Physics (BIOPHYSICS), Department of Physics, and Center of Excellence for Vectors and Vector-Borne Diseases, Faculty of Science, Mahidol University, Bangkok, Thailand
 c Department of Mathematics, Faculty of Science, Mahidol University, Bangkok, Thailand

Received 6 January 2007; received in revised form 14 May 2007; accepted 18 May 2007

Abstract

Genetic alterations such as point mutations, chromosomal rearrangements, modification of DNA methylation and chromosome aberrations accumulate during the lifetime of an organism. They can be caused by intrinsic errors in the DNA replication and repair as well as by external factors such as exposure to mutagenic substances or radiation. The main purpose of the present work is to begin an exploration of the stochastic nature of non-equilibrium DNA alteration caused by events such as tautomeric shifts. This is done by modeling the genetic DNA code chain as a sequence of DNA-bit values ('1' for normal bases and '-1' for abnormal bases). We observe the number of DNA-bit changes resulting from the random point mutation process which, in the model, is being induced by a stochastic Brownian mutagen (BM) as it diffuses through the DNA-bit systems. Using both an analytical and Monte Carlo (MC) simulation techniques, we observe the local and global number of DNA-bit changes. It is found that in 1D, the local DNA-bit density behaves like $1/\sqrt{t}$, the global total number of the switched (abnormal) DNA-bit increases as \sqrt{t} . The probability distribution P(b, 0, t) of b(0, t) is log-normal. It is also found that when the number of mutagens is increased, the number of the total abnormal DNA-bits does not grow linearly with the number of mutagens. All analytic results are in good agreement with the simulation results.

© 2007 Elsevier Ireland Ltd. All rights reserved.

PACS: 87.15.Aa

Keywords: DNA alteration; Genetic instability; Stochastic process; Mathematical modeling

1. Introduction

Genetic alterations such as point mutations, chromosomal rearrangements, unequal crossing over, loss of heterozygosity, modification of DNA methylation and chromosome aberrations accumulate during the lifetime of the organism. They are caused by intrinsic errors in the

0303-2647/\$ – see front matter © 2007 Elsevier Ireland Ltd. All rights reserved. doi:10.1016/j.biosystems.2007.05.004

^{*} Corresponding author.

*E-mail addresses: scwtr@mahidol.ac.th, wtriampo@yahoo.com
(W. Triampo).

2

DNA replication and repair as well as by external factors such as exposure to mutagenic substances or radiation. Since the discovery that the configuration of a DNA or RNA molecule is a double helix (Watson et al., 1988), molecular biologists and geneticists have been studying the crucial role of DNA in the genome organization. Once it was recognized that DNA is the informational active chemical component of essentially all genetic materials, it was assumed that this macromolecule must be extraordinarily stable in order to maintain the degree of fidelity required of a master blueprint.

It was something of a surprise to learn that the primary structure of DNA is quite dynamic and subject to constant changes. For example, gene transposition is a well-established phenomenon in prokaryotic and eukaryotic cells (Finnegan, 1990; Kleckner, 1981). In addition, DNA is subject to alteration in the chemistry or sequence of individual nucleotides (Lindahl, 1993; Roberts, 1978; Singer and Kusmierek, 1982). Many of these changes arise as a consequence of errors introduced during replication, recombination and repairing itself. Other basic alterations arise from the inherent instability of specific chemical bonds that constitute the normal chemistry of nucleotides under physiological conditions of temperature and pH. Finally, the DNA of living cells reacts to a variety of chemical compounds and a smaller number of physical agents, many of which are present in the environment. Each of these modifications of the molecular structure of genetic material is appropriately considered to be a DNA damage. DNA damages can be classified into two major classes, spontaneous and environmental. However, in some cases the actual chemical changes in DNA that occur "spontaneously" are indistinguishable from those brought about through interaction with certain environmental agents. The term "spontaneous" may merely imply that we have not identified a particular environmental culprit. Changes in the DNA sequence may result from processes such as insertion, deletion, transversion and transition. For example, the genetic instability characteristic of cancer cells may be due, in part, to mutations in genes whose products normally function to ensure DNA integrity. DNA replication in normal human cells is an extremely accurate process. During the cell division cycle, copy errors occur with probabilities less than 10^{-9} to 10^{-10} per nucleotide. In contrast, the malignant cells that constitute cancer tissues are markedly heterogeneous and exhibit alterations in nucleotide sequence of DNA.

As initially proposed by Delbruck et al. (1935) and Watson and Crick (1953), spontaneous mutations are initiated by quantum jump events such as tautomeric shifts in single protons of DNA bases. Even what may

be the most common of spontaneous mutations involves a chemical mechanism which must involve quantum uncertainty, since it occurs when individual electrons shift their positions to produce "tautomers".

Specifically, nucleotide transitions can be induced by exposure to endogeneous and exogeneous mutagens (agents causing genetic changes) such as chemical carcinogens. However, not all mutagens are carcinogenic. The nucleotide transitions are the interchange of bases of the same shape, e.g., the purine bases transition, $C(\text{cytosine}) \leftrightarrow T(\text{thymine})$ or the pyrimidine bases transitions, $A(\text{adenine}) \leftrightarrow G(\text{guanine})$. One of the mechanisms that can cause the transition is the shift of the positions of the electrons for the bases to become a transient form (known in organic chemistry as a *tautomeric shift*).

In standard complementary pairing, G pairs with C and A with T. Keto-enol tautomeric shift leads to nonstandard form of G: $G \leftrightarrow G^*$ resulting in G^* pairing with T. Amino-imino tautomeric shift leads to a non-standard form of A: A \leftrightarrow A* resulting in A* pairing with C. Nonstandard bases alter the pairing specificity, i.e., modified purine pairs with the wrong pyrimidine and modified pyrimidine pairs with the wrong purine. Fig. 1 shows an example of the keto-enol tautomeric shift that results in a transition mutation of the complementary strand. Consider the pairing of ATGC with TACG: Let G in the first strand undergo a tautomeric shift to G*. The complementary strand that is generated would be TATG, not TACG. This would be a transition from $C \leftrightarrow T$. To complete the process of producing a mutation, a tautomeric shift must take place during replication, either in the template chain, or in the deoxyribonucleotide being added by the DNA polymerase. Since the shifted form retains its rare mis-matching structure for only a brief period, the next replication cycle will most likely find itself reverted

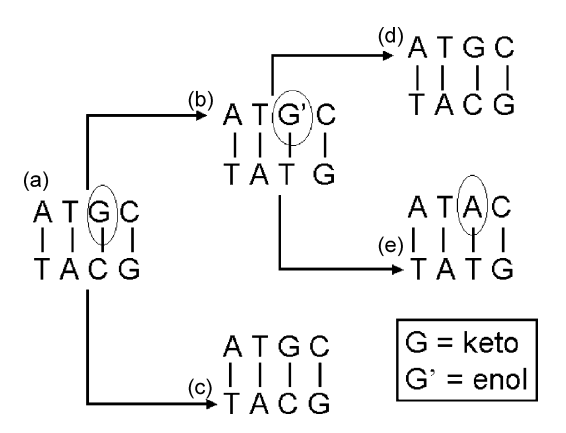


Fig. 1. A diagram of the keto-enol tautomeric shift that results in a transition mutation of the complementary strand.

D. Triampo et al. / BioSystems xxx (2007) xxx-xxx

to its normal form, and the polymerase will pair it with its normal mate. Thus, in two cycles of replication, an A-T pair is changed to a G-C pair, or vice versa. This, in turn, can often result in a change in a triplet code,

leading to an amino acid substitution in a protein, and a modification of some visible phenotypic property of the organism.

Although it has never been demonstrated experimentally that rare tautomers are responsible for spontaneous mutations, subsequent experimental and theoretical investigations (Leszczynski, 1999; Radchenko et al., 1983) seem to confirm the essential correctness of this postulate. It should be remarked that Neo-Darwinian evolutionary theory is founded on the principle that mutations occur randomly, and the direction of evolutionary change is provided by selection for advantageous mutations. However, the central tenet, that mutations occur randomly, has recently been challenged by the finding of the phenomenon termed adaptive or directed mutation.

There have been a few approaches used to investigate this mutation complex process ranging from wet lab research to highly complicated computational calculations. Theoretical models fall into two very broad classes: deterministic and stochastic models. Deterministic models attempt to model or predict the average behavior of systems according to some precise rules. In contrast, stochastic models describe the probability of very specific behaviors of individuals rather than average behavior of the population. Stochasticity has been recognized in the biology field of research and modeling as the description of life systems (Kurakin, 2006). It had appeared as general principles underlying the dynamics and organization of biological systems at all scales: gene expression (Kurakin, 2005), enzymes (Xie and Lu, 1999), self-organization of macromolecular complexes mediating transcription (Dundr et al., 2002; Kimura et al., 2002), and DNA repair (Essers et al., 2002; Hoogstraten et al., 2002).

Because a gene or DNA is a molecule, the statistical fluctuations of atomic or molecular scale cannot be avoided. Mathematical modeling of genetic instability has led to considerable insight into human tumorigenesis. One study of the mutational spectrum gave the type, location and frequency of DNA changes in a particular gene (Hussain and Harris, 1999). Claytong and Robertson (1955) proposed a random walk mutation model as a model for genetic analysis. It was later proposed explicitly by Crowj and Kimura (1964), by Kimura (1965), and subsequently popularized by Lander (1975). Zeng and Cockerham (1993) proposed a more general mutation model, called the regression mutation model. This model regards the regression coefficient of the effect of an allele after mutation on the effect of the allele before mutation as a parameter.

In 1989, Nowak and Schuster (1989) investigated error thresholds in finite populations. They determined that, at error rates above the critical value, the quasispecies ceases to be localized in sequence space and start to drift randomly. Sole' and Deisboeck (2004) used a quasispecies model to investigate the error threshold in cancer cells. They demonstrated that, once the threshold is reached, the highly unstable cancer cells become unable to maintain their genetic information, leading to a decrease in the velocity of tumor growth. The original quasispecies model assumes that genomes replicate conservatively, i.e., each single-stranded genome replicates by producing a new, possibly error-prone, single stranded copy without affecting the original. In this form, the quasispecies model predicts the existence of an error catastrophe or "error threshold", a threshold mutation rate above which no viable species can exist. This threshold depends on the replication rate of the fittest sequence, the master sequence (Komarova et al., 2002) utilize a stochastic model to evaluate the rate of formation of dysplastic crypts by chromosomal instability (CIN) and microsatellite instability (MIN) mechanisms in sporadic colon cancer to obtain broad qualitative agreement with the relative importance of CIN and MIN and the number of polyps generated under these conditions.

The main purpose of the present work is to begin an exploration of the stochastic nature of non-equilibrium DNA alteration caused by events such as tautomeric shifts in a theoretical DNA-bit alteration model This is done by modeling the genetic DNA (or RNA) code chain as a sequence of DNA-bit values ('1' for normal bases and -1 for abnormal bases). This is similar to what is used in computers or electronics. We observe the number of DNA-bit changes resulting from the random point mutation process (to mimic tautomeric shifts) which is being induced by a stochastic Brownian mutagen (BM) as it diffuses through the DNA-bit systems. We will make analytic predictions and simulate the non-equilibrium process using the Monte Carlo (MC) method. To the best of our knowledge, there has not been a stochastic approach to investigate the nonequilibrium stochastic kinetics of DNA-alteration. This work therefore represents a new avenue for studying non-equilibrium mutation.

2. Theoretical model and analytic predictions

As mentioned, earlier theoretical models fall into two very broad classes: deterministic and stochastic models.

3

ARTICLE IN PRESS

D. Triampo et al. / BioSystems xxx (2007) xxx-xxx

Stochastic models evaluate the entire probability distribution of random individual events. This kind of model is potentially more informative in that it considers rare events, not just average properties. Typically one defines a variety of discrete states, and the rates or probabilities of transition between the states. Often the different states of a phenomenon of interest can be represented as a Markov process. In a Markov process, the system

passes through the defined states in discrete steps with

a given set of transition probabilities. The possibilities

for where the system will go next, and the chance it will

"select" a particular option, depend only on where the system is at the moment (i.e., its present state) rather than on how it got there (its history). This type of analysis can in principle give the chance that the system is in a given state as a function of time or other key variables. However, utilizing this approach often requires a detailed understanding of individual states and transitions, which is not always available. As the system complexity increases, the definition of all the relevant states and the mathematical analysis of all the transitions between them can become daunting. The results will

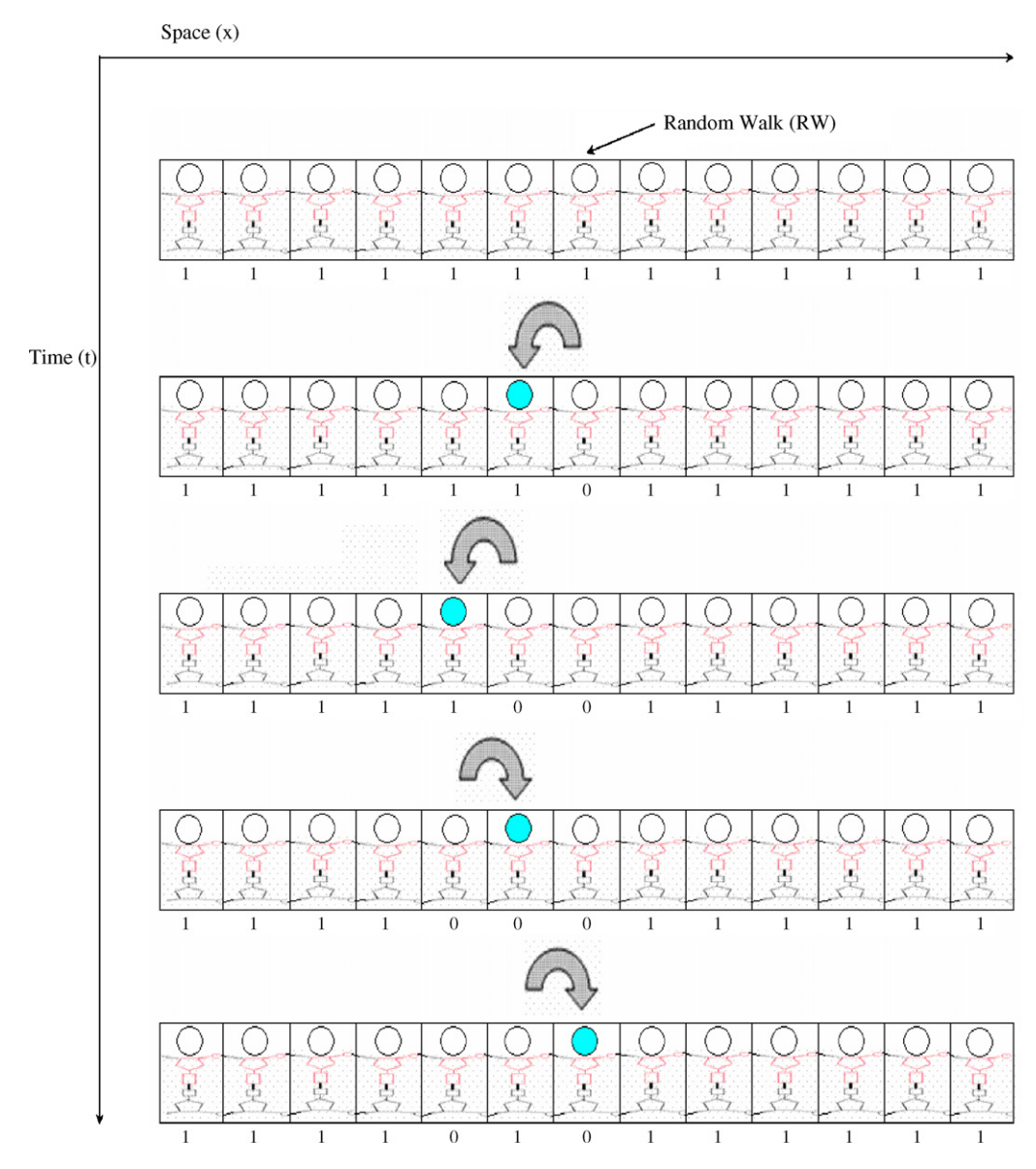


Fig. 2. Illustration of the discrete system incorporated with DNA-bit switching processes for 1D and switching rate q = 1. The initial 100% normal DNA-bit state is shown on the top, with the Brownian mutagen (BM) represented by the filled circle. From the top, we show a possible configurations after 3 step-moves. The BM switches a DNA-bit each visit, so those DNA-bits visited an even number of times are restored to their original value.

Please cite this article in press as: Triampo, D. et al., The stochastic model of non-equilibrium mutagen-induced alterations of DNA: Implication to genetic instability in cancer, BioSystems (2007), doi:10.1016/j.biosystems.2007.05.004

4

be probabilities of discrete events, rather than average properties.

We now look at a system of one-dimensional (1D) chain of the DNA-bits (Fig. 2). The position of each DNA-bit is labeled by "x" and that of a mutagen by a lattice vector R(t). The DNA-bits are described by the variables σ_x which may take the values "1" or "-1". The bit variables encode the information about the status of the nucleotide sequences for the transition creation process. As we stated above, normal DNA-bits are denoted by "1" and abnormal DNA-bits by "-1". The mutagen has a probability p for moving to one of its two nearest neighbor sites in a time step δt . After making such a jump, there is a probability q that the DNA-bit on the site departed from is switched. As known, parameters are the variables which, based on the theoretical analysis, are expected to influence the outcome of interest. In some cases, values of the parameters are known from prior experiments, and therefore these values can be fixed. In other cases, the values of the parameters are unknown or could reasonably be expected to vary over a known range. In this case, the parameters are adjustable. The greater the excess of independent experimental data points over adjustable parameters, the more valid the experimental confirmation of the theory. Starting with the initial condition that all bits are "1", we monitor the time evolution of the numbers of the abnormal "-1" and normal bits "1" for the different situations which shall be specified later.

To mathematically model the stochastic mutagenesis, we write the temporal probability distribution $P(R, \{\sigma_x\}, t)$ which is the probability that at time t, the mutagen is at position R(t) and the DNA-bits have values given by the set, $\{\sigma_x\}$. This distribution evolves according to a master equation (Gardiner, 1985) of the form

$$P(R, \{\sigma_x\}, t + \delta t)$$

$$= (1 - p)P(R, \{\sigma_x\}, t) + \frac{p(1 - q)}{2d} \sum_{l} P(R + l, \{\sigma_x\}, t)$$

$$+\frac{pq}{2d}\sum_{l}P(R+l,\ldots,-\sigma_{R+l},\ldots,t)$$
 (1)

where l represents the two orthogonal lattice vectors or go-left and go-right vector (which have magnitude l). In principle one can solve this system by the use of linear difference equations. This approach would suffer from having a too large of a number of degrees of freedom. For the case of Brownian mutagen, we focus on the specific case where p = 1 and q = 1.

An alternative continuum description was obtained by viewing the process as a stochastic cellular automaton (SCA). The process is then defined in terms of the position R(t) of the BM. Each time step the agent makes a random jump to one of its nearest neighbors and in which the bit at the site it leaves behind definitely switches. This corresponds to setting p = q = 1. Let us denote a randomly chosen unit lattice vector by l(t), and the time-dependent value of the spin at site x by $\sigma_x(t)$. Then we have

$$R(t + \delta t) = R(t) + l(t), \tag{2}$$

and

$$\sigma_{x}(t+\delta t) = \sigma_{x}(t)(1-2\delta_{x,R(t)}) \tag{3}$$

We are interested in a continuum limit of these two equations. In this limit, the first equation becomes the Langevin stochastic equation for the random walk,

$$\frac{\mathrm{d}R}{\mathrm{d}t} = \xi(t),\tag{4}$$

where $\xi(t)$ is an uncorrelated Gaussian random variable with zero mean (i.e., $\xi(t)$ is a white noise process). The correlator of $\xi(t)$ is given by

$$\langle \xi(t)\xi(t')\rangle = D\delta(t-t'),\tag{5}$$

where δ is the Dirac delta function and D is the diffusion constant. $\langle \cdots \rangle$ indicates an average over the noise (or equivalently the paths of the agent). The agent is chosen to reside initially at the origin.

The equation governing the evolution of the DNA-bit density denoted by ϕ is described by

$$\partial_t \phi(x, t) = -\lambda \phi(x, t) \delta(x - R(t)), \tag{6}$$

where λ is a phenomenological parameter which describes how strongly the DNA-bit density is coupled to the BM. It is the coarse-grained version of σ . Taking an initial condition $\phi(x, 0) = 1$ for all x and straightforward integration of Eq. (6) gives the explicit functional solution

$$\phi(x,t) = \exp[-\lambda \int_0^t dt' \delta(x - R(t')). \tag{7}$$

We will now use the stochastic solution of local DNAbit density to calculate several interesting quantities. The simplest quantity to consider is the mean local DNA-bit density given by

$$b(x,t) = \langle \phi(x,t) \rangle = \sum_{n=0}^{\infty} (-\lambda)^n \chi_n(x,t), \tag{8}$$

where $\chi_0(x, t) = 1$ and for n > 0,

$$\chi_n(x,t) = \frac{1}{n!} \left\langle \left[\int_0^t d\tau \, \delta(x - R(\tau)) \right]^n \right\rangle. \tag{9}$$

ARTICLE IN PRESS

D. Triampo et al. / BioSystems xxx (2007) xxx-xxx

6

It can be shown that

$$\chi_n(x,t) = \int_0^t d\tau_1 \int_0^{\tau_1} d\tau_2 \cdots \int_0^{\tau_{n-1}} d\tau_n \ g(0,\tau_1 - \tau_2)$$

$$\times \cdots \times g(0,\tau_{n-1} - \tau_n) g(x,\tau_n), \tag{10}$$

where $g(x, t) = (2\pi Dt)^{-1/2} \exp(-x^2/2Dt)$ is the probability density of the random walk. Eq. (10) is an *n*-fold convolution. Therefore, if we apply the temporal Laplace transform, we get (for n > 0)

$$\tilde{\chi}_n(x,s) \equiv \int_0^\infty dt \, e^{-st} \chi_n(x,t) = \frac{1}{s} \tilde{g}(0,s)^{n-1} \tilde{g}(x,s),$$
(11)

where

$$\tilde{g}(x,s) = \frac{1}{(2DS)^{1/2}} \exp\left[-\left(\frac{2S}{D}\right)^{1/2}|x|\right].$$
 (12)

where $\tilde{g}(x, s)$ is the Laplace transform of the diffusion equation Green function.

Summing over these function as given in Eq. (6) we find

$$\tilde{b}(x,s) = \frac{1}{s} \left[1 - \frac{\lambda \tilde{g}(x,s)}{1 + \lambda \tilde{g}(0,s)} \right]. \tag{13}$$

This exact result allows one to extract a great deal of statistical information about the process. First, one can simply invert the Laplace transform to find the average local DNA-bit density (or average density of switching relative to 1/2) as a function of x and t. The explicit forms are given as

$$b(x,t) = \operatorname{erf}\left[\frac{|x|}{(2Dt)^{1/2}}\right] + \exp\left(\frac{\lambda|x|}{D} + \frac{\lambda^2 t}{2D}\right)$$

$$\times \operatorname{erfc}\left[\lambda\left(\frac{t}{2D}\right)^{1/2} + \frac{|x|}{(2Dt)^{1/2}}\right] \tag{14}$$

where $\operatorname{erf}(z)$ and $\operatorname{erfc}(z)$ are the error function (Abramowitz and Stegun, 1972). Considering the long time behavior of the above expression, we find that the average local DNA-bit density at the origin (x = 0) decays asymptotically as

$$b(0,t) = \left(\frac{2D}{\pi\lambda^2 t}\right)^{1/2} \left[1 + O\left[\frac{D}{\lambda^2 t}\right]\right]. \tag{15}$$

We note here that the continuum solution has the important property that $\langle \phi(x, t; \lambda)^n \rangle = \langle \phi(x, t; nt) \rangle$. This allows us to utilize the exact solution to reconstruct the probability density for the local DNA-bit density. Theoretically, it can be proved that the average DNA-bit density by N agents $\equiv b_N(0, t)$ is proportional to $b(0, t)^N$, i.e.,

$$b^{(N)}(0,t) = [b^{(1)}(0,t)]^N = t^{N/2}, \quad \text{as } t \gg 1.$$
 (16)

Another interesting quantity which may be extracted from b(0, t) is the global switched DNA-bits, B(t), defined as

$$B(t) = \int dx [\langle b(x,0) \rangle - \langle b(x,t) \rangle].$$

This quantity obeys the exact relation

$$\frac{\mathrm{d}B(t)}{\mathrm{d}t} = \lambda b(0, t). \tag{18}$$

We find that asymptotically $B(t) \approx (t)^{1/2}$, independent of the coupling. In other words, the total amount of disorder created by a single BM on average increases as $t^{1/2}$ that is rather independent of the coupling between the BM and the DNA-bits for large time.

We now consider the probability distribution function P(b, x, t) of the local corrupted bit density. This P function will provide the information about the time evolution of the probability distribution that describes the local corruption behavior. Obviously, at the very early times, the peak of the distribution is supposed to occur in the vicinity of the origin. The complete analytic structure of $b(x, t; \lambda)$ is needed to reconstruct the distribution function P. This suggests that by knowing the first moment of the corruption density, we can generate the higher moment. Therefore, we can reconstruct the probability density function. We define P via

$$P(b, x, t) = \langle \delta(b - b_R(x, t)) \rangle \tag{19}$$

where $b_R(x, t)$ is the stochastic field solution given in Eq. (15). We can express the δ function using a frequency integral, and then expand it in powers of the field as follows:

$$P(b, x, t) = \int_{-\infty}^{\infty} \frac{d\omega}{2\pi} e^{-i\omega b} \langle e^{i\omega b_R(x, t)} \rangle$$

$$= \int_{-\infty}^{\infty} \frac{d\omega}{2\pi} e^{-i\omega b} \sum_{n=0}^{\infty} \frac{(i\omega)^n}{n!} \langle b_R(x, t)^n \rangle$$

$$= \int_{-\infty}^{\infty} \frac{d\omega}{2\pi} e^{-i\omega b} \sum_{n=0}^{\infty} \frac{(i\omega)^n}{n!} \langle b(x, t; n\lambda) \rangle.$$
(20)

We next take the Laplace transform of $b(x, t; n\lambda)$. From Eq. (12) we have

$$b(x, s; n\lambda) = \frac{1}{s} \left[1 - \frac{n\lambda \tilde{g}(x, s)}{1 + n\lambda \tilde{g}(0, s)} \right] = \frac{\tilde{g}(0, s) - \tilde{g}(x, s)}{s\tilde{g}(0, s)} + \frac{\tilde{g}(x, s)}{s\tilde{g}(0, s)[1 + n\lambda \tilde{g}(0, s)]}.$$
 (21)

The first term is handled as it is independent of n. Thus, the sum over n for this yields a factor $e^{i\omega}$ which leads to

ARTICLE IN PRESS

D. Triampo et al. / BioSystems xxx (2007) xxx-xxx

TTI 1 . 1 . C

the factor $\delta(1-b)$ when integrated over ω . The details of how to perform the sum over n for the second term, we refer to a reference by Newman and Triampo (1999). The final result for $\hat{P}(b, x, s)$ is

$$\hat{P}(b, x, s) = \frac{\hat{g}(0, s) - \hat{g}(x, s)}{s\hat{g}(0, s)} \delta(1 - b) + \frac{\hat{g}(x, s)}{\hat{g}(0, s)^2} \frac{1}{s\lambda b}$$

$$\times \exp\left[-\frac{1}{\lambda \hat{g}(0, s)} \ln\left(\frac{1}{b}\right)\right]. \tag{22}$$

To this end, we need the explicit form for $\hat{g}(x, s)$ which is given by Eq. (11). Inserting this into Eq. (22) and inverting the Laplace transform, we have our final result

$$P(b, x, t) = \delta(1 - b) \operatorname{erf} \left[\frac{|x|}{(2Dt)^{1/2}} \right] + \frac{1}{(\pi t)^{1/2}} \frac{1}{\tilde{\lambda}b} \times \exp \left\{ -\left[\frac{|x|}{(2Dt)^{1/2}} - \frac{\ln b}{2\tilde{\lambda}t^{1/2}} \right]^2 \right\}$$
(23)

where erf(z) is the error function where $\tilde{\lambda} = \lambda/(2D)^{1/2}$. In particular, the probability distribution for the average bit corruption density at the origin takes the form

$$P(b, 0, t) = \frac{1}{(\pi t)^{1/2}} \frac{1}{\tilde{\lambda}b} \times \exp\left\{ \left[-\frac{\ln(b)^2}{4\tilde{\lambda}^2 t} \right] \right\}$$
 (24)

which is a log–normal distribution and where we have defined $\tilde{\lambda} = \lambda/\sqrt{2}$. This indicates the extreme nature of the fluctuations in the system. For instance, the typical value of the magnetization density can be found from the above expression to decay exponentially.

For the asymptotic behavior of b(0, t) as $b(0, t) \approx 1/\sqrt{t}$, P(b, 0, t) in Eq. (24) becomes

$$P(b, 0, t) = \frac{1}{\sqrt{\pi \tilde{\lambda}}} \times \exp\left\{-\frac{1}{4\tilde{\lambda}^{2}t} \left[\ln \frac{1}{\sqrt{t}}\right]^{2}\right\}$$

$$\approx \exp\left\{-\frac{(\ln t)^{2}}{t}\right\} = \exp\left\{-\frac{1}{144t} - \frac{1}{6t^{2}}\right\}$$

$$-\frac{3}{4t^{3}} + \frac{26}{9t^{4}} + O\left(\frac{1}{t^{5}}\right)\right\} \approx \exp\left\{-\frac{1}{t}\right\}$$

$$= \exp\left\{-\left(\frac{1}{\sqrt{t}}\right)^{2}\right\} = \exp\{-b^{2}\}$$
(25)

which is a normal distribution and where $O(1/t^5)$ is the correction to the order of $1/t^5$. We now claim that log-normal distribution approaches normality when t is infinitely large. Finally, we analyze the effects of many BM's within the system. We assume the BM's to be non-interacting, i.e., they are unaware of each other's immediate presence. The non-trivial statistics reside in

the fact that the mutating effects of the BM's statistically interact via the overlapping of the BM histories. As we have already seen, a single BM interferes with the previous switched DNA-bit it has created, such that the amount of mutating does not simply increase linearly in time. This effect is more severe when more than one BM is present, as each BM can disturb the mutation that another BM has previously created. We measure the strength of this interference via a quantity called the "mutation efficacy" of the mutagents, defined as

$$\sigma_N \equiv \lim_{t \to \infty} \frac{B^N(t)}{B(t)}$$

where $B^N(t)$ is the average global mutation created by N mutagents. If the BM's were truly independent (in terms of the mutation they create), then we would expect $\sigma_N \propto N$.

3. Monte Carlo numerical results and discussion

Our aim in this section is to show the validity of our predicted results obtained in the previous section. To do so, we have performed the Monte Carlo simulations of the discrete model defined in Section 2. All results are obtained for a 1D chain of DNA-bits which at each site can take either the value 1 (normal) or -1 (abnormal). The chain length is considered negligible, as long as one ensures that the BM never touches the system boundaries in any of its realizations up to the latest time at which data is extracted. Thus, the system is infinitely large. We performed an average over realizations (or runs) with each run starting with the same initial configuration; namely all DNA-bits are normal. The DNA-bit at the starting point has value = 1 as shown in Fig. 2, then the BM are introduced to the starting point (origin). At each Monte Carlo step, the BM randomly walks to either one of its two neighboring sites and switches the DNA-bit of visited site before leaving. We let the BM mutate the system independently with the consequence that multiple occupancies are allowed.

We have focused on the local DNA-bit density at the origin so we measured the average altered DNA-bits density at the origin where the BM started switching the system denoted by b(0, t). To investigate the accumulated DNA alteration, we measure the total number of abnormal DNA-bits B(t) versus time. Then we defined a coarse-grained bit corruption over a patch containing 20 bits representing the bit at the origin to measure the probability distribution of the local DNA-bit density, P(b, 0, t). The 20 bit patch size is chosen because, computationally, this is primarily as a consequence of

7 i_

the optimization of the simulation technique. This is technically to compromise the length and time scale of BM versus the DNA global alteration time scale. If the patch size is too small (it has been tested), it would not quite allow us to obtain the data for the reasonably good enough histogram data resulting in the good quality probability distribution. In contrast, if the patch size is too large, it could lead to the scenario where the BM would be spending to long time in just one site in unreasonable large frequency to alter each DNA coarse-grained bit. This situation could lead to the local change as unrealistic "over-express" of a spontaneous or one time-step of a single DNA in relation with global change that is not in the reasonable time scales. Biologically, this optimal bit patch size might imply some biological counterparts, i.e., how could each BM be able to induce DNA-alteration. In addition, this optimal size might reflect the BM capability or efficiency to alter DNA. Moreover, it is known that several factors like the sensitivity of each genetic site to BM, specificity of BM/DNA matching, the fluctuation of the response due to either "on or off" genes or the inhomogeneity of DNA array landscape, etc.

In addition, the BM is initially allocated evenly on boundary of the patch to avoid the internal decimation by the transient motion of the BM. Lastly, we consider the situation of more than one BMs. We have measured the asymptotic long time value of the ratio between the number of the abnormal DNA-bit when many agents are present and that when only one agent is present. It is denoted by σ_N .

In Fig. 3, the plot between the local DNA-bit density and time is shown. b(0, t) can be viewed as being the

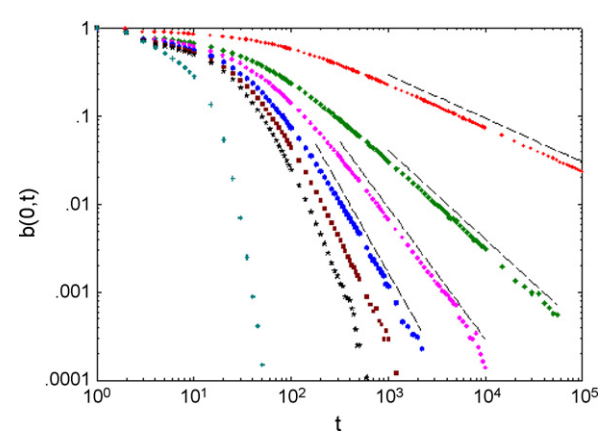


Fig. 3. The log-log plot of local DNA-bit density at the origin b(0, t) vs. time, d=1, p=1 and q=1 due to 1, 2, 3, 4, 5, 6, 16 and 32 BMs. The arrow directs the increment of number of BMs. The dash lines have slope -0.4992, -1.0104, -1.4999 and -1.9487, respectively, along the arrow direction and show the range of time in which the exponent is attracted.

frequency of the local changes of DNA-bit caused by the random or stochastic induction of the mutagen(s). It is found that $b(0, t) \approx \sqrt{t}$ for one BM and $b^{(N)}(0, t)$ $t = [b^{(1)}(0, t)]^N = t^{N/2}$ for N > 1 which are in good agreement with the analytic prediction. This indicates that b(0,t) depends sensitively on the number of BMs in terms of the overlap of the paths of different walkers and how often the BMs have visited the origin. The decay of b(0,t) due to N BAs is not linearly proportional to b(0, t)due to 1 BM but instead it varies as the power N of b(0,t). For N = 2, it gives $b(0, t) \approx t$. This result is consistent with observations that the between-population genetic variance (Roychoudhury and Nei, 1988; Lynch and Hill, 1986), and that the cumulative selection response from mutation (Hill, 1982) asymptotically increase linearly with time. It should be pointed out that the origin is strongly altered by the multiple BMs since all of the independent BMs always return to the origin and switched its DNA-bits. In the process of N agents which are noninteracting, they will interfere strongly with each other. In other words, the overlap of their histories is found. When time is infinitely large, b(0, t) approaches 0. It implies 50% chance of finding the site to be normal or abnormal. This agrees with the time limit of b(0, t). The fluctuation at this equilibrium is relatively large compared to that in the scaling regime. This results from thermal fluctuation (Burgess, 1969).

Fig. 4 shows the probability distribution P(b, 0, t) of b(0, t). In the early time regime, the simulated probability distribution is log–normal. The distribution curve has a robust tail for larger value of average DNA-bit density. This reveals the extreme fluctuation at the origin and the high probability that the origin will only be slightly mutated. The fact that BM on 1D lattice always returns to the origin (Hughes, 1995) is critical for this event. At large time the distribution has completely changed from

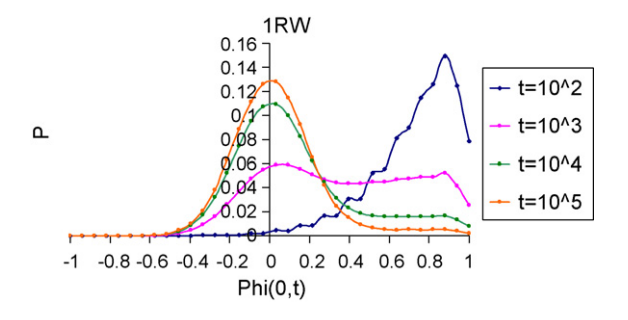


Fig. 4. The simulated probability distribution of a local DNA-bit density at the origin b(0,t), d=1, p=1 and q=1 due to 1 BM. In the early time regime when the simulated probability distribution is log–normal (Eq. (24)) and at large time the distribution has completely changed from log–normal to normal.

log–normal to normal. The peak occurs with a probability of 0.1275. An important feature that this distribution unambiguously points out is that the realizations where the DNA-bits at the origin will be half abnormal and half normal will have the highest probability of occurrence. The distribution approaches normality as time proceeds with the highest probability occurring at b(0, t) = 0. This means that the origin is steadily altered. It is expected that the distribution approaches a normal distribution quicker when there are more than one BM. The peak of the normal distributions remains at the same place. In contrast to b(0, t), the characteristics of the normal distributions are independent of N and time.

In Fig. 5, we present the results of the numerical simulations which gives the values of σ_N . We have performed numerical simulations of the many mutagens system in order to test the prediction result. The microscopic rule we use is that there is no hard-core exclusion between the mutagens, and that for each time step the N mutagens are in turn moved to a randomly chosen nearest neighbor site. A DNA-bit which is occupied by two mutagens, say, will thus (for q = 1) be switched twice in that time step. We observe the evolution of the ratio of the average global DNA-bit switching for N agents as compared to one agent for d = 1. Asymptotically, this ratio is the mutating efficacy by definition. Results are shown for N=2, 3, and 4. The curves are asymptotic to constants as expected. As we see, σ_N does not increase linearly as the number of mutagens is increased. From the stochastic point of view, this implies that there is a degree of interference between the mutagens. In the process of N BMs which are non-interacting, they will interfere strongly with each

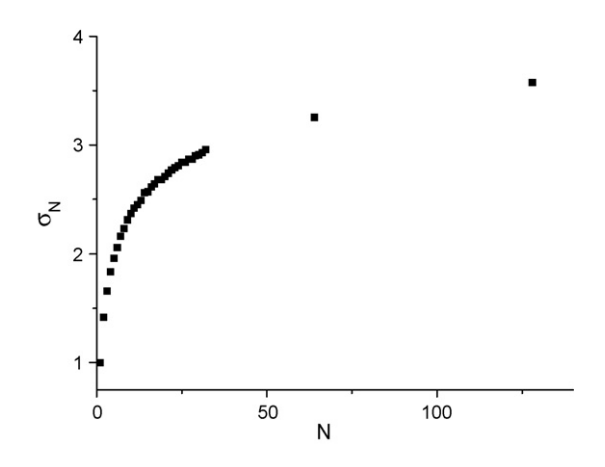


Fig. 5. Plot of σ_N vs. number of BMs. It shows that σ_N does not increase linearly as the number of mutagens is increased and, from the stochastic point of view, this implies that there is a degree of interference between the mutagens.

other. In other words, the overlap of their histories is found

Lastly, we suggest that our theoretical results can be tested, at least in principle, directly by experiments. Recently, it was shown that CIN and MIN can be introduced in cancerous cell lines through specific mutagenesis (Bardelli et al., 2001). In addition, Greenman et al. (2007) and Haber and Settleman (2007) have shown large scale analysis of DNA mutations across cancer arrays. While an in-depth study of dynamics above the error threshold along with careful consideration of the enzymatic interactions, both subjects of future research, would be necessary to rigorously quantify this statement particularly to non-equilibrium aspects. This is one example of a quantifiable and testable hypothesis that can be used to experimentally test our theoretical work. Theoretical modeling frequently uses simplifying assumptions. Simplifying assumptions eliminate complexities which may be peripheral to the issue under consideration, allowing a focus on key features of a complex biological system. For example, most models of genetic instability assume that the rate of genetic change is constant at any location in the genome, even though there is evidence of mutation "hot spots" which violate this assumption (Schaaper and Dunn, 1991). In determining whether this simplifying assumption impacts the results when modeling genetic change in carcinogenesis, one would need to know whether mutation "hot spots" exist at key loci within cancer-associated genes.

4. Implication to genetic instability in cancer and conclusion

In this work, we have modeled the stochastic kinetics of the spontaneous mutation induced by nucleotide transition as a problem of a mutagen. The dynamics in the model is to mimic the mutagenesis due to the tautomeric shift which may occur when a mutagen interacts with one of the bases in the DNA chain. The "tautomers" are created when the interaction causes some of the electrons in the base to shift their positions. To understand how this model may feature the real world phenomena, we have used both analytical model and computer simulation techniques. Analytically, we have set up the master equation and solved for local DNA-bit density, global abnormal DNA-bits, and the probability distribution function to describe the non-equilibrium nature of mutagenesis. To confirm the theoretical findings, we have performed computer simulations by applying some stochastic cellular automata rules to a DNA-bit system. Evidently, the model is non-trivial since the values of DNA-bits depend very sensitively on the path of the

10

BM, i.e., how often the BM has visited and switched the DNA-bits. We find that the local DNA-bit density, $b(0,t) \approx 1/\sqrt{t}$ the global DNA-bit $B(t) \approx \sqrt{t}$, probability density function P(b,0,t) is log-normal, and also for the case of many mutagens, σ_N does not increase linearly as the number of the BMs increases. Instead, it increases more slowly due to interference effects occurring along the path of the mutagens. Our work may relate to genetic instability in cancer.

Genetic instability is a hallmark of human cancers (Lengauer et al., 1998; Loeb, 2001). Genetic changes which are required in carcinogenesis are divided into two very broad classes: those which are dominant, requiring alteration of only one gene copy to contribute to a premalignant or malignant phenotype, and those which are recessive, requiring alteration of both gene copies to contribute to a premalignant or malignant phenotype. Genetic alterations can happen in stem cells and differentiated cells. If those genetic alterations affect genes involved in cellular proliferation, cell-cycle regulation or apoptosis, then neoplastic growth might be initiated (Levine, 1993; Mitelman et al., 1994; Kinzler and Vogelstein, 1998; Lengauer et al., 1998; Knudson, 2001; Hahn and Weinberg, 2002). The alteration of one gene, however, does not suffice to give rise to full-blown cancer. For progression towards malignancy and invasion, further mutational hits are necessary (Knudson, 2001). Hence the risk of cancer development does not only depend on mutations initiating tumourigenesis, but also on subsequent mutations driving tumor progression.

One point that we wish to make is that biological processes such as mutagenesis can be modeled by a simple model with reasonable assumptions. Although for very complex biological system, perhaps such simple model may not be valid or can only be partially modeled. To date, the number of theoretical investigation of the kinetics of mutagenesis is scant, which is one of the reasons we have modeled this problem. This work gives an example of how an interaction between a living system and its environment can be described as a stochastic process. This work can also be viewed as a problem in non-equilibrium disordering. Here, we started with an initially ordered configuration and by applying local update rules (the dynamics), we can tract the time evolution of the degree of disordering. A more detailed model would require, for example, a complete description of the tautomeric shifts, in order to understand the kinetics of mutagenesis more fully. This may involve quantum mechanics theory since one would need to know position of the localization of the electrons in the bases as they shift from a nitrogen ion to a hydrogen ion. It should be pointed out that we have not addressed a very important issue, the survivability of the mutation. At what degree of mutagenesis is the DNA sequence not able to replicate itself. In order to correct the errors which occur during the DNA synthesis, DNA polymerase checks the newly-synthesized DNA strand and corrects most of the incorrect bases (Kornberg, 1974; Watson, 1970). It was shown experimentally that this "proof-reading" step reduces the number of mutations by a factor of 10^2 to 10^3 . Such significant reduction should be also considered while comparing the calculated and observed frequencies of the mutations. Therefore, the frequency of the spontaneous $GC \rightarrow AT$ before the checking step should be in the approximate range of 10^{-6} to 10^{-8} .

Also we would like to note that the values of the predicted non-equilibrium quantities are sensitive to the level of calculations (level of theory and the basis set), which suggests that a higher-level calculations should be also performed. So far, computational calculations of the nucleotide sequences done within the framework of the "human genome" have proven to be useful since they provide deeper insight into the principle of genome organization and function. Much more work has to be done to close the gap between the complexities of real biological entities and grossly oversimplified mathematical (modeling) descriptions used to study biological and medical systems. The increase appreciation of stochasticity in biological research is observed in all scales of biological systems (Kurakin, 2005, 2006; Xie and Lu, 1999; Dundr et al., 2002; Kimura et al., 2002; Essers et al., 2002; Sirakoulis, 2004; Hoogstraten et al., 2002). We believe our model will complement detailed stochastic modeling by providing a set of powerful mathematical tools and concepts to visualize DNA alteration.

Acknowledgements

This research work was financially supported in part by Mahidol University, The Thailand Research Fund (TRF), The National Center for Engineering and Biotechnology, Thailand (BIOTEC), and the Third World Academy of Sciences (TWAS 04-446 RG/PHYS/AS). The authors thank the reviewer of the manuscript for all the valuable recommendations and comments.

References

Abramowitz, M., Stegun, I.A., 1972. Handbook of Mathematical Functions, 10th ed. Dover, New York.

Bardelli, A., Cahill, D.P., Lederer, G., Speicher, M.R., Kinzler, K.W., Vogelstein, B., Lengauer, C., 2001. Genetic instability and the quasispecies model. Proc. Natl. Aacd. Sci. 98, 5770.

ARTICLE IN PRESS

D. Triampo et al. / BioSystems xxx (2007) xxx-xxx

- Burgess, R.E., 1969. Fluctuation Phenomena in Solid. Academic Press, New York
- Claytong, A., Robertson, A., 1955. Mutation and quantitative variation. Am. Nat. 89, 151–158.
- Crowj, F., Kimura, M., 1964. The theory of genetic loads. Proc. XI Int. Congr. Genet., 495–505.
- Delbruck, M., Timofeeff, N.W., Zimmer, K.G., 1935. Nachr. Biol. Ges. Wiss. Gottingen 1, 189.
- Dundr, M., Hoffmann-Rohrer, U., Hu, Q., Grummt, I., Rothblum, L.I., Phair, R.D., Misteli, T., 2002. A kinetic framework for a mammalian RNA polymerase in vivo. Science 298, 1623–1626.
- Essers, J., Houtsmuller, A.B., van Veelen, L., Paulusma, C., Nigg, A.L., Pastink, A., Vermeulen, W., Hoeijmakers, J.H., Kanaar, R., 2002. Nuclear dynamics of RAD52 group homologous recombination proteins in response to DNA damage. EMBO J. 21, 2030–2037.
- Finnegan, D.J., 1990. Transposable elements and DNA transposition in eukaryotes. Cuur. Opin. Cell Biol. 21, 471–477.
- Gardiner, C.W., 1985. Handbook of Stochastic Processes, second ed. Springer-Verlag, Berlin.
- Greenman, C., et al., 2007. Patterns of somatic mutation in human cancer genomes. Nature 446, 153–158.
- Haber, D.A., Settleman, J., 2007. Drivers and passengers. Nature 446, 145–146.
- Hahn, W.C., Weinberg, R.A., 2002. Rules for making human tumor cells. N. Engl. J. Med. 347, 1593–1603.
- Hill, W., 1982. Rates of change in quantitative traits from fixation of new mutations. PNAS 79, 142–145.
- Hoogstraten, D., Nigg, A.L., Heath, H., Mullenders, L.H., van Driel, R., Hoeijmakers, J.H., Vermeulen, W., Houtsmuller, A.B., 2002. Rapid switching of TFIIH between RNA polymerase I and II transcription and DNA repair in vivo. Mol. Cell 10, 1163–1174.
- Hughes, B.H., 1995. Random Walks and Random Environments, vol. 1. Clarendon Press, Oxford.
- Hussain, S.P., Harris, C.C., 1999. Mutation spectrum and load: the generation of hypotheses linking the exposure of endogeneous or exogeneous carcinogens to human cancer. Mutat. Res. 428, 33–39.
- Kimura, M., 1965. A stochastic model concerning the maintenance of genetic variability in quantitative characters. Proc. Natl. Acad. Sci. U. S. A. 54, 731–736.
- Kimura, H., Sugaya, K., Cook, P.R., 2002. The transcription cycle of RNA polymerase II in living cells. J. Cell Biol. 159, 777–782.
- Kinzler, K.W., Vogelstein, B., 1998. The Genetic Basis of Human Cancer. McGraw-Hill, Toronto, CA.
- Kleckner, N., 1981. Transposable elements in prokaryotes. Annu. Rev. Genet. 15, 341–404.
- Knudson, A.G., 2001. Two genetic hits to cancer. Nat. Rev. Cancer 1, 157, 162
- Komarova, N.L., Lengauer, C., Vogelstein, B., Nowak, M.A., 2002. Dynamics of genetic instability in sporadic and familial colorectal cancer. Cancer Biol. Ther. 1, 685–692.
- Kornberg, A., 1974. DNA Synthesis. W.H. Freeman & Co, San Francisco.
- Kurakin, A., 2005. Self-organization versus watchmaker: stochastic gene expression and cell differentiation. Dev. Genes Evol. 215, 46–52.

Kurakin, A., 2006. Self-organization versus watchmaker: Molecular motors and protein translocation. Biosystems 84, 15– 23

11

- Lander, R., 1975. The maintenance of genetic variability by mutation in a polygenic character with linked loci. Genet. Res. 26, 221– 235
- Lengauer, C., Kinzler, K.W., Vogelstein, B., 1998. Genetic instabilities in human cancers. Nature 396, 643–649.
- Leszczynski, J. (Ed.), 1999. Computational Molecular Biology of "Theoretical and Computational Chemistry Book Series, vol. 8. Elsevier
- Levine, A.J., 1993. The tumor suppressor genes. Annu. Rev. Biochem. 62, 623–651.
- Lindahl, T., 1993. Instability and decay of the primary structure of DNA. Nature (London) 362, 709–715.
- Loeb, L.A., 2001. A mutator phenotype in cancer. Cancer Res. 61, 3230–3239.
- Lynch, M., Hill, W.G., 1986. Phenotypic evolution by neutral mutation. Evolution 40, 915–935.
- Mitelman, F., Johansson, B., Mertens, F., 1994. Catalog of Chromosome Aberrations in Cancer, vol. 2. Wiley–Liss, New York.
- Newman, T.H., Triampo, W., 1999. Binary data corruption due to a Brownian agent. Phys. Rev. E 59 (5), 5172–5186.
- Nowak, M., Schuster, P., 1989. Error tresholds of replication in finite populations, mutation frequencies and the onset of Muller's ratchet. J. Theor. Biol. 137, 375.
- Radchenko, E.D., Plohotnichenko, A.M., Sheina, G.G., Blagoi, Yu.P., 1983. Ab initio study of the prototropic tautomerism of cytosine and guanine and their contribution to spontaneous point mutations. Biophysics (Engl. Ed.) 28, 559.
- Roberts, J.J., 1978. The repair of DNA modified by cytotoxic, mutagenic and carcinogenic chemicals. Adv. Radiat. Biol. 7, 211–425
- Roychoudhury, A.K., Nei, M., 1988. Human polymorphic genes: world distribution. Oxford University Press, New York.
- Schaaper, R.M., Dunn, R.L., 1991. Spontaneous mutation in the Escherichia coli lacI gene. Genetics 129, 317–326.
- Singer, B., Kusmierek, J.T., 1982. Chemical mutagenesis. Annu. Rev. Biochem. 51, 655–693.
- Sirakoulis, G.Ch., 2004. An algorithm for the study of DNA sequence evolution based on the genetic code. BioSystems 77, 11– 23.
- Sole, R.V., Deisboeck, T.S., 2004. An error catastrophe in cancer. J. Theor. Biol. 228, 47–54.
- Watson, J.D., Crick, F.H.C., 1953. Genetic implications of the structure of deoxyribonucleic acid. Nature 171, 964–969.
- Watson, J.D., 1970. Molecular Biology of Gene. W.A. Benjamin Inc., New York.
- Watson, J.D., Hopkins, N.H., Roberts, J.W., Steitz, J.A., Weiner, A.M., 1988. Molecular Biology of the Gene. The Benjamin/Cummings Publishing Company Inc., CA/Reading, MA.
- Xie, X.S., Lu, H.P., 1999. Single-molecule enzymology. J. Biol. Chem. 274, 15967–15970.
- Zeng, Z.B., Cockerham, C., 1993. Mutation models and quantitative genetic variation. Genetics 133, 729–736.

Effect of lipid peroxidation on the properties of lipid bilayers: a molecular dynamics study

Jirasak Wong-ekkabut^{a,b}, Zhitao $Xu^{b,c}$, Wannapong Triampo^{a,d}, I-Ming Tang^{a,e}, D. Peter Tieleman^b, Luca Monticelli^{b,*}

^a Department of Physics, Mahidol University, Bangkok 10400, Thailand

^b Department of Biological Sciences, University of Calgary, Calgary, Alberta T2N 1N4, Canada

^c Present address: Materials and Process Simulation Center, California Institute of Technology, Pasadena, California, USA

^d Center for Vector and Vector-Borne Diseases, Mahidol University, Bangkok 10400, Thailand

^e Center of Nanoscience and Nanotechnology, Mahidol University, Bangkok 10400, Thailand

*Corresponding author

luca.monticelli@ucalgary.ca

Dept. of Biological Sciences, University of Calgary

2500, University Dr NW

Calgary, AB, Canada, T2N 1N4

Phone: +1 403 220-4039 Fax: +1 403 289-9311

Abstract

Lipid peroxidation plays an important role in cell membrane damage. We investigated the effect of lipid peroxidation on the properties of 1-palmitoyl-2-linoleoyl-sn-glycero-3phosphatidylcholine (PLPC) lipid bilayers using molecular dynamics simulations. We focused on four main oxidation products of linoleic acid with either a hydroperoxide or an aldehyde group: 9-trans, cis-hydroperoxide linoleic acid, 13-trans, cis-hydroperoxide linoleic acid, 9-oxononanoic acid, and 12-oxo-9-dodecadienoic acid. These oxidized chains replaced the sn-2 linoleate chain. The properties of PLPC lipid bilayers were characterized as a function of the concentration of oxidized lipids, with concentrations from 2.8 to 50% for each oxidation product. The introduction of oxidized functional groups in the lipid tail leads to an important conformational change in the lipids: the oxidized tails bend towards the water phase and the oxygen atoms form hydrogen bonds with water and the polar lipid head group. This conformational change leads to an increase in the average area per lipid and, correspondingly, to a decrease of the bilayer thickness and the deuterium order parameters for the lipid tails, especially evident at high concentrations of oxidized lipid. Water defects are observed in the bilayers more frequently as the concentration of the oxidized lipids is increased. The changes in the structural properties of the bilayer and the water permeability are associated with the tendency of the oxidized lipid tails to bend towards the water interface. Our results suggest that one mechanism of cell membrane damage is the increase in membrane permeability due to the presence of oxidized lipids.

Keywords: lipid peroxidation, membrane damage, membrane permeability, computer simulation, water defect, bilayer structure.

Introduction

Lipid peroxidation alters the physiological functions of cell membranes and plays an important role in cellular membrane damage. Peroxidation is believed to be involved in cellular ageing and in various diseases, such as Parkinson's and Alzheimer's disease (1-9) as well as schizophrenia (10), atherosclerosis (11,12), inflammatory diseases (13) and cardiac ischemia reperfusion injury (14,15). Unsaturated lipids are easily susceptible to peroxidation (16). The effect of both unsaturation and peroxidation on the properties of lipid bilayers has been well characterized experimentally (17-22). Still, the exact mechanism of membrane damage by oxidized lipids is unclear. Oxidized lipid tails are more polar and can be shorter in length, due to the presence of aldehyde or hydroperoxide groups (23,24). Lipid peroxidation has been shown to perturb the bilayer structure and modify membrane properties such as membrane fluidity, permeability to different substances and bilayer thickness. The existence of a direct relationship between lipid peroxidation and membrane leakiness has been suggested (25-28). Increased membrane permeability caused by oxidation of lipids and membrane proteins can disrupt ion gradients, therefore altering metabolic processes. Lipid peroxidation can influence the permeability of lipid membranes by increasing the dielectric constant of the membrane interior and by increasing the microviscosity, possibly through cross-linking of lipid radicals (23). Focusing on structural and dynamic properties, a decrease in membrane thickness upon oxidation has been observed using X-ray diffraction analysis, along with interdigitation of the terminal methyl segments (22). The effect of peroxidation on lipid dynamics and membrane order is less clear. According to some researchers, peroxidation does not affect the fluidity of the membrane (29) nor the reorientational dynamics of the lipids (18). According to others, membrane fluidity is decreased (30-33) and the decrease is higher near the double bonds of the bilayer, whereas other regions are less affected (30). Some have reported an increase in the lipid tails order parameter (30,33-36), others no change (37) or a decrease (18,38). Several reasons can explain the differences in experimental results, including the use of different methodologies to generate peroxides, leading to different (and usually not well-defined) lipid compositions of the membrane (22). Despite the numerous studies on the effect of oxidation on the structure and dynamics of lipid membranes, the relationship between increased membrane permeability and modifications in the structure and dynamics of lipid bilayers is not clear.

In recent years, computational studies of model membranes proved to be particularly useful in the description of the structure and dynamics of lipid bilayers (39,40) and in the

interpretation of experimental results (41). Both pure lipid bilayers (42-44) and mixtures of lipids with proteins and cholesterol have been investigated using computational methods (43,45-48). Unsaturated lipid bilayers also have been studied using computer simulations (49-53), but the structural consequences of the presence of oxidized lipids have never been investigated using computational methods, to the best of our knowledge.

In the present work, we use molecular dynamics simulations to characterize the effect of lipid oxidation on the properties of 1-palmitoyl-2-linoleoyl-sn-glycero-3-phosphatidylcholine (PLPC) lipid bilayers. In particular, we describe the effect of four different products of PLPC peroxidation (54) at five concentrations, ranging from 2.8% to 50%. We focused on four main oxidation products of linoleic acid, including either a hydroperoxide or an aldehyde group: 9-trans, cis-hydroperoxide linoleic acid, 13-trans, cis-hydroperoxide linoleic acid, 9oxononanoic acid, and 12-oxo-9-dodecadienoic acid (Figure 1). These oxidized chains replaced the sn-2 linoleate chain in PLPC. The goal of this work is to understand how oxidized lipids change the membrane properties. In particular, we seek to characterize the relationship between the changes in membrane permeability and the modifications of structural and dynamic properties of the lipid bilayer, and to provide a detailed description at the atomistic level of the chemical interactions responsible for the changes in the properties of the membrane. The paper is organized as follows. First we describe the methods used to derive the simulation parameters for the lipids and the simulation methods. Then we describe a number of properties of a PLPC bilayer and how they change upon increasing the concentration of oxidized lipids, and compare simulation results to experimental ones reported in the literature. Finally, we discuss the relationship between permeability, structure and dynamics of oxidized bilayers.

Methods

Force field parameters

A united atom force-field was used for the lipids in all simulations. The parameters for the phosphatidylcholine (PC) head group and the lipid tails were taken from previous works on PLPC and DPPC lipids (42,51). The hydroperoxide lipid tails were created by addition of a hydroperoxide group at position C9 or C13 of the linoleate tail and shifting the double bonds, as shown in Figure 1a and 1b. The aldehyde lipid tails were also built starting from linoleic acid (Figure 1c, 1d). The bonded parameters for the O-O and O-H bonds and for the O-O-H angle were taken from previous calculations on hydrogen peroxide (55), while all

other missing parameters were derived using quantum chemistry calculations on 3hydroperoxy-1-butene (Figure 2a). The charges at the last carbon and oxygen and dihedral angle parameters of C-C-C=O in aldehyde lipid tail were calculated from propanal (Figure 2b) by using the same procedure as for the hydroperoxide lipid tail. We used the Jaguar software package (56) for all quantum calculations, with the B3LYP method of density functional theory (57,58) and the LACV3P**++ basis set. Partial atomic charges were estimated using natural population analysis (NPA) (59) and the electrostatic surface potential (ESP) fitting method with Merz-Kollman atomic radii (60) after the geometry optimization. The results for partial charges are reported in Table 1. For the calculation of bond and angle force constants, we restrained the bond lengths and angles at seven different values, then fitted a harmonic potential functions to the energy profile. For dihedral parameters, dihedral angles were restrained at 36 different values from 0 to 360 degrees, and the standard proper dihedral function $(V(\omega) = \sum_{n=0}^{\infty} \frac{V_n}{2} [1 + \cos(n\omega - \gamma)])$ was fitted to the potential energy. For all bonded parameters, the Lennard-Jones and electrostatic energy were calculated for different geometries and subtracted from the total energy before fitting. Results for all bonded parameters are reported in Table 2 and 3.

Bilayer setup and simulation details

The systems were generated starting from the equilibrium structure of a PLPC bilayer containing 72 lipids. We replaced 2, 4, 8, 18, and 36 PLPC lipid molecules with each oxidized lipid, obtaining 20 different bilayers with oxidized lipid concentrations of 2.8%, 5.6%, 11.1%, 25%, and 50% respectively. The two bilayer leaflets always contained the same number of oxidized lipids. All 21 simulation systems contained 72 lipid (including PLPC and oxidized lipids) and 2880 water molecules. All simulations were carried out with version 3.3.1 of the GROMACS package (61). After energy minimization, molecular dynamics simulations were run for 180 ns, and the initial 80 ns were considered as an equilibrium period. The integration time step was 2 fs. Periodic boundary conditions were applied in all dimensions. A 1.0 nm cutoff was employed for the electrostatic and Lennard-Jones interactions and the neighbor list was updated at every time step. The long range electrostatics was calculated using particle mesh Ewald (62,63); the real-space interactions were evaluated on a 0.12 nm grid with fourth-order B-spline interpolation. The relative error for the Ewald sum

in the direct and reciprocal space, controlled in GROMACS by the parameter ewald_rtol, was set to 10^{-5} . The LINCS algorithm was used to constrain all bond lengths (64). The weak temperature coupling scheme was applied separately to the lipids and water (65), with a temperature of 298 K and a time constant of 0.1 ps. The semi-isotropic pressure was applied (65), with and equilibrium pressure of 1 bar both in the x-y plane and in the z direction (bilayer normal) with a time constant of 4.0 ps and a compressibility of 4.5×10^{-5} bar⁻¹. Molecular graphics were made using VMD (66).

Potential of mean force and permeability of water

Constraint simulations were used to calculate the potential of mean force (PMF) of water as a function of the distance from the center of the bilayer, the local diffusion coefficient at different depths and water permeability through the lipid bilayer (67,68). A series of 31 simulations was run with the distance between water and the center of bilayer constrained between 0 and 3.0 nm, with 0.1 nm spacing. Only the component of the distance along the bilayer normal (Z axis) was constrained, while water was completely free to move in the X and Y directions. The SHAKE algorithm was used, with a relative tolerance of 10⁻⁵. Two water molecules were constrained at the chosen depths inside the bilayer, at a distance of 3.0 nm from each other. In the first simulation, one water molecule was restrained at 0 nm (corresponding to the center of the bilayer) and the second at 3 nm (corresponding to the bulk water phase). This setup allows for increased sampling at no computational cost. Each simulation was 15 ns long and the forces were calculated as a function of the simulation time. The free energy of water transfer from the bulk phase to various depths in the membrane can be expressed as:

$$\Delta G(z) = -\int\limits_{bulk-}^{z} < F(z') >_{\iota} dz' \; , \; \left(\; 1 \; \right) \label{eq:deltaG}$$

where $\langle F(z') \rangle_t$ indicates the average force over the simulation time; the limits of the integration range from bulk water to depth z. In order to estimate the error on the force, we used a block averaging procedure on five intervals, each 3 ns long. We used the force autocorrelation method for the calculation of the local time-dependent friction coefficient, $\xi(t)$, as described by Marrink (67,68). The static friction coefficient, ξ , is inversely proportional to the local diffusion coefficient (D(z)) (68-70) and the permeability coefficient (P) of the solute is defined as the inverse of the resistance (R). The resistance R to permeate through the bilayer is obtained by integrating over the local resistances $\Re(z)$:

$$R = \int_{\text{outside}}^{z} \Re(z') dz' = \int_{\text{outside}}^{z} \frac{\exp(\Delta G(z') / RT)}{D(z')} dz' = \frac{1}{P} . \tag{2}$$

Results and discussion

Structural and dynamic properties of the lipid bilayer

The first important change in the simulations of all the oxidized lipids is in the conformation of the lipid tails. Snapshots showing the conformation of oxidized and nonoxidized lipids are shown in Figure 3. The portion of the lipid tail containing oxygen atoms is found, on average, close to the interface region. This is confirmed by the distribution of aldehyde and peroxide oxygen atoms in the bilayer, shown in Figure 4. For both the aldehyde-containing and the peroxide-containing lipids, the maximum density of oxygen atoms is around the carbonyl group, and the distribution is broader for aldehyde-containing lipids. Together with the conformational change, hydrogen bonding is observed between the oxidized lipid tail and water, carbonyl groups and phosphate groups. Table 4 shows the average number of hydrogen bonds formed by the hydroperoxide and aldehyde groups with other groups, in each simulation. In all cases, oxidized lipid tails form hydrogen bonds mostly with water molecules. For hydroperoxide-containing lipids, hydrogen bonds with phosphate groups are more probable than with carbonyl groups. The average total number of hydrogen bonds per lipid does not change significantly with the concentration of oxidized lipids. Its average value is 1.00 ± 0.13 for hydroperoxide lipids and 0.48 ± 0.05 for aldehyde lipids. This highlights a correlation between oxygen density distribution and hydrogen bonding: hydroperoxide lipids have higher propensity to form hydrogen bonds with water and narrower density distributions. These findings corroborate the model initially proposed by van Kuijk et al., suggesting that the hydroperoxide moieties reside in the proximity of the lipid head group region, because of their hydrophilic character (71).

The presence of hydrogen bonding interactions involving the lipid tails affects most of the properties of the lipid bilayer. Figure 5A shows the electron density profile calculated from our simulations of pure PLPC and for bilayers containing 50% concentration of each oxidized lipid. The total density at the center of the bilayer is increased in the presence of oxidation, and the maxima are shifted towards the center. The increase of the density at the center of the bilayer corresponds to partial interdigitation of the phospholipids acyl chain terminal methyl segment when the thickness of bilayer decreases. While experimental data on

PLPC are not available, the change in the electron density profile upon peroxidation has been characterized experimentally for dilinoleoyl phosphatidylcholine (DLPC) bilayers, as shown in Figure 5B (reproduced from reference (22)). Simulation results on PLPC compare favorably with the experimental ones on DLPC, showing a decrease in the bilayer thickness and a higher density in the center.

We calculated the average area per lipid and bilayer thickness in the 25 simulated systems, and compared the results to previous simulations and experimental data. The thickness of the bilayer was calculated from the simulations as the average distance between phosphate groups in the two leaflets. Figure 6 shows the area per lipid molecule and the bilayer thickness at different concentrations of each oxidized lipid. For the pure PLPC bilayer, we found an average area per lipid of 0.651 ± 0.015 nm² and an average thickness of $3.62 \pm$ 0.01 nm. The difference with previous calculations (51,72) and experimental findings (50,73) is within 6% for the area and 3% for the thickness. For all the bilayers containing oxidized lipids, the area increases with increasing concentrations of the oxidized lipids, and the thickness decreases. Visual inspection of the trajectories suggests that the increase in area per lipid and the corresponding decrease in the thickness are related to the preference of the more polar oxidized tails for the interface and the head group region. The relationship between area and thickness is not straightforward, since both the length of the oxidized lipid tail and the position of the oxygen in tail have a specific effect on the structural properties of the bilayer. The thickness is generally less when the bilayer contains aldehyde lipids, for which one of the acyl tails is shorter. On the other hand, lipids with the peroxide or aldehyde groups farther away from the carbonyl ester tend to give larger areas. Bilayers containing 13-tc generally have the largest area per lipid, but not the smallest thickness.

The increase in the area per lipid observed in our simulations is consistent with experimental results by Pradhan et al. showing that peroxidized lipids increase the phospholipids spacing in erythrocyte membranes (74). Sabatini et al. characterized DPPC monolayers containing oxidized lipids, in particular 9-al (referred to as PoxnoPC, in their study) and the carboxylic acid analogue (75). They found that both oxidized lipids expanded the monolayers, similarly to our results. Interestingly, film expansion was larger with the carboxylic terminal group, the more polar group. They also proposed a model for the arrangement of the *sn*-2 acyl chains in monolayers that is similar to the model of van Kuijk (71), and consistent with our results.

The degree of ordering of the tail is also influenced by the presence of the oxygen atoms, as shown by the deuterium order parameter (Figure 7). The deuterium order parameter can be measured by NMR, and is defined as:

$$S_j = \frac{1}{2} < 3\cos^2(\theta_j) - 1 > ,$$
 (3)

where θ_j is the angle between a C-D bond and the membrane normal. The brackets indicate averaging over the two bonds in a certain CD₂ group, over all the lipids and over time. Since we used a united atoms representation in our simulations, the positions of the deuterium atoms were reconstructed assuming ideal tetrahedral geometry of the methylene groups. The order parameter was calculated for all the CD bonds in the sn-1 and sn-2 chains of both PLPC and the oxidized lipids in all the simulations. As expected, in PLPC molecules the unsaturated lipid tail has lower order parameters compared to the saturated one. The average order parameter for the acyl chains decreases with increasing concentration of oxidized lipids, both for PLPC and for the oxidized lipids. The order parameter for both the sn-1 and the sn-2 tails of oxidized lipids is lower than for the linoleate tail of the pure PLPC bilayer. The disordering effect induced by the presence of the oxidized lipid tail is stronger for aldehyde lipids than for hydroperoxide ones. This effect can possibly be due to the lower hydrogen bonding propensity of the aldehyde tails, which makes them more mobile, and to the larger free volume available for the sn-1 chain when the sn-2 chain is shorter.

Wratten et al. (18) measured the membrane ordering in PLPC and DLPC bilayers containing hydroperoxide and hydroxide groups using angle-resolved fluorescence depolarization. Their results showed that the presence of oxidized lipid molecules cause a decrease in membrane order. However, other studies showed an increase (30,34-36) or no change (37) in the order parameter. It has been suggested that this discrepancy depends on the presence of numerous oxidative products, different from our case.

Together with the changes in the structural properties of the bilayer, dynamic properties of the lipids were also modified. We calculated the lateral diffusion coefficient from the mean square displacements (MSD) of the lipids as a function of time. We observed that the two monolayers move relative each other and relative to water during the simulations. Both types of motion are artifacts due to the finite size of the simulated systems and to periodic boundary conditions (76). We therefore subtracted the center of mass motion of each monolayer before calculating the MSD. We then utilized the model proposed by Wohlert and Edholm for the calculation of the lateral diffusion coefficient at short and long time scales (76). This model considers two different types of diffusion occurring on different time scales. The diffusion at

short times (described by the D_1 coefficient) takes place within a circular area of radius R and is not Brownian, while the diffusion at long times (described by the D_2 coefficient) involves large displacements and is Brownian. Both diffusion coefficients can be calculated by fitting the MSD curve to the following expression (76);

$$\langle r^2 \rangle = \frac{4D_1 t r_0^2}{r_0^2 + 4D_1 t} + 4D_2 t$$
, where $r_0^2 \equiv \frac{R^2}{2}$ (4)

In order to estimate the error of diffusion coefficients, we split our 100 ns trajectories in five intervals of 20 ns each and fitted the MSD curves between 0 and 10 ns. For the pure PLPC bilayer we found values of $10.3 \pm 0.8 \cdot 10^{-7}$ cm²/s for D₁, 0.27 nm² for r_0^2 and $0.60 \pm 0.05 \cdot 10^{-7}$ cm²/s for D₂. Previous simulations of a PLPC bilayer gave a diffusion coefficient of $1.3 \pm 0.3 \cdot 10^{-7}$ cm²/s for the diffusion at long times (53). This value is significantly higher than our result, but it was obtained at a higher temperature (310K). Our results compare favorably to previous simulation results for a DMPC bilayer, with D₁ = $13 \cdot 10^{-7}$ cm²/s, D₂ = $0.79 \cdot 10^{-7}$ cm²/s and $r_0^2 = 0.3$ nm² (76). The agreement with experimental diffusion coefficients is also very reasonable: the diffusion coefficient at long times can be compared with results from neutron scattering experiments, measuring D = $1 \sim 10 \cdot 10^{-7}$ cm²/s (77,78), while D₂ can be compared with diffusion coefficients from fluorescence recovery after photo bleaching (FRAP) experiments, which typically give values around $0.5 \sim 1 \cdot 10^{-7}$ cm²/s (79).

Short-time and long-time diffusion coefficients for all the simulated systems are reported in Figure 8. Short-time diffusion coefficients decrease very slightly with increasing concentration of oxidized lipids, while long time diffusion coefficients are not significantly affected by peroxidation. Early experimental studies suggested an increase of membrane microviscosity upon peroxidation (30-32,80), while more recent results indicated that the effect of lipid oxidation causes pronounced structural effects but minimal effects on the membrane dynamics (18,29). Our study suggests that, while the presence of oxidized lipids has a large influence on structural properties, its effect on lipid diffusion is relatively small. However, the diffusion appears to be faster for aldehyde lipids compared to hydroperoxide lipids. This can be related to the stronger hydrogen bonding interactions observed for hydroperoxide lipids, which involve not only water but also polar head groups of neighboring lipids.

Water permeation through PLPC bilayers

The presence of oxidized lipids has a profound influence on the permeability of water through PLPC bilayers. Water pores are observed in all the simulations containing 5% or more oxidized lipids, and they are relatively stable at higher oxidation levels. Figure 9 shows a water defect in a bilayer containing 13-tc lipids at 50% concentration. Based on visual inspection of the trajectories, water defects can form independently in both leaflets and they are larger in the presence of 12-al and 13-tc. This difference correlates well with the higher area per lipid in bilayers containing 12-al and 13-tc lipids, which have polar oxygen atoms closer to the terminal methyl group.

In order to understand the energetics of water penetration inside different bilayers, we calculated the potential mean force (PMF) of water as a function of the distance from the center of the bilayer using constraint simulations. Due to the high computational cost, we limited the calculations to 9 systems, including pure PLPC and bilayers containing 11.1% and 50% of each oxidized lipid. For the same systems we also calculated the local diffusion coefficient and the permeability of water across the bilayer. PMF profiles are shown in Figure 10. The shape of free energy profile for pure PLPC is very similar to previously published profiles for DPPC (67,68,81). The free energy increases moving from the water interface to the hydrophobic tail region, reaching a maximum of 29.4 ± 2.3 kJ/mol at 0.5 nm from the center of bilayer. A dip of about 1 kJ/mol is observed at the center of bilayer, which can be interpreted as the effect of the slightly lower local density (67,68). Free energy values in our simulation are higher than those obtained by Marrink and Bemporad simulating DPPC bilayers (67,81). The difference might be explained by the different nature of the lipids and the lower temperature used in our simulations (300K instead of 350K or higher). For the pure PLPC bilayer, we compared PMF results obtained from constraint and umbrella sampling simulations (data not shown), and did not find significant differences. For the mixtures containing oxidized lipids, the shape of the PMF becomes Gaussian-like when the concentrations of oxidized lipids increases, and the dip at the center of the bilayer disappears. Since the density at the center of the bilayer increases with increasing level of oxidation, this result is consistent with the idea that the dip in the PMF depends on the local density. The free energy barrier to translocation across the bilayer decreases as the concentration of oxidized lipids increases, with all four oxidized lipids. The free energy at the center of bilayer is decreased by 0.6~1.6 kJ/mol in the presence of 11.1% oxidized lipids, and by 4.0 to 11.1 kJ/mol in the presence of 50% oxidized lipids. Like for the bilayer thickness, 12-al and 13-tc lipids have a stronger effect on the free energy barrier compared to 9-tc and 9-al.

Local diffusion coefficients and the local resistance were calculated for water at different depths in the membrane. In the case of the pure PLPC bilayer, we observe a decrease in the local diffusion coefficient from bulk water to lipid tail interior and an increase in the central portion of the bilayer. Although this behavior is qualitatively similar to that observed by Marrink and Bemporad on DPPC bilayers (67,81), the discrepancy in the actual values is significant. In the central region, the local diffusion coefficient of water is lower in oxidized bilayers than in the non-oxidized bilayer. This is related to the increase in the local density at the center of oxidized bilayers. As expected, the free energy barrier dominates the local resistance profiles for water in the bilayers, and therefore water permeability. To our knowledge, water permeability through PLPC bilayer has never been reported in the literature. However, several papers reported experimental results for water permeability through different saturated and unsaturated lipid bilayers. A value of $4.9 \pm 0.6 * 10^{-3}$ cm/s has been reported for 1-stearoyl-2-linoleoyl phosphatidylcholine (SLPC), $9.1 \pm 2.4 * 10^{-3}$ cm/s for 1,2-dilinoleoyl phosphatidylcholine (DLPC) (82). Although comparable, these values are higher than our findings for pure PLPC, $1.6 \pm 0.5 * 10^{-3}$ cm/s at $25 ^{\circ}$ C.

Table 5 shows the permeability of water through PLPC bilayers at two different concentrations of oxidized lipids. As all oxidized lipids decrease the free energy barrier for water penetration, all of them increase water permeability. This effect is not very large at the concentration of 11.1%, but at 50% the increase in permeability is between one and two orders of magnitude. The increase in water permeability with increasing concentration of oxidized lipids is consistent with experimental results (25-28) and correlates with looser packing of lipids. In our simulations, 12-al and 13-tc lipids have a larger effect on water permeability compared to 9-al and 9-tc lipids. This result suggests a relationship between permeability and the bilayer structural features. Water permeability appears to be related to the position of the oxygen in the lipid tail more than to the length of the tail and the hydrogen bonding capability of the oxidized moiety. Therefore, water permeability correlates better with the area per lipid than with the bilayer thickness and hydrogen bonding capability.

Although our calculations are limited to the permeability of water through a lipid membrane, we expect similar trends to be valid for any polar solute (27). An increase in the permeability of all polar substances would lead to an imbalance for numerous substances in a cell and therefore to cell death.

Conclusions

In the present work we studied the effect of lipid peroxidation on the properties of 1palmitoyl-2-linoleoyl-*sn*-glycero-3-phosphatidylcholine (PLPC) lipid bilayers molecular dynamics simulations. We simulated PLPC lipid bilayers containing different concentrations of four oxidation products of linoleic acid, containing either a hydroperoxide or an aldehyde group, in two different positions in the lipid tails. The aldehyde lipids have different chain length compared to the hydroperoxide ones, and the hydroperoxide group is more hydrophilic than the aldehyde group. These simple chemical features of the individual lipid molecules lead to well-defined changes in the properties of the bilayers. While the structural properties of the lipid membrane are strongly affected by the presence of oxidized lipids, the dynamic properties are affected to a much lesser extent. All the oxidized tails show a significant conformational difference compared to non-oxidized tails: the oxidized moiety is generally close to the lipid head group region and forms hydrogen bonds mainly with water. This tendency is more pronounced for hydroperoxide lipids compared to aldehyde lipids, due to the higher hydrophilicity of the hydroperoxide group. Structural properties of the lipid bilayer are found to depend on the different chemical features of the oxidized lipids: nature and position of the functional group, length of the lipid tail. The area per lipid has a stronger dependence on the position of the oxidized moiety, while the bilayer thickness depends strongly also on the length of the tail. The changes in area per lipid and bilayer thickness are reflected by a decrease in the order parameter of the lipid tails, which is stronger in the case of aldehyde lipids. Despite the large changes in the structural properties of the lipid bilayer, lipid dynamics does not appear to be significantly affected by the presence of oxidized lipids. Water permeability through the bilayer is significantly increased in the presence of oxidized lipids, and water defects are observed frequently at high concentrations of oxidized lipids. Our results suggest that one mechanism of cell membrane damage is the increase in membrane permeability due to the presence of oxidized lipids.

Acknowledgement.

This research has been supported by the Natural Science and Engineering Research Council (NSERC). Jirasak Wong-ekkabut and I-Ming Tang are supported by the Royal Golden Jubilee Ph.D. Program (PHD/0240/2545). WT is supported by the National Center for Genetic Engineering and Biotechnology (BIOTEC) and Thailand Research Fund (TRF).

DPT is an Alberta Heritage Foundation for Medical Research (AHFMR) Senior Scholar and Canadian Institutes of Health Research New Investigator, LM is an AHFMR postdoctoral fellow. Calculations were performed in part on WestGrid facilities.

References

- 1. Markesbery, W.R. 1997. Oxidative stress hypothesis in Alzheimer's disease. *Free Radical Biol. Med.* 23(1):134-147.
- 2. Sohal, R.S., and R. Weindruch. 1996. Oxidative stress, caloric restriction, and aging. *Science* 273(5271):59-63.
- 3. Dexter, D.T., C.J. Carter, F.R. Wells, F. Javoyagid, Y. Agid, A. Lees, P. Jenner, and C.D. Marsden. 1989. Basal lipid-peroxidation in substantia nigra is increased in Parkinsons-disease. *J. Neurochem.* 52(2):381-389.
- 4. Mark, R.J., Z. Pang, J.W. Geddes, K. Uchida, and M.P. Mattson. 1997. Amyloid betapeptide impairs glucose transport in hippocampal and cortical neurons: involvement of membrane lipid peroxidation. *J. Neurosci.* 17(3):1046-1054.
- 5. Mark, R.J., M.A. Lovell, W.R. Markesbery, K. Uchida, and M.P. Mattson. 1997. A role for 4-hydroxynonenal, an aldehydic product of lipid peroxidation, in disruption of ion homeostasis and neuronal death induced by amyloid beta-peptide. *J. Neurochem.* 68(1):255-264.
- 6. Halliwell, B., and J.M. Gutteridge. 1990. Role of free radicals and catalytic metal ions in human disease: an overview. *Methods Enzymol*. 186:1-85.
- 7. Halliwell, B. 2000. The antioxidant paradox. Lancet 355(9210):1179-1180.
- 8. Butterfield, D.A., J. Drake, C. Pocernich, and A. Castegna. 2001. Evidence of oxidative damage in Alzheimer's disease brain: central role for amyloid beta-peptide. *Trends Mol. Med.* 7:548-554.
- 9. Everse, J., and P.W. Coates. 2005. Role of peroxidases in Parkinson disease: a hypothesis. *Free Radic. Biol. Med.* 38:1296-1310.
- 10. Zhang, X.Y., Y.L. Tan, L.Y. Cao, G.Y. Wu, O. Xu, Y. Shen, and D.F. Zhou. 2006. Antioxidant enzymes and lipid peroxidation in different forms of schizophrenia treated with typical and atypical antipsychotics. *Schizophr. Res.* 81:291-300.
- 11. Berliner, J.A., and J.W. Heinecke. 1996. The role of oxidized lipoproteins in atherogenesis. *Free Radical Biol. Med.* 20(5):707-727.
- 12. Diaz, M.N., B. Frei, J.A. Vita, and J.F. Keaney. 1997. Mechanisms of disease antioxidants and atherosclerotic heart disease. *New Engl. J. Med.* 337(6):408-416.
- 13. Wood, L.G., P.G. Gibson, and M.L. Garg. 2003. Biomarkers of lipid peroxidation, airway inflammation and asthma. *Eur. Respir. J.* 21:177-186.
- 14. Downey, J.M. 1990. Free radicals and their involvement during long-term myocardial ischemia and reperfusion. *Annu. Rev. Physiol.* 52:487-504.

- 15. McCord, J.M. 1985. Oxygen-derived free radicals in postischemic tissue injury. *New Engl. J. Med.* 312(3):159-163.
- 16. Brodnitz, M.H. 1968. Autoxidation of saturated fatty acids: A review. *J. Agric. Food Chem.* 16:994-999.
- 17. Binder, H., and K. Gawrisch. 2001. Effect of unsaturated lipid chains on dimensions, molecular order and hydration of membranes. *J. Phys. Chem. B* 105(49):12378-12390.
- Wratten, M.L., G. Vanginkel, A.A. Vantveld, A. Bekker, E.E. Vanfaassen, and A. Sevanian. 1992. Structural and dynamic effects of oxidatively modified phospholipids in unsaturated lipid-membranes. *Biochemistry* 31(44):10901-10907.
- 19. Baenziger, J.E., H.C. Jarrell, R.J. Hill, and I.C.P. Smith. 1991. Average structural and motional properties of a di-unsaturated acyl chain in a lipid bilayer effects of 2 cisunsaturated double bonds. *Biochemistry* 30(4):894-903.
- 20. Chamulitrat, W., and R.P. Mason. 1989. Lipid peroxyl radical intermediates in the peroxidation of poly-unsaturated fatty-acids by lipoxygenase direct electron-spin resonance investigations. *J. Biol. Chem.* 264(35):20968-20973.
- 21. Tamm, L.K., and J. Seelig. 1983. Lipid solvation of cytochrome-C oxidase deuterium, N-14, and P-31 nuclear magnetic resonance studies on the phosphocholine head group and on cis-unsaturated fatty acyl chains. *Biochemistry* 22(6):1474-1483.
- 22. Mason, R.P., M.F. Walter, and P.E. Mason. 1997. Effect of oxidative stress on membrane structure: small-angle X-ray diffraction analysis. *Free Radical Biol. Med.* 23(3):419-425.
- 23. Stark, G. 1991. The effect of ionizing radiation on lipid membranes. *Biochim. Biophys. Acta* 1071(2):103-122.
- 24. Porter, N.A., S.E. Caldwell, and K.A. Mills. 1995. Mechanisms of free radical oxidation of unsaturated lipids. *Lipids* 30(4):277-290.
- 25. Mandal, T.K., and S.N. Chatterjee. 1980. Ultraviolet- and sunlight-induced lipid peroxidation in liposomal membrane. *Radiat. Res.* 83(2):290-302.
- 26. Chatterjee, S.N., and S. Agarwal. 1988. Liposomes as membrane model for study of lipid peroxidation. *Free Radical Biol. Med.* 4:51-72.
- 27. Kunimoto, M., K. Inoue, and S. Nojima. 1981. Effect of ferrous ion and ascorbate-induced lipid peroxidation on liposomal membranes. *Biochim. Biophys. Acta Biomembranes* 646:169-178.
- 28. Nakazawa, T., S. Nagatsuka, and O. Yukawa. 1986. Effects of membrane stabilizing agents and radiation on liposomal membranes. *Drugs Exp. Clin. Res.* 12(9-10):831-835.

- 29. Leyko, W., D. Ertel, and G. Bartosz. 1991. Effect of hyperthermia and lipid peroxidation on the erythrocyte membrane structure. *Int. J. Radiat. Biol.* 59(5):1185-1193.
- 30. Bruch, R.C., and W.S. Thayer. 1983. Differential effect of lipid peroxidation on membrane fluidity as determined by electron spin resonance probes. *Biochim. Biophys. Acta* 733(2):216-222.
- 31. Dobretsov, G.E., T.A. Borschevskaya, P.V. A., and V.Y. A. 1977. The increase of phospholipid bilayer rigidity after lipid peroxidation. *FEBS Lett.* 84:125-128.
- 32. Sevanian, A., M.L. Wratten, L.L. McLeod, and E. Kim. 1988. Lipid peroxidation and phospholipase A2 activity in liposomes composed of unsaturated phospholipids: a structural basis for enzyme activation. *Biochim. Biophys. Acta Lipids and Lipid Metabolism* 961:316-327.
- 33. Richter, C. 1987. Biophysical consequences of lipid peroxidation in membranes. *Chem. Phys. Lipids* 44(2-4):175-189.
- 34. Cavatorta, P., L. Masotti, G. Sartor, M.B. Ferrari, E. Casali, S. Borello, G. Minotti, and T. Galeotti. 1985. in Cell Membranes and Cancer (Galeotti, T., et al., Eds.). Elsevier, New York.
- 35. Gut, J., S. Kawato, R.J. Cherry, K. Winterhalter, and C. Richter. 1985. Lipid peroxidation decreases the rotational mobility of cytochrome P-450 in rat liver microsomes. *Biochim. Biophys. Acta* 817:217-228.
- 36. Eichenberger, K., P. Bohni, K. Winterhalter, and C. Richter. 1982. Microsomal lipid peroxidation causes an increase in the order of the membrane lipid domain. *FEBS Lett.* 142:59-62.
- Galeotti, T., S. Borello, G. Palombini, L. Masotti, M.B. Ferrari, P. Cavatorta, A. Arcioni,
 C. Stremmena, and C. Zanonni. 1984. Lipid peroxidation and fluidity of plasma membranes from rat liver and Morris hepatoma 3924A. *FEBS Lett.* 169:169-173.
- 38. Grzelinska, E., G. Bartosz, K. Gwozdzinski, and W. Leyko. 1979. A spin-label study of the effect of gamma radiation on erythrocyte membrane. Influence of lipid peroxidation on membrane structure. *Int. J. Radiat. Biol.* 36(4):325-334.
- 39. Feller, S.E. 2000. Molecular dynamics simulations of lipid bilayers. *Curr. Op. Colloid In.* 5(3-4):217-223.
- 40. Tieleman, D.P., S.J. Marrink, and H.J.C. Berendsen. 1997. A computer perspective of membranes: molecular dynamics studies of lipid bilayer systems. *Biochim. Biophys. Acta Rev. Biomembranes* 1331(3):235-270.
- 41. Nagle, J.F., and S. Tristram-Nagle. 2000. Structure of lipid bilayers. *Biochim. Biophys. Acta* 1469(3):159-195.

- 42. Berger, O., O. Edholm, and F. Jahnig. 1997. Molecular dynamics simulations of a fluid bilayer of dipalmitoyl-phosphatidylcholine at full hydration, constant pressure, and constant temperature. *Biophys. J.* 72(5):2002-2013.
- 43. Lindahl, E., and O. Edholm. 2000. Mesoscopic undulations and thickness fluctuations in lipid bilayers from molecular dynamics simulations. *Biophys. J.* 79(1):426-433.
- 44. Mukhopadhyay, P., L. Monticelli, and D.P. Tieleman. 2004. Molecular dynamics simulation of a palmitoyl-oleoyl phosphatidylserine bilayer with Na+ counterions and NaCl. *Biophys. J.* 86(3):1601-1609.
- 45. Edholm, O., and A.M. Nyberg. 1992. Cholesterol in model membranes. A molecular dynamics simulation. *Biophys. J.* 63(4):1081-1089.
- 46. Faller, R., and S.J. Marrink. 2004. Simulation of domain formation in DLPC-DSPC mixed bilayers. *Langmuir* 20(18):7686-7693.
- 47. de Vries, A.H., A.E. Mark, and S.J. Marrink. 2004. The binary mixing behavior of phospholipids in a bilayer: A molecular dynamics study. *J. Phys. Chem. B* 108(7):2454-2463.
- 48. Tieleman, D.P., J.L. MacCallum, W.L. Ash, C. Kandt, Z. Xu, and L. Monticelli. 2006. Membrane protein simulations with a united-atom lipid and all-atom protein model: lipid-protein interactions, side chain transfer free energies and model proteins. *J. Phys.- Condens. Mat.* 18(28):S1221.
- 49. Feller, S.E., D.X. Yin, R.W. Pastor, and A.D. MacKerell. 1997. Molecular dynamics simulation of unsaturated lipid bilayers at low hydration: Parameterization and comparison with diffraction studies. *Biophys. J.* 73(5):2269-2279.
- 50. Hyvonen, M.T., and P.T. Kovanen. 2005. Molecular dynamics simulations of unsaturated lipid bilayers: effects of varying the numbers of double bonds. *Eur. Biophys. J.* 34(4):294-305.
- 51. Bachar, M., P. Brunelle, D.P. Tieleman, and A. Rauk. 2004. Molecular dynamics simulation of a polyunsaturated lipid bilayer susceptible to lipid peroxidation. *J. Phys. Chem. B* 108(22):7170-7179.
- 52. Niemela, P.S., M.T. Hyvonen, and I. Vattulainen. 2006. Influence of chain length and unsaturation on sphingomyelin bilayers. *Biophys. J.* 90(3):851-863.
- 53. Ollila, S., M.T. Hyvonen, and I. Vattulainen. 2007. Polyunsaturation in Lipid Membranes: Dynamic Properties and Lateral Pressure Profiles. *J. Phys. Chem. B.* 111(12):3139-3150.
- 54. Pratt, D.A., J.H. Mills, and N.A. Porter. 2003. Theoretical calculations of carbon-oxygen bond dissociation enthalpies of peroxyl radicals formed in the autoxidation of lipids. *J. Am. Chem. Soc.* 125(19):5801-5810.

- 55. Swart, M. 2002. Density functional theory applied to copper proteins. *In* Materials Science Centre and Laboratory for Chemical Physics. Rijksuniversiteit Groningen, Groningen. 240.
- 56. Schrodinger, I. 2000. Jaguar 4.1. Portland, Oregon.
- 57. Becke, A.D. 1993. Density-functional thermochemistry. 3. The role of exact exchange. *J. Chem. Phys.* 98:5648-5652.
- 58. Lee, C.T., W.T. Yang, and R.G. Parr. 1988. Development of the Colle-Salvetti correlation-energy formula into a functional of the electron-density. *Phys. Rev. B* 37(2):785-789.
- 59. Reed, A.E., R.B. Weinstock, and F. Weinhold. 1985. Natural population analysis. *J. Chem. Phys.* 83(2):735-746.
- 60. Singh, U.C., and P.A. Kollman. 1984. An approach to computing electrostatic charges for molecules. *J. Comput.. Chem.* 5(2):129-145.
- 61. Lindahl, E., B. Hess, and D. van der Spoel. 2001. GROMACS 3.0: a package for molecular simulation and trajectory analysis. *J. Mol. Model.* 7(8):306-317.
- 62. Darden, T., D. York, and L. Pedersen. 1993. Particle Mesh Ewald an N.Log(N) method for Ewald sums in large systems. *J. Chem. Phys.* 98(12):10089-10092.
- 63. Essmann, U., L. Perera, M.L. Berkowitz, T. Darden, H. Lee, and L.G. Pedersen. 1995. A smooth particle mesh ewald method. *J. Chem. Phys.* 103(19):8577-8593.
- 64. Hess, B., H. Bekker, H.J.C. Berendsen, and J.G.E.M. Fraaije. 1997. LINCS: A linear constraint solver for molecular simulations. *J. Comp. Chem.* 18(12):1463-1472.
- 65. Berendsen, H.J.C., Postma, J. P. M., van Gunsteren, W. F., Di Nola, A. and J. R. Haak. 1984. Molecular dynamics with coupling to an external bath. *J. Chem. Phys.* 81:3684-3690.
- 66. Humphrey, W., A. Dalke, and K. Schulten. 1996. VMD: visual molecular dynamics. *J. Mol. Graph.* 14(1):33-38, 27-38.
- 67. Marrink, S.J., and H.J.C. Berendsen. 1994. Simulation of water transport through a lipid membrane. *J. Phys. Chem.* 98:4155-4168.
- 68. Marrink, S.J., and H.J.C. Berendsen. 1996. Permeation process of small molecules across lipid membranes studied by molecular dynamics simulations. *J. Phys. Chem.* 100(41):16729-16738.
- 69. Kubo, R. 1966. The fluctuation-dissipation theorem. Rep. Prog. Phys. 29:255-284.
- 70. Kirkwood, J.G. 1946. The statistical mechanical theory of transport processes. I. general theory. *J. Chem. Phys.* 14(3):180-201.

- 71. van Kuijk, F.J.G.M., A. Sevanian, G. Handelman, and E.A. Dratz. 1988. A new role for phospholipase A2: protection of membranes from lipid peroxidation damage. *Trends Biochem. Sci.* 12:31-34.
- 72. Kupiainen, M., E. Falck, S. Ollila, P. Niemelä, A.A. Gurtovenko, M.T. Hyvönen, M. Patra, M. Karttunen, and I. Vattulainen. 2005. Free Volume properties of sphingomyelin, DMPC, DPPC, and PLPC bilayers. *J. Comput. Theor. Nanosci.* 2:1-13.
- 73. Lewis, B.A., and D.M. Engelman. 1983. Lipid bilayer thickness varies linearly with acyl chain length in fluid phosphatidylcholine vesicles. *J. Mol. Biol.* 166(2):211-217.
- 74. Pradhan, D., M. Weiser, K. Lumley-Sapanski, D. Fazier, S. Kemper, P. Williamson, and R.A. Schlegel. 1990. Peroxidation-induced perturbations of erythrocyte lipid organization. *Biochim. Biophys. Acta* 1023:398-404.
- 75. Sabatini, K., J.P. Mattila, F.M. Megli, and P.K.J. Kinnunen. 2006. Characterization of Two Oxidatively Modified Phospholipids in Mixed Monolayers with DPPC. *Biophys. J.* 90:4488-4499.
- Wohlert, J., and O. Edholm. 2006. Dynamics in atomistic simulations of phospholipid membranes: Nuclear magnetic resonance relaxation rates and lateral diffusion. *J. Chem. Phys.* 125:204703-204710.
- 77. Tabony, J., and B. Perly. 1990. Quasielastic neutron scattering measurements of fast local translational diffusion of lipid molecules in phospholipid bilayers. *Biochim. Biophys. Acta.* 1063:67-72.
- 78. Konig, S., W. Pfeiffer, T. Bayerl, D. Richter, and E. Sackmann. 1992. Molecular dynamics of lipid bilayers studied by incoherent quasi-elastic neutron scattering. *J. Phys. II Fr.* 2:1589-1615.
- 79. Almeida, P.F., W.L. Vaz, and T.E. Thompson. 1992. Lateral diffusion in the liquid phases of dimyristoylphosphatidylcholine/cholesterol lipid bilayers: a free volume analysis. *Biochemistry* 31(29):6739-6747.
- 80. Ianzini, F., L. Guidoni, P.L. Indovina, V. Viti, G. Erriu, S. Onnis, and P. Randaccio. 1984. Gamma-irradiation effects on phosphatidylcholine multilayer liposomes: calorimetric, NMR, and spectrofluorimetric studies. *Radiat. Res.* 98(1):154-166.
- 81. Bemporad, D., J.W. Essex, and C. Luttmann. 2004. Permeation of small molecules through a lipid bilayer: a computer simulation study. *J. Phys. Chem. B* 108(15):4875-4884.
- 82. Olbrich, K., W. Rawicz, D. Needham, and E. Evans. 2000. Water Permeability and Mechanical Strength of Polyunsaturated Lipid Bilayers. *Biophys. J.* 79:321-327.

Table 1. Partial atomic charges in the oxidized lipid tails.

functional group	СН	0	0	Н	reference molecule
hydroperoxide tails	0.30	-0.30	-0.45	0.45	3-hydroperoxy-1-butene
aldehyde tails	0.53	-0.53	-	-	propanal

Table 2. Force constant F_C for optimized bonds and angles and dihedral angles.

Bond	r ₀ (nm)	F _C [kJ/(mol*nm ²)]	reference molecule
C-O	0.14180	225670	3-hydroperoxy-1-butene
0-0	0.14430	269580	H ₂ O ₂ (55)
О-Н	0.09810	444130	H ₂ O ₂ (55)

Angle	α_0 (degree)	F _C [kJ/(mol*rad ²)]	reference molecule
=C-C-O	104.00	418.40	3-hydroperoxy-1-butene
C-C-O	109.50	418.40	3-hydroperoxy-1-butene
C-O-O	105.90	598.37	3-hydroperoxy-1-butene
O-O-H	100.00	506.92	H ₂ O ₂ (55)

Table 3. Force constants for dihedral angles. The functional form is the following: $a(1 + \cos(x - b)) + c(1 + \cos(2x - d)) + e(1 + \cos(3x - f))$

dihedral angles	a*	b [#]	c*	d [#]	e*	f [#]	reference molecule
C=C-C-O	2.12	223.90	0	0	3.62	180.50	3-hydroperoxy-1-butene
C-C-O-O	2.13	334.25	0	0	7.04	8.10	3-hydroperoxy-1-butene
C-O-O-H	8.46	23.30	6.51	18.40	0	0	3-hydroperoxy-1-butene
C-C-C=O	0.47	180.00	1.58	180.00	2.67	180.00	propanal

^{*} kJ/(mol*rad²)

[#] degrees

Table 4. Average of the number of hydrogen bonds per oxidized lipid molecule. Hydrogen bonds are between hydroperoxide or aldehyde groups and the lipid head group or water.

Lipid bilayer	% oxidized lipids	carbonyl group	phosphate group	water
PLPC with 13-tc	2.8%	0.34	0.41	0.77
	5.6%	0.36	0.44	0.85
	11.1%	0.14	0.62	1.04
	25.0%	0.30	0.45	0.94
	50.0%	0.20	0.38	0.89
PLPC with 9-tc	2.8%	0.35	0.41	1.06
	5.6%	0.50	0.20	0.93
	11.1%	0.21	0.50	1.15
	25.0%	0.22	0.53	1.04
	50.0%	0.26	0.51	0.96
PLPC with 12-al	2.8%	-	-	0.54
	5.6%	-	-	0.45
	11.1%	-	-	0.54
	25.0%	-	-	0.45
	50.0%	-	-	0.41
PLPC with 9-al	2.8%	-	-	0.45
	5.6%	-	-	0.45
	11.1%	-	-	0.52
	25.0%	-	-	0.54
	50.0%	-	-	0.46

Table 5. Water permeability through PLPC bilayers containing four different oxidized lipids (concentration of 11.1% and 50 %).

Lipid bilayer	% oxidized lipid	permeability of water (*10 ⁻³ cm/s)
PLPC	0	1.6 ± 0.5
PLPC with 9-tc	11.1%	3.3 ± 0.6
	50%	11.6 ± 4.5
PLPC with 13-tc	11.1%	2.1 ± 0.8
	50%	92 ± 40
PLPC with 9-al	11.1%	3.2 ± 1.9
	50%	16.1 ± 4.7
PLPC with 12-al	11.1%	4.0 ± 2.2
	50%	66 ± 32

Figure 1. Products of the oxidation of linoleic acid considered for this work.

13-hydroperoxy-trans-11, cis-9-octadecadienoic acid (13-tc)

9-hydroperoxy-trans-10, cis-12-octadecadienoic acid (9-tc)

12-oxo-cis-9-dodecenoic acid (12-al)

9-oxo-nonanoic acid (9-al)

Figure 2. Lipid fragments used for the calculation of bonded parameters and partial charges for the oxidized lipid tails.

3-hydroperoxy-1-butene

propanal

Figure 3. Snapshots of a single PLPC and 13-tc taken at 5 ns intervals. Lipids are colored by atom type: nitrogen is blue, carbon is cyan, oxygen is red, phosphorus is tan. Molecules are oriented along the z axis and superimposition was done on the phosphorus and oxygen atoms.

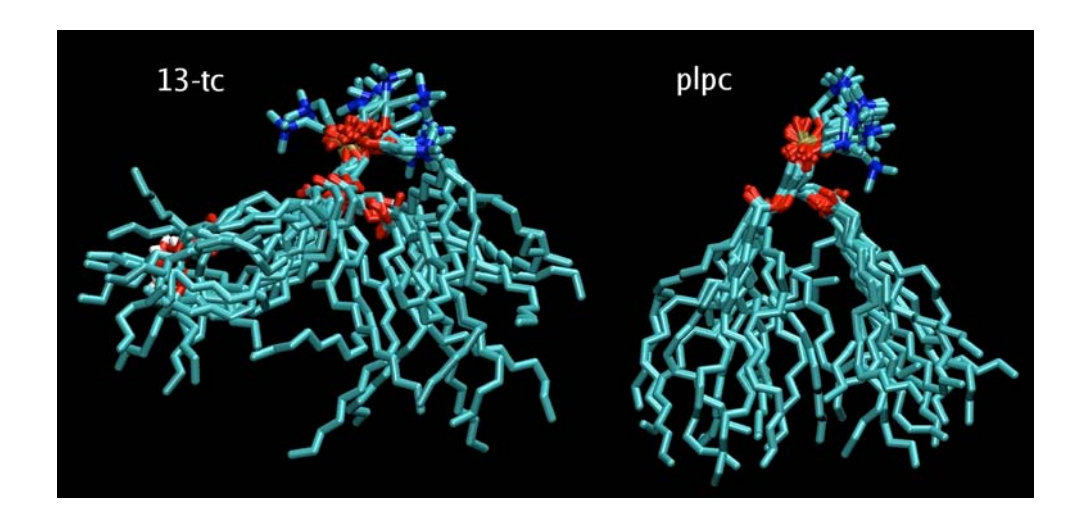


Figure 4. Electron density profiles for the oxygen atoms of the oxidized acyl chains in PLPC bilayers containing 11.1% of oxidized lipids. The maximum density of the phosphate group is 1.85 nm from the center in a pure PLPC bilayer.

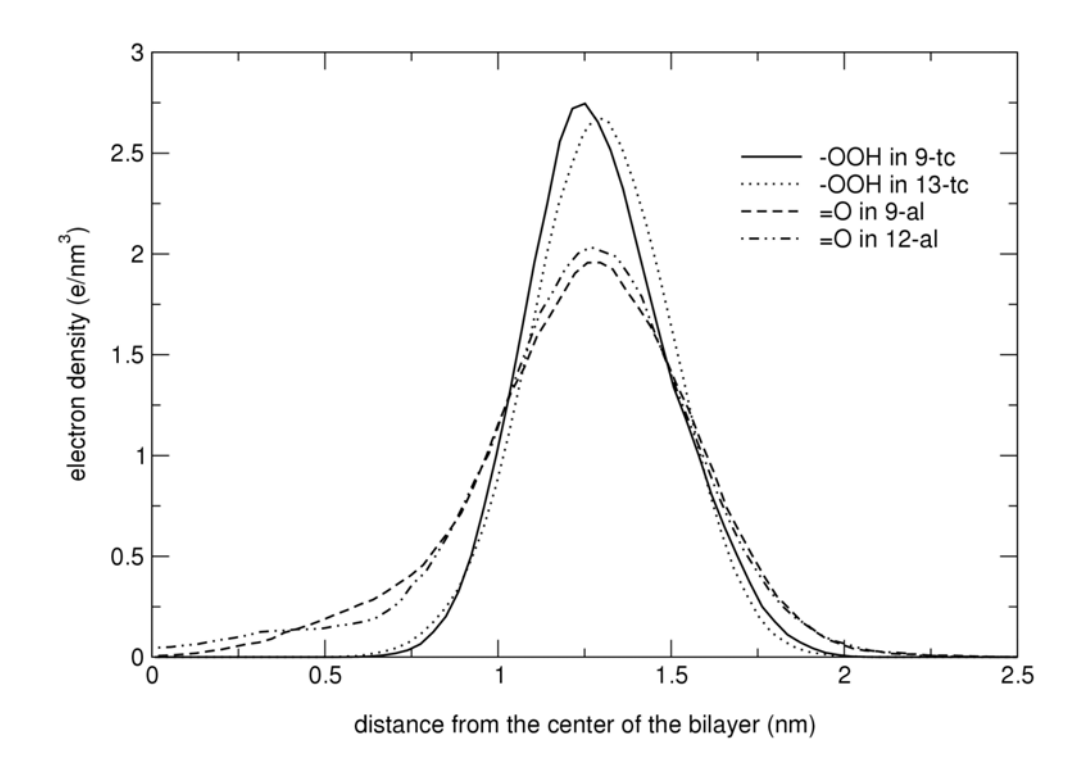


Figure 5. (A) Total electron density in simulations of PLPC bilayers including two oxidation products, 12-al and 9-tc, at 50% concentration. (B) Relative electron density in X-ray diffraction experiments on DLPC and peroxidized products (reproduced from reference (22)).

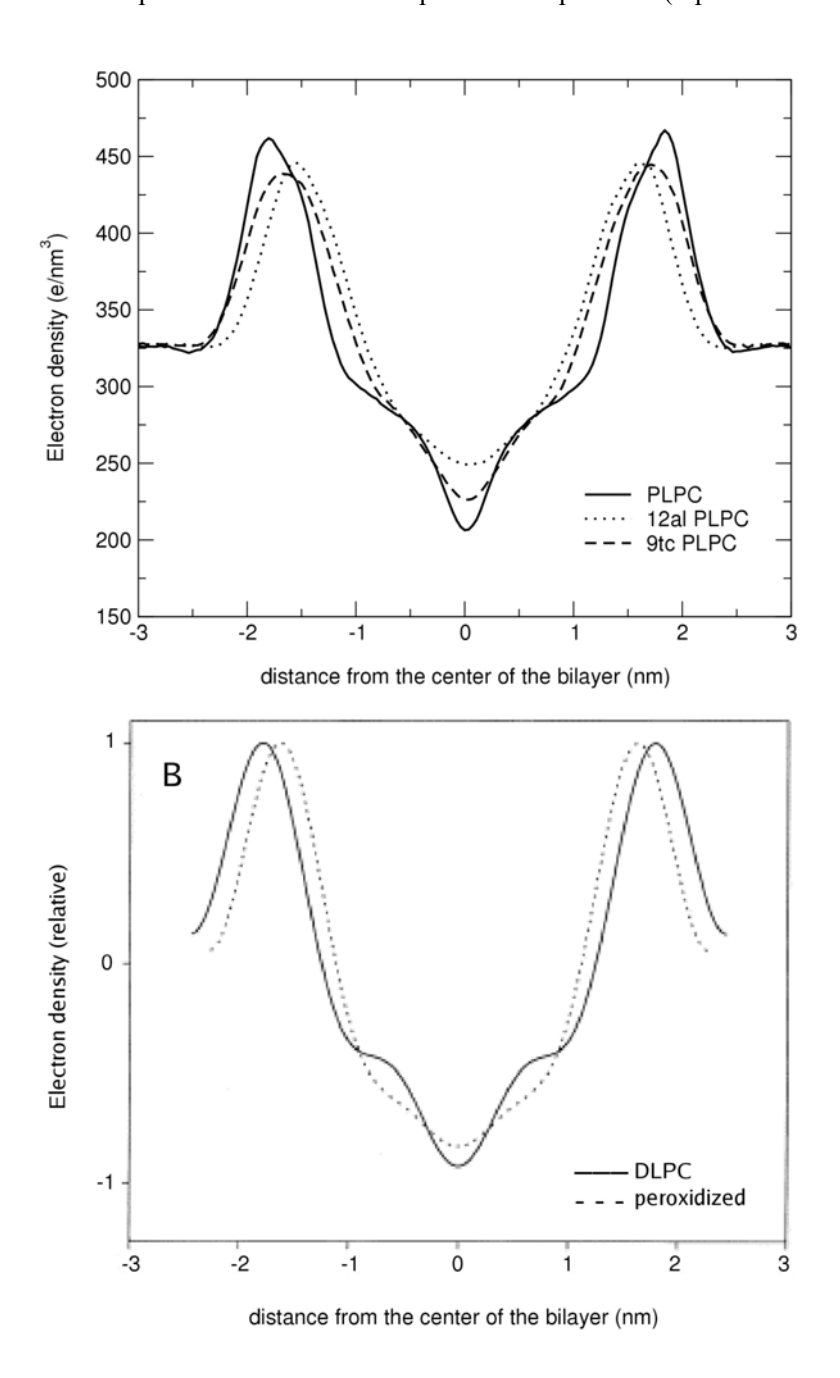


Figure 6. The thickness and area per lipid of lipid bilayer, containing various concentrations of each oxidized lipid.

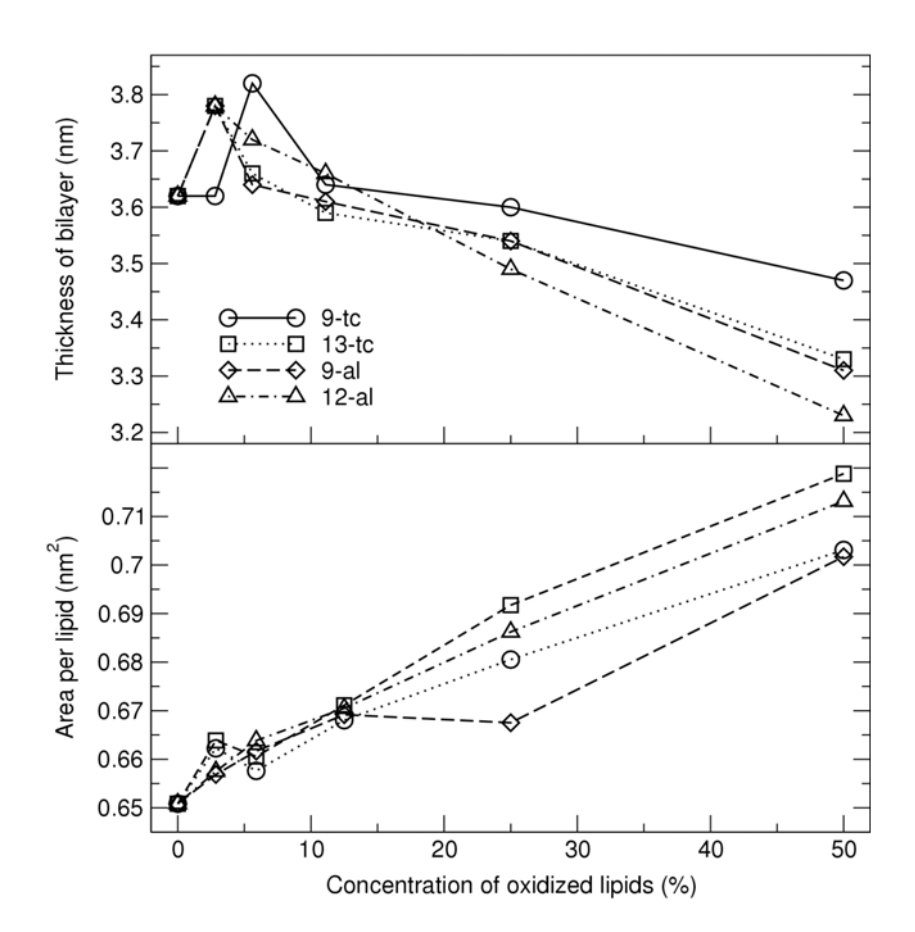


Figure 7. Deuterium order parameter in the *sn*-2 lipid chains of PLPC and each oxidized lipid, in the 11% mixtures.

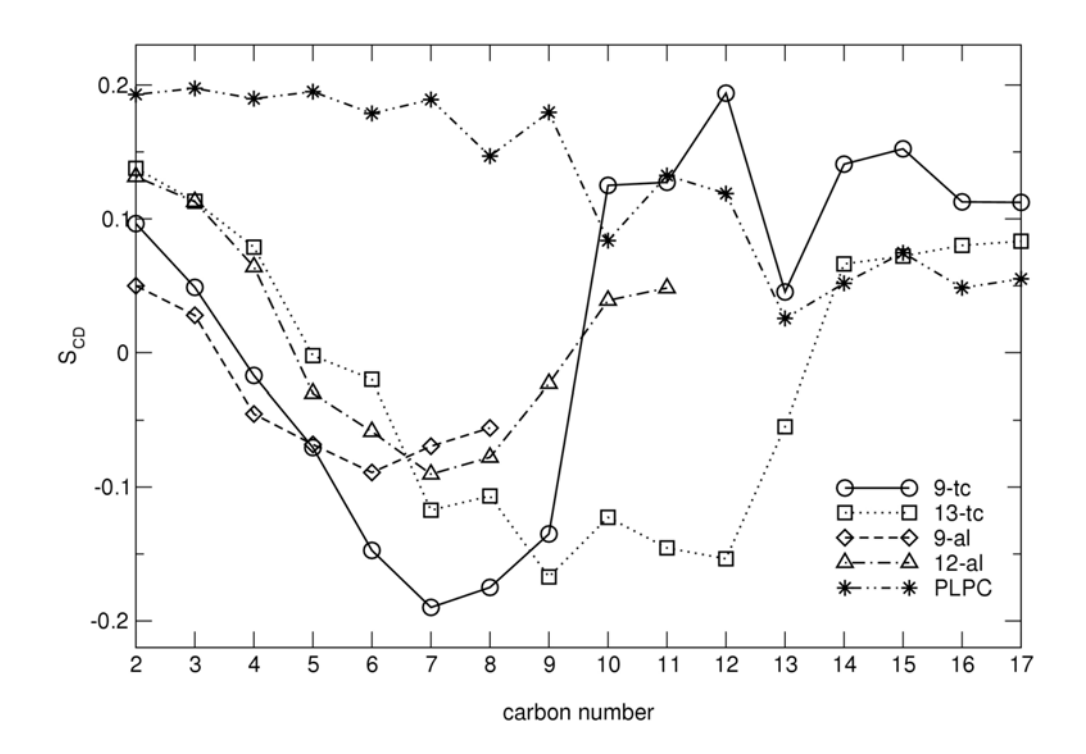


Figure 8. Short time (D_1) and long time (D_2) lateral diffusion coefficient for each oxidized lipid as a function of the concentration.

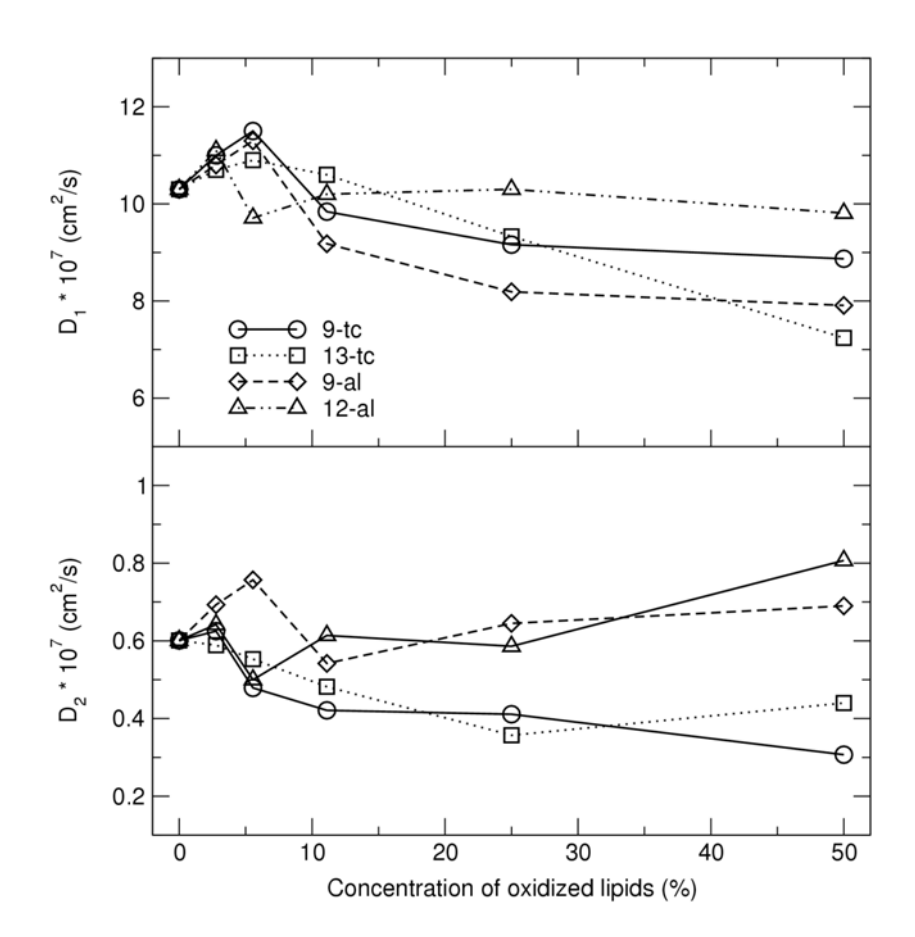


Figure 9. Snapshot showing a stable water defect in a PLPC bilayer containing 50% 13-tc lipids. PLPC is shown as sticks in grey, PLPC in cyan; all phosphate atoms are shown as tan spheres, oxygen atoms in the hydroperoxide group are shown as red spheres; water oxygen atoms are shown as blue spheres (with bigger size inside the bilayer).

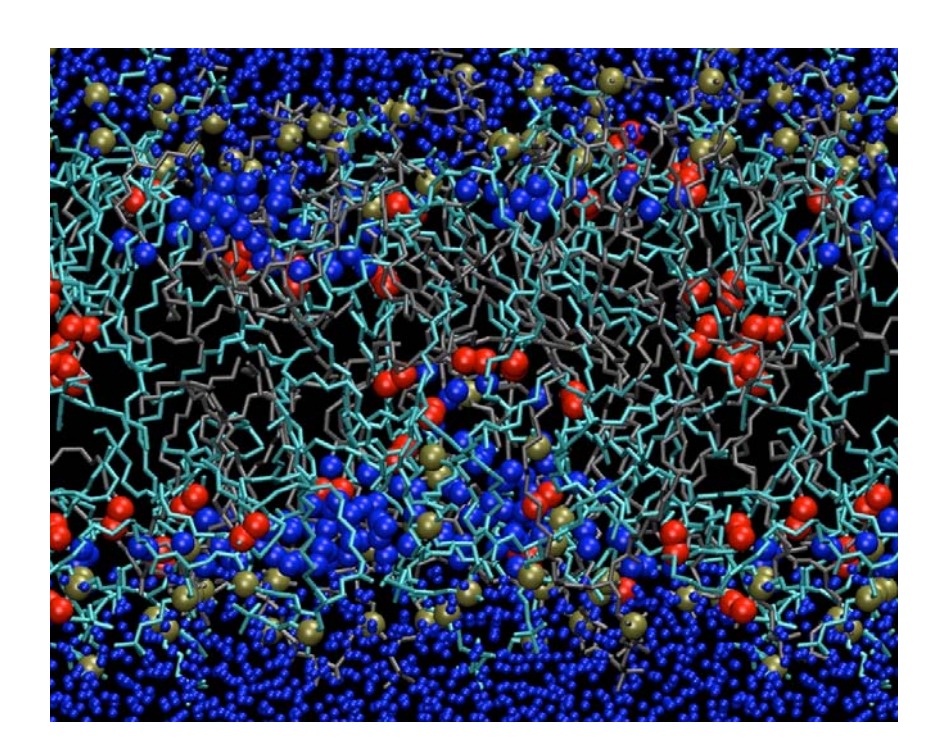
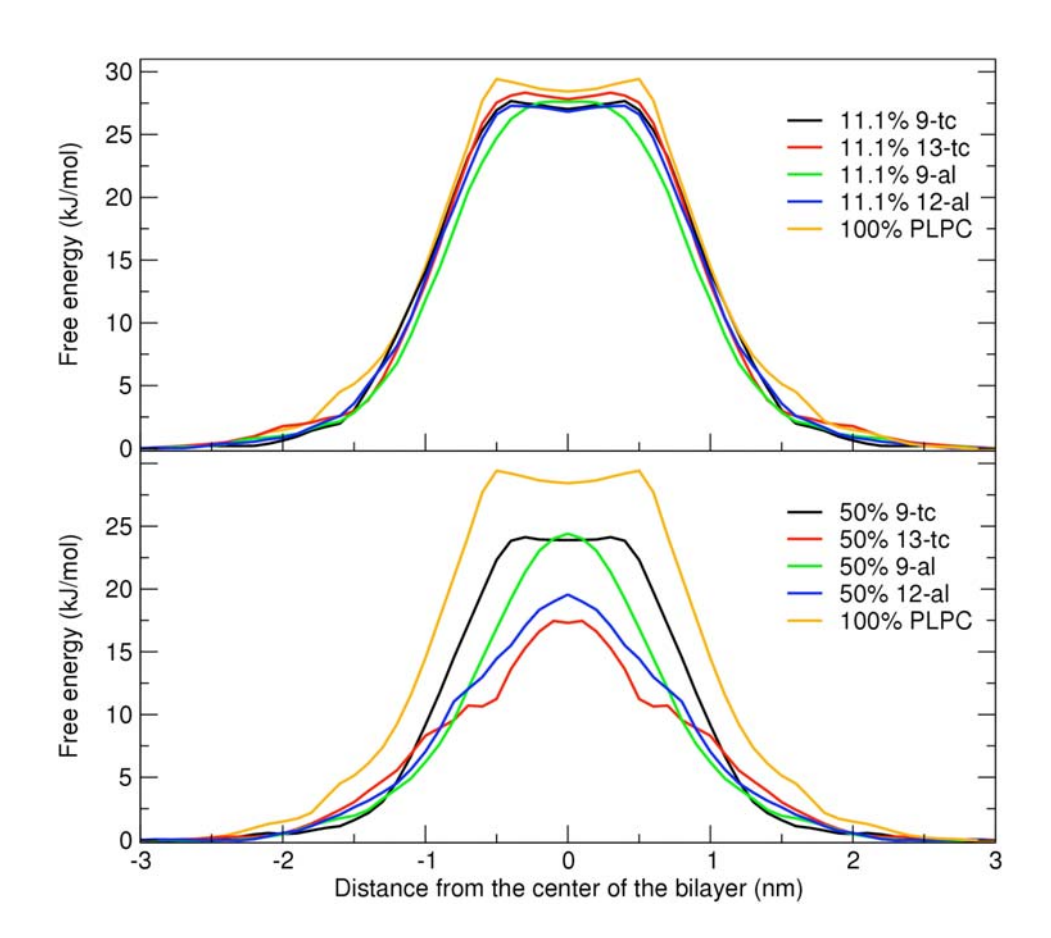


Figure 10. Potential of mean force for water as a function of the distance from the center of the bilayer, in a bilayer containing pure PLPC or 11.1% oxidized lipids or 50% oxidized lipids. Error bars are omitted for clarity.



Elsevier Editorial System(tm) for BioSystems

Manuscript Draft

Manuscript Number: BIO-D-07-00117

Title: Stochastic modeling of the effect of an external electric field on the Min protein Dynamics in E. coli

Article Type: Full Length Article

Keywords: Electric fields; E. coli; Cell division; Min proteins; MinCDE oscillation; stochastic process

Corresponding Author: Dr. Wannapong Triampo,

Corresponding Author's Institution:

First Author: Charin Modchang

Order of Authors: Charin Modchang; Wannapong Triampo; Paisan Kangthang; Udorn Junthorn; Somrit Unai; Waipot Ngamsaad; Narin Nuttawut

Abstract: Cell division in Escherichia coli and other rod-shaped bacteria depends on the precise placement of a division septum at the cell center. The MinCDE system consisting of three proteins: MinC, MinD, and MinE, controls accurate cell division at the center of the cell through pole-to-pole oscillation. With some simplifying assumptions and relying on our deterministic model, we present a one-dimensional stochastic model describing effects of an external electric field to the MinCDE system. Computer simulations were performed to investigate the response of the oscillatory dynamics to various strength of the electric field and the total number of Min proteins. Providing a strong enough electric field, it has been found, is capable of interfering with the MinCDE dynamics as a consequence of the possible change in the division process. Interestingly, it was found that the effects of an electric field do not depend on the total number of Min proteins. The noise involved has shifted the correct trend of Min proteins behavior. However, as a consequence of the robustness of the dynamics, the oscillatory pattern of the proteins still exists even though the number of Min proteins is relatively low. However, consideration of the correlations between the local and global minimum (maximum) of MinD (MinE) suggests that using high enough Min protein

concentration would reduce the local minimum (maximum) effect, which is related to the probability of polar division in each single oscillator cycle.

Though the studied model is simple and neglects some complex mechanisms concerning protein oscillation in correlation with cell division, it is demonstrated to be good enough for positioning the dividing site.

Therefore, with regards to this problem, more experimental and theoretical works are needed. Especially, more realistic model (of course more complicated model) development through deterministic and stochastic approaches is still very much in need. Lastly, it is to be mentioned that this study may be of significant importance in the development of new technological processes in the fields of agriculture, food and medicine.

Stochastic modeling of the effect of an external electric field on the Min protein Dynamics in *E. coli*

5 Charin MODCHANG, Wannapong TRIAMPO*, Paisan KANGTHANG, Udorn JUNTHORN, Somrit UNAI, Waipot NGAMSAAD, Narin NUTTAWUT

R&D Group of Biological and Environmental Physics (BIOPHYSICS),

Department of Physics, Faculty of Science, and Center of Excellence for Vector and Vector-Borne

Diseases, Mahidol University, Bangkok, Thailand

Yongwimon Lenbury

Department of Mathematics, Faculty of Science, Mahidol University, Bangkok, Thailand

15

10

PACS number: 87.15.Aa

Keywords: Electric fields, E. coli, Cell division, Min proteins, MinCDE oscillation, stochastic process

20

Corresponding author

scwtr@mahidol.ac.th or wtriampo@yahoo.com

25 R&D Group of Biological and Environmental Physics,

Department of Physics, Faculty of Science,

Mahidol University, Rama 6 Rd., Ratchatewee, Bangkok, 10400 Thailand

Phone: 662 441-9816 ext. 1131

Fax: 662 441-9322

Abstract

Cell division in Escherichia coli and other rod-shaped bacteria depends on the precise placement of a division septum at the cell center. The MinCDE system consisting of three proteins: MinC, MinD, and MinE, controls accurate cell division at the center of the cell through pole-to-pole oscillation. With some simplifying assumptions and relying on our deterministic model, we present a one-dimensional stochastic model describing effects of an external electric field to the MinCDE system. Computer simulations were performed to investigate the response of the oscillatory dynamics to various strength of the electric field and the total number of Min proteins. Providing a strong enough electric field, it has been found, is capable of interfering with the MinCDE dynamics as a consequence of the possible change in the division process. Interestingly, it was found that the effects of an electric field do not depend on the total number of Min proteins. The noise involved has shifted the correct trend of Min proteins behavior. However, as a consequence of the robustness of the dynamics, the oscillatory pattern of the proteins still exists even though the number of Min proteins is relatively low. However, consideration of the correlations between the local and global minimum (maximum) of MinD (MinE) suggests that using high enough Min protein concentration would reduce the local minimum (maximum) effect, which is related to the probability of polar division in each single oscillator cycle.

Though the studied model is simple and neglects some complex mechanisms concerning protein oscillation in correlation with cell division, it is demonstrated to be good enough for positioning the dividing site. Therefore, with regards to this problem, more experimental and theoretical works are needed. Especially, more realistic model (of course more complicated model) development through deterministic and stochastic approaches is still very much in need. Lastly, it is to be mentioned that this study may be of significant importance in the development of new technological processes in the fields of agriculture, food and medicine.

5

10

15

20

1. Introduction

Cell division in *Escherichia coli* and other rod-shaped bacteria depends on the precise placement of a division septum at the cell center in order to ensure the equipartition of cytoplasmic components into the two daughter cells. It has been known that the dynamics of Min proteins, MinCDE, consisting of three proteins: MinC, MinD, and MinE, play a key role in determining the site of septal placement in *E. coli* (de Boer *et al.*, 1989). Previous studies (Rothfield *et al.*,1999;Margolin,2001;Addinall *et al.*,2002) have shown that the earliest event in this process is the polymerization of the tubulin-like protein FtsZ at mid-cell into an annular structure called the Z-ring. In the absence of the Min system, Z-rings form at mid-cell as well as cell poles, resulting in the production of minicells (Akerlund et al.,1992). It has been shown that the three Min proteins must act in the certain way for cell dividing process to be achieved (de Boer et al.,1989).

MinC and MinD act in concert to form a nonspecific inhibitor of septation. MinC interacts with the division protein FtsZ to prevent formation of stable FtsZ ring marking the dividing site (Hu Z et al., 1999). In other words, MinC is an antagonist of FtsZ polymerization and a specific inhibitor of Z-ring formation (Hu et al.,1999; Hu and lutkanhaus,2000), while MinD plays a role is making MinC-mediated division inhibition sensitive to suppression by MinE (de Boer et al.,1992). Because MinC binds to MinD, the movement of MinC from pole to pole with relatively long polar dwell times and a short transit time blocks the formation of polar Z-rings but not medial rings (Meinhardt and de Boer, 2001; Margolin,2001). Therefore, the ATPase activity of MinD is presumed to provide the driving force for the pole-to-pole oscillation of the MinC division inhibitor.

The MinCD division inhibitor lacks site specificity, as evidenced by the observation that expression of MinC and MinD in the absence of MinE leads to a block in septation at all potential division sites, leading to formation of long nonseptate filaments. Filamentation is suppressed by MinE, which acts as a topological specificity factor to prevent the division inhibitor from acting at the midcell site while permitting it to block septation at polar division sites. Consistent with the ability of MinE to specifically counteract the division inhibitor at midcell, a MinE-green fluorescent protein (MinE-GFP) localizes to a ring-like structure at sites adjacent to the midcell, and this localization pattern requires the simultaneous expression of MinD (Raskin and de Boer, 1997). MinD is required to localize MinE at midcell (Raskin and de Boer, 1997). It was shown in a related study that MinD localizes to the cell pole in a MinE-dependent fashion and undergoes a rapid oscillation from pole to pole (Raskin and de Boer 1999).

The necessity for quantitative modeling and simulations is especially compelling when the process of interest displays spatiotemporal pattern formation, such as the oscillations of the Min proteins. Several studies have been made with different reaction-diffusion models to explain these oscillations (Meinhardt and de Boer, 2001; Howard *et al.*, 2001; Kruse, 2002; Howard and Rutenberg, 2003; Huang 2003, Modehang *et al.*, 2005). It has also recently emerged that MinD forms helical filaments in living cells (Shih, 2003); recent mathematical models (Drew *et al.*, 2005; Meacci and Kruse, 2005; Pavin *et al.*, 2005) have attempted to include this feature. The model by Drew et al. (Drew *et al.*, 2005) includes polymer growth from nucleation sites at the ends of the cell. Both of these models use continuous partial differential equations. The model by Pavin *et al.* (Pavin *et al.*, 2005) differs in that it is a three-dimensional stochastic model, but it does not exhibit the observed large scale helical filaments. Incorporating stochastic feature introduced into Min modeling is nevertheless likely to be important for systems of this type (Howard and Rutenberg, 2003, Tostevin and Howard, 2006, Fange and Elf, 2006, Pavin *et al.*, 2006, Kerr *et al.*, 2006).

Given the significance of the protein oscillation in correlation with the cell division, another interesting question may be asked: how the abnormal or unsuccessful cell division is affected by the abnormal protein oscillation? More specifically, under externally perturbation of stresses such as pH, heat, electric field, or magnetic field, how does each perturbation or combined perturbation affect protein oscillation in correlation with the cell division? Focusing on the effect of electric field is the central issue of this research work. Because the protein is typically charged, it thus could interact with the electric field (Simonson, 2003). For Min protein, MinCDE, they are membrane-bound and are diffusive in the cytoplasm and on the membrane. We believe that a high enough field could effect the dynamic movement of these proteins assuming that the cell survives. However, the motion mode and spatial distribution of these electric charged proteins may be greatly effected by this external electric field perturbation.

Motivated in part by this debate, in this study the effect of constant electric fields on MinCDE protein dynamics in *E. coli* has been examined. We present a simple one-dimensional stochastic model that may predict the experimental observations of the Min oscillations in the near future. The stochastic modeling approach is used in order to take into account the fluctuations or noises. With this approach, it will allow us to understand how the intrinsic chemical fluctuations in spatially extended systems can cause different properties than what would be described by a mean-field model or deterministic counterpart. The noise or fluctuation in non-homogeneous systems has, for instance, been shown to create new steady states (Togashi and Kaneko, 2004), drive spatial oscillations (Howard

and Rutenberg, 2003), cause spatial phase separation of a bistable system (Elf and Ehrenberg, 2004), or drive the irregular relocation dynamics of Soj protein in *Bacillus subtilis* (Doubrovinski and Howard, 2005). Random fluctuations in genetic networks are inevitable as chemical reactions are probabilistic and many genes, RNAs and proteins are present in low numbers per cell (Paulson, 2004).

In this paper, the relative concentrations of MinD and MinE are to be reported as functions of space and time. For each Min protein species considered, the characteristic model parameters, field strength J, and the number of Min proteins, are varied and comparatively interpreted. The highlighting aim of this study is to enhance the understanding of protein dynamic phenomena related to different intensity of electric treatments under various conditions. Here, we have tested the hypothesis that a direct current (dc) electric field may be one other extrinsic factor that can perturb cell division via protein oscillation. In addition, it has been reported that dc electric fields are able to induce directional responses such as cell migration (galvanotaxis/electrotaxis) and cell division in many cell types (Robinson, 1985; Song et al., 2002; Wang et al., 2000; Zhao et al., 1999). We attempt to find out whether small dc physiological electric field can change the protein dynamic oscillation in E. coli cell division by using a computational stochastic modeling as a tool.

The discoveries and conclusions of this study may be of significant importance in the development of new technological processes in the fields of agriculture and food science, particularly fermenting process controls and eliminating the undesirable pathogenic microorganisms. Electric and electromagnetic treatments are among the many food preparation processes and /or conservation techniques used in recent years [Pathak *et al.*, 2003, Espachs-Barroso *et al.*, 2003, Giner *et al.*, 2003, Martin *et al.*, 2003). The main objective of such treatments is to reduce or eliminate part of the often-undesirable microorganisms present.

Recently in cancer research, low-intensity, intermediate-frequency, alternating electric fields, delivered by means of insulated electrodes, have been found to have a profound inhibitory effect on the growth rate of a variety of human and rodent tumor cell lines. These findings demonstrate the potential applicability of the described electric fields as a novel therapeutic modality for malignant tumors (Kirson *et al.*, 2004, Hernandez-Bule *et al.*, 2007, Janigro *et al.*, 2006, Cucullo *et al.*, 2005).

2. Model rationale of protein oscillatory perturbation under an external electric field

It has been known that studies of the response of living systems to uniform physical fields (i.e., electric, gravitational, and magnetic) are capable of yielding novel insight into a variety of biological processes(Denegre *et al.*, 1998; Gerhart *et al.*, 1989; Helmstetter, 1997.; Henderson *et al.*, 1998.; Valles, 2002; Yokota *et al.*, 1992.; Zhao *et al.*, 1999). Particularly, the direct current electric fields are able to induce directional responses such as cell division in many cell types (Robinson, 1985; Song *et al.*, 2002; Zhao *et al.*, 1999). For example, Zhao *et al.* (1999) showed that the application of static electric fields to dividing human corneal epithelial cells causes the division planes to orient(Kirson *et .*, 2004).

Electrical phenomena govern many biological processes from molecular binding interactions to intercellular communication. Endogenous or exogenous perturbations of small extracellular electric fields have been observed to affect cellular processes, and several different mechanisms for these effects have been proposed (Weaver and Astumian, 1990). Diverse biological responses to electric fields continue to motivate experimental searches for mechanisms of electromagnetic interactions with cells. It has been shown that development (Jaffe, 1979), regeneration (Borgens *et al.*, 1981.; Borgens *et al.*, 1977; Jaffe and M-m., 1979.), and repair (Kenner *et al.*, 1975.) are all effected by electric fields and that many other basic cellular functions including motility (Cooper and Keller, 1984.; Cooper and Schliwa, 1985.; Luther *et al.*, 1983) and receptor regulation (Young and M-m, 1983.) are modulated by applied external electric fields. In addition, cell membrane permeabilization and fusion are effected by applied fields (Knight and F, 1982.; Tessie *et al.*, 1982.; Zimmermann and Vienken.J, 1982.). Local perturbation of plasma membrane potentials provides a hypothetical mechanism of interaction of applied electric fields with cells. Electric fields of high strength applied as short time pulses (microsecond) to aqueous suspensions of living cells have remarkable effects on the cell membranes or even kill the organisms.

Electric fields can be applied to cell suspensions by the use of capacitor discharges as a part of a high voltage circuit (Hilsheger and Niemann, 1980; Sale and Hamilton, 1967). Some investigators have observed that sinusoidal electric fields alter fundamental cellular functions (Goodman et al., 1983); such studies have led to concern about potential biological hazards from exposure to environmental sinusoidal fields. Most of the proposed coupling mechanisms are the subject of substantial debate. The possibility of applying low-intensity electricity has been studied because of its

effects on viable microbial interactions (Bawcom *et al.*, 1995; Rajnicek *et al.*, 1994). In order to study the effects of a high-voltage electric current application (intensity > 25 kW cm⁻¹) on microorganisms, experiments were carried out on different yeasts and bacterial species (Palaniappan *et al.*, 1990). In other experiments, the same authors (Palaniappan *et al.*, 1992) demonstrated that there was a notable reduction in the viability of bacterial cultures, indicating that this was due to chemical reactions induced by electric treatment. From the above mentioned reports, it can be seen that the behavior of a single cell or cell clusters in an external electric field may not be yet thoroughly understood. Moreover, to the best of our knowledge, no study has been performed to assess the effects of the electric field on the protein oscillatory dynamics of the cell, either theoretically or experimentally.

10

15

20

25

30

5

It is hypothesized that *E. coli*'s cell membrane may act as a "shield" or "absorber" to the cytoplasmic organelles including cytoplasmic and membrane bound Min proteins. It is possible that the field will eventually penetrate the membrane and interact with those interior components of the cell and consequently generate the electric force on charged objects including Min proteins. It is important to note that, if the field is too strong, the cell membrane may be damaged possibly resultint in cell death or abnormality (Bowcom, 1995; Zimmermann, 1974; Zimmermann, 1976; Zimmermann, 1982).

Another possibility is due to the generation of induced secondary field. High enough field strength could polarize or redistribute the somewhat mobile charges. With this induced polarization, it is possible to generate the secondary field inside the E. coli in the direction parallel but opposite to the direction of a primary applied field. This is based on the consideration that the cell membrane is a dielectric material as shown in Figure 1. It has been shown previously that these membrane dielectric properties are highly characteristic of, and rapidly affected by, alterations in physiological activities and induction of pathologic states in cells (Huang et al., 1992; Gascoyne et al., 1993; Gascoyne et al., 1994; Ginsa et al., 1991; Huang et al., 1996; Huang et al., 1999; Yang et al., 1999). Such differences can be not only used for cell characterization, but also exploited for selective cell manipulation, separation and sorting (Gascoyne., 1997; Pethig and Markx, 1997; Yang et al., 1999; Yang et al., 2000). This situation is, in fact, very complicated and highly dependent on the electrolytic conditions. It is known that even in the absence of an external electric field, particles exposed to an ion cloud become charged. Ions will collide with the particle due to their thermal motions. As the particle becomes charged, it will repel ions of the same sign and leads to a nonhomogenous distribution of ions in its neighborhood. This phenomena can be viewed as nonlinear feedback. However, here our first step model will assume that this effect is somewhat negligible as far as the protein oscillatory behavior is concerned.

3. Possible experiments using fluorescent microscopy together with single particle tracking (SPT) technique

In the past decade, two important technological innovations have contributed to reshaping molecular biology research. The first was the development of fluorescent proteins that allow researchers to selectively label single proteins. The second is high-resolution fluorescence imaging that is made possible by the new generation of bright-field and confocal microscopes (Pierce *et al.*, 1997; Endow, 2001; Kain and Kitts, 1997). Because of new tools, biologists are able to study molecular dynamics within the living cell at sub-micron resolutions. They can record time-lapse series to study molecular transport or conformal changes within the cell. While these methods offer an enormous potential for increasing our understanding of biology, they also constitute a challenge for researchers in the field who have not yet devised efficient ways to exploit and quantitatively interpret this unprecedented flow of data. Currently, the large majority of data analysis and feature extraction is done manually, which is very time consuming, so that image processing technique have been developing to solve this problem.

Adopting the above mentioned techniques, a number of previous studies of Min protein oscillations focuses on the spatial-temporal pattern formation and the biochemical basis function (Rothfield *et al.*, 2005; Shih *et al.*, 2002.). However, the experimental data of spatial-temporal pattern formation has been poorly interpreted for quantitative study. To cope with this drawback, here for the first time ever, we apply the Single Particle Tracking (SPT) technique (Saxton and Jacobson, 1997; Qian,1991) to explore the dynamics of GFP-MinD protein as the indicator of MinD dynamics. The analysis does not only concentrate on the ensemble positions of GFP:MinD, but also on the dynamics and localization via the ensemble positions. Data analysis is performed to provide the qualitative and quantitative interpretation is turn of the behavior of MinD oscillation. To the best of our knowledge, this SPT method has not yet been used for this specific protein problem. All previous quantitative results of the MinD dynamics were mostly obtained by either experimental approach via other techniques or modeling and simulations (Rothfield *et al.*, 2005; Shih *et al.*, 2002., Meinhardt and de Boer, 2001; Howard *et al.*, 2001; Kruse, 2002; Howard and Rutenberg, 2003; Huang 2003).

Here we will briefly describe how one may use SPT technique to experimentally investigate the focused problem, namely the effect of an electric field on the Min protein oscillation. However, since works are still on going, we here present the framework for the case in the absence of the field.

Briefly, SPT technique is the method or an image processing technique used to follow the spot – like particle in the fluorescence image under the intensity of fluorescence signal. The data from SPT measurement generally yield a key characteristic of a cell membrane or membrane-bound proteins. It is not only a probe of membrane microstructure but it also has major influence upon reaction kinetics within the cell membrane. Therefore, the SPT technique has been used in a large field of biophysical research to measure the trajectory of individual proteins or lipids in the cell membrane, such as plasma and nuclear membrane (Saxton and Jacobson, 1997), nuclear trafficking of Viral Genes (Babcock *et al.*, 2004), chromosome dynamics (Sage *et al.*, 2005), and bacterial actins motion (Kim *et al.*, 2006). To demonstrate the idea of how one can perform the experiment to support our theoretical predictions (at least in principle), here the materials and experimental procedure are briefly described as follow.

5

10

15

20

25

30

35

In the experiment, E. coli RC1/pFX9 [$\Delta min/P_{lac}$ -gfp:: $\Delta minD$ $\Delta minE$] was used. For examination of MinD labeled with green fluorescent proteins (GFP), a starter of RC1/pFx9 cells were grown in the optimal condition media until the OD_{600nm} is approximately 0.4 (log phase). The centrifugation was performed to collect the cells. Finally, the sample will be treated with isopropyl-β-Dthiogalactopyranoside (IPTG) for protein induction, diluted with a media before use. In our experiment, the 5-7 µl of each E. coli sample was dropped in a glass slide coated with Poly-L-lysine then covered with a coverslip at room temperature before examination. After that fluorescence microscopy were used with an InVivo software to obtain fluorescence image sequence. In this process, a charge-coupled device (CCD) camera was attached to the video port of microscope to acquire images and movies. After the images are obtained, the SPT technique is used to follow the region of interest (ROI) which consists of the highest GFP:MinD concentration signal. The collected data in SPT measurement are supported by SpotTracker Java plugin of public domain ImageJ software. Typically, the acquired images are in the configuration of fluorescence signal that could have faded after about 4-5 minutes have passed and subsequently the final image sequence is noisy. Hence, to improve the quality of the acquired images, we used the software's function called Gaussian filter to reduce the noise. The improved images are further enhanced by using the rescaling option of SpotTracker plugin. Lastly, the tracking of ROI with SpotTracker plugin was performed to collect the positions at given times in text file (Sage et al., 2005). The positions of ensemble were then analyzed by MATLAB software. In this work, the focus is on the dynamics and localization patterns of MinD protein in quantitative manner. The summary of the procedure is shown in the Figure 2.

From the data without the field exposure, the ensemble GFP:MinD oscillations from pole to pole with the approximately 45 seconds of period was shown in **Fig.3(B)**, the 2D image sequence of pole-to-pole MinD oscillations at each successive time for the rescaled and enhanced signal is shown.

Each fluorescence image represents the ensemble of GFP:MinD signal locating at polar zones. The time(s) labeled on the left side of the column is the first time at which GFP:MinD assembles after switching to the new pole. The sequence of positions (x,y) at successive times can be used to determine the trajectory of GFP-MinD in x and y components as shown in **Figure 3** (C) and (D), respectively.

To sum up, with the described technique the protein oscillatory dynamics can be studied. Though the case study of the protein oscillation under an electric field treatment has not been carried ort experimentally, with the modification and optimization, it is believed to be accomplished in the future. It is worth noting that things must be done with special care because of many possible problems including the noise, frame-shift, and optimal electric field strength. We believe that this particular research problem will open up very rich areas of future research and investigations in various aspects.

4. A Stochastic Model

Here, we present a simple one-dimensional stochastic model which predicts Min proteins oscillations in *E. coli*. Based on our deterministic model at the mean-field level (Modchang *et al.*, 2005.), the dynamics of these Min proteins in the presence of an external field, are described by

$$\frac{\partial \rho_D}{\partial t} = D_D \frac{\partial^2 \rho_D}{\partial x^2} + J_D \frac{\partial \rho_D}{\partial x} - \frac{\sigma_1 \rho_D}{1 + \sigma_1' \rho_e} + \sigma_2 \rho_e \rho_d , \qquad (1)$$

$$\frac{\partial \rho_d}{\partial t} = D_d \frac{\partial^2 \rho_d}{\partial x^2} + J_d \frac{\partial \rho_d}{\partial x} + \frac{\sigma_1 \rho_D}{1 + \sigma_1' \rho_e} - \sigma_2 \rho_e \rho_d, \tag{2}$$

25

30

5

10

15

20

$$\frac{\partial \rho_E}{\partial t} = D_E \frac{\partial^2 \rho_E}{\partial x^2} + J_E \frac{\partial \rho_E}{\partial x} - \sigma_3 \rho_D \rho_E + \frac{\sigma_4 \rho_e}{1 + \sigma_4' \rho_D}, \tag{3}$$

and

$$\frac{\partial \rho_e}{\partial t} = D_e \frac{\partial^2 \rho_e}{\partial x^2} + J_e \frac{\partial \rho_e}{\partial x} + \sigma_3 \rho_D \rho_E - \frac{\sigma_4 \rho_e}{1 + \sigma_4' \rho_D}$$
(4)

where ρ_D and ρ_E are the concentrations of the MinD and the MinE proteins in the cytoplasm, respectively, and ρ_d and ρ_e are the concentrations of the MinD and the MinE proteins on the cytoplasmic membrane, respectively. The first equation describes the time rate of change of the

concentration of MinD (ρ_D) in the cytoplasm. The second is for the change in the MinD concentration (ρ_d) on the cytoplasmic membrane. The third is for the change of the concentration of MinE (ρ_E) in the cytoplasm. The last one is for the change in the MinE concentration (ρ_e) on the cytoplasmic membrane. The constant σ_1 represents the spontaneous association of MinD to the membrane wall (Rowland *et al.*, 2000), whereas the constant σ_2 describes ejection of MinD from the cell membrane by membrane-bound MinE. Similarly, the constant σ_4 represents the spontaneous membrane dissociation of MinE, whereas the constant σ_3 describes the recruitment of cytoplasmic MinE to the membrane by cytoplasmic MinD (Huang *et al.*, 1996). The constant σ_1' corresponds to the membrane-bound MinE suppression of the binding of MinD to the membrane, and σ_4' corresponds to the cytoplasmic MinD suppression of the release of the membrane-bound MinE. Since the experimental results given in the work of Raskin and de Boer (1999) show that the MinC dynamics simply follows that of the MinD protein, so, for the sake of simplicity, consideration of the MinC dynamics is omitted. In this model, we adopted the dynamic model of compartmentization in the bacterial cell division process proposed by Howard and Rutenberg (2003) (as schematically summarized in **Figure 4**) by adding an extra term that depends on the external electric field.

To investigate how the intrinsic chemical fluctuations in spatially extended systems can give rise to properties radically different from what would be described by a mean-field model in the Min systems, we modify our deterministic model to a discrete particle model, where the Min protein molecule is represented as a particle and may hop between lattices. The number of protein molecules at site k is n_i^k , with $i = \{D, d, E, e\}$ representing cytoplasmic MinD, membrane-bounded MinD, cytoplasmic MinE, and membrane-bounded MinE, respectively. Here, the dynamics of Min system is a reaction-diffusion system consisting of two processes. The first one is the diffusion process that describes diffusion of the Min proteins. At the molecular level the diffusion process often results in a net flow of chemical species from regions of higher concentration to regions of lower concentration. The second one is the reaction process that describes self-organization of biological systems.

For the diffusion process, in the absence of external electric field, at each time step Δt , these particles have an equal probability $D_i \Delta t / (\Delta x)^2$ to hop to one of its neighboring sites with lattice space Δx and time step Δt . When the external electric field is present, the probabilities for a particle to hop to the left neighboring site or to the right neighboring site are no longer equal, but, in this case, they become

$$P_{L} = \frac{D_{i}\Delta t}{\left(\Delta x\right)^{2}} \left(0.5 + \frac{J_{i}\Delta t}{2\Delta x}\right); P_{R} = \frac{D_{i}\Delta t}{\left(\Delta x\right)^{2}} \left(0.5 - \frac{J_{i}\Delta t}{2\Delta x}\right),$$

where P_L , and P_R are probabilities for a particle to hop to the left and right neighboring sites, respectively. J_i is an external field parameter. We assume that a chemical substance moving in the region of an external field will experience a force that is proportional to the external field parameter J_i . In general, $J_i = \mu_i E$, $i = \{D, d, E, e\}$, where E is the field strength and μ is the ionic mobility of the chemical substance, which is proportional to the diffusion coefficient and depends on the total amount of free charges in that substance.

For the reaction processes, at site k the following reactions may occur

$$\begin{aligned} & \text{Probability:} \\ n_D^k \to n_D^k - 1, \quad n_d^k \to n_d^k + 1 & P_{D \to d} &= \sigma_1 \Delta t / \left(1 + \sigma_1' n_e^k \right), \\ n_D^k \to n_D^k + 1, \quad n_d^k \to n_d^k - 1 & P_{d \to D} &= \sigma_2 \Delta t \, n_e^k, \\ n_E^k \to n_E^k - 1, \quad n_e^k \to n_e^k + 1 & P_{E \to e} &= \sigma_3 \Delta t \, n_D^k, \\ n_E^k \to n_E^k + 1, \quad n_e^k \to n_e^k - 1 & P_{e \to E} &= \sigma_4 \Delta t / \left(1 + \sigma_4' n_D^k \right). \end{aligned}$$

The first (third) reaction indicates that each MinD (MinE) molecule at site k in the cytoplasm may bind to the cell membrane with equal probability $P_{D\to d}$ ($P_{E\to e}$) and the second (fourth) reaction indicates that each membrane-bound MinD (MinE) molecule at site k may be released to the cytoplasm with equal probability $P_{d\to D}$ ($P_{e\to E}$). These reactions are stochastic analogs of the reaction processes in our deterministic model (Modchang $et\ al.$, 2005.). Since the protein synthesis can be blocked without affecting the protein oscillation (Raskin and de Boer, 1999), we do not include the protein synthesis or degradation in our model. We also assume that the total amount of MinD and MinE is conserved.

5

5. Simulations, conditions, and parameters

In our simulation, we use lattice spaces $\Delta x = 0.02 \,\mu\text{m}$ and time steps $\Delta t = 2 \times 10^{-4} \,\text{s}$. The length of the *E. coli* is taken to be $2 \,\mu\text{m}$, there are 100 lattice sites covering the bacterium cell. We use $D_D = 0.28 \,\mu\text{m}^2\text{s}^{-1}$, $D_d = 0.003 \,\mu\text{m}^2\text{s}^{-1}$, $D_E = 0.6 \,\mu\text{m}^2\text{s}^{-1}$, $D_e = 0.006 \,\mu\text{m}^2\text{s}^{-1}$, $\sigma_1 = 20 \,\text{s}^{-1}$ and $\sigma_4 = 0.8 \,\text{s}^{-1}$ (Howard and Rutenberg, 2003; Howard *et al.*, 2001). To see how the effects of an external electric field on the oscillatory behaviors of Min proteins may change when the number of Min protein is changed, four representative parameter sets shown in Table 1 are used, where *N* is the total number of MinD which is equal to the total number of MinE. We use equal numbers of Min proteins because "wild type" oscillations are observed when both proteins are equally expressed on plasmids (Shih et al., 2002.).

To preserve the strength of the interaction between Min proteins when the total number of Min proteins is changed, the four parameters σ'_1 , σ_2 , σ_3 and σ'_4 are scaled as in Table 1. (Howard and Rutenberg, 2003).

Table 1. Scaled parameters used in the simulations

20

25

N	$\sigma_{\scriptscriptstyle 1}'$	$\sigma_2(s^{-1})$	$\sigma_3(s^{-1})$	$\sigma_{\scriptscriptstyle 4}'$
200	25.0	0.27	30.0	20.0
400	2.0	0.135	15.0	10.0
800	0.6	0.0675	7.5	5.0
1500	0.25	0.036	4.0	2.7

Since there are no experimental values of μ for either MinD and MinE, we assume that they have the same type of free charges and define a new parameter J such that

$$J_i = \mu_i E \equiv \frac{D_E J}{D_i} \,,$$

where $i = \{D, d, E, e\}$. Initially, we assume that MinD and MinE are mainly at the opposite ends of the cell. The hard wall boundary conditions are imposed at both ends of the bacterium.

6. Results and discussions

5

10

15

20

25

30

Figure 5 shows space-time plots of the total $(n_D^k + n_d^k)$ MinD (above) and total $(n_E^k + n_e^k)$ MinE (below) concentration for J = 0.0 m/s to J = 0.3 m/s and (a) N = 400, (b) N = 1500. Clearly, in the absence of the field J = 0.0 m/s, the MinD and MinE are in good agreement with experimental results. Namely, the MinE are more localized at midcell which then sweeps toward a cell pole, displacing the MinD to localize at the poles. Once the MinE cluster reaches the cell pole it disappears in the cytoplasm, only to reform at midcell where the process repeats, but in the other half of the cell. This process is repeated forever resulting in the Min proteins oscillations. When the external electric field is turned on $J \neq 0$, the oscillation patterns are no longer symmetric about the mid-cell. This is mainly because Min proteins themselves are charged macromolecules (MinD, molecular weight = 29,936.61D and charge: 4.5e; MinE, molecular weight = 10,416.08 D and charge: 0.5e. See www.eolproject.org:8080/). Hence, when protein molecules are in the electric field, they will be pushed in the direction of the fields (or opposite to the field direction, depending on its charges). In our simulation, we assume that MinD and MinE have the same type of charges which are consistent with the above data. As the external field parameter J increases from 0.0 m/s to 0.3 m/s, the period of the oscillation of both MinD and MinE increases from 100 s to 150 s. The periods measured from our systems are in good agreement with experiments, with periods from 30-120 s in the absence of the field. With respect to fluctuation driven instability, it is also found that in the case of a low N the stochastic fluctuated data could be very far off from the average behavior or those results obtained from the deterministic model. The noise involved has shifted the correct trend of Min proteins behavior. However, as a consequence of the robustness of the dynamics, the oscillatory pattern of the proteins still exists even though the number of min proteins is relatively low.

In **Figure 6**, the relative MinD and MinE concentrations as functions of x for J = 0.3 m/s with N = 400 and N = 1500 are shown. From their average lines, the minima of MinD and maxima of MinE are significantly shifted from the midcell (x = 1). It is also indicated by both **Figures 1 and 2** that, although both MinD and MinE are pushed in the same direction by the electric field, they tend to be more concentrated at the opposite ends when J is increased. A possible explanation is that this phenomenon arises because, in nature, MinD and MinE tend to repel each other, so that in the absence of an electric field, the location of the minimum of MinD is the location of the maximum of MinE. Moreover, although there is an electric force to push them in the same direction, this force cannot overcome the repelling forces between them. The fluctuations around the solid lines can be very large when N is small.

Figure 7 shows the relative concentration profiles of MinD (above) and MinE (below) as functions of position x along the bacterium length under the influence of an electric field with J = 0.3m/s, at various total numbers of Min proteins. It indicateds that the position of the global minimum of MinD and a position of the global maximum of MinE do not change as the total number of Min proteins is changed. This implies that only J controls these global extremum positions. Moreover, the values of the global minimum relative concentrations of MinD protein appears to be lowered as N increases, while the global maximum of MinE protein concentration is higher. These demonstrate the significance of using fewer protein copies that could result in not only the degradation of the accuracy of the extremum, but also the central features. Of course the correlation between these minimum and maximum is constrained by the conservative law of the total number of the both Min protein copies, but fluctuation sets bounds on the concentration levels. These effects can also be discussed in the context of nucleoid occlusion (Yu, 1999) as follows. In the absence of the field, MinCDE system normally tends to prevent polar FtsZ rings, because the nucleoids will inhibit FtsZ rings elsewhere away from midcell. Considering the correlations between the local and global minimum (maximum) of MinD (MinE), it suggests that using high enough Min protein concentration would reduce the local minimum (maximum) effect, which is related to the probability of polar division in each single oscillator cycle. This leads us to believe that too low a concentration of Min proteins can result in an unacceptable probability of polar division. This may suggest that E. coli may be using the optimal number of Min proteins, trading off midpoint precision against the cost of protein synthesis [Howard 2003 PRL]. This activity of E. coli is believed to be even more subtle when the situation is more complicated including the presence of the electric field. .

5

10

15

20

25

30

Figure 8 shows relative concentrations of MinD (above) and MinE (below) as functions of position x along the bacterium length under the influence of an electric field for N = 1500. It is seen that, in the case of no external field (J = 0.0 m/s), the relative concentrations of MinD and MinE are symmetric about the midcell. MinD has a minimum at the midcell, whereas MinE has a maximum, which is in good agreement with that which was reported in a previous studies [Howard 2003]. When the external electric field is turned on, a shift in the minimum of MinD and maximum of MinE were once again observed to be J dependent. Both the positions of MinD concentration minimum and MinE concentration maximum are more pronouncedly shifted toward the left pole as J increases. It is noted that the minimum of MinD and the maximum of MinE are always shifted to the left pole. This difference arises because of the relative magnitudes of the forces acting on the two proteins. First of

all, there is an internal force between the MinD and the MinE proteins. This force causes MinE to repel MinD. In the absence of any other forces, this explains why the location of the maximum of MinE is the location of the minimum of MinD. When an external field is applied (as expressed by a non-zero value of J), then one must take into account the relative magnitudes of the two forces. These results are consistent, at least qualitatively, with those obtained with a deterministic partial differential model proposed by Modchang *et al.*(2005).

In **Figure 9** (a) and (b), we show the concentrations of the MinD and the MinE proteins at the left end grid and the right end grid versus time. In these figures, it is easy to see that when J = 0.0 m/s, the concentrations of MinD (or MinE) at the left end grid and the right end grid have the same patterns of oscillation with the same frequencies and amplitudes, but with a phase difference of 180° . When an external field is applied, the amplitudes of the oscillations at the two end grids are no longer equal. As J is increased, the amplitude of the oscillation at the left end grid of MinD is seen to decrease while those of the MinE increase.

6. Concluding remarks

20

25

30

15

5

10

We have used a stochastic model to study the effects of an external electric field and noise on the *E. coli* MinCDE system. Proper divisions of bacteria require accurate definition of the division site. This accurate identification of the division site is determined by the rapid pole-to-pole oscillations of MinCDE. The stochastic approach is motivated by previous studies of how the intrinsic chemical fluctuations in spatially extended systems can give rise to properties that are radically different from what would be described by a mean-field model. The model itself has been modified from that of Howard and Rutenberg (2003) together with that of Modchang *et al.*(2005).

We found that a strong enough external electric field can shift the MinD concentration minimum and MinE concentration maximum position from the mid-cell. Shifting from the mid-cell appears to depend on the strength of the electric field. We have also found evidence that the effects of an electric field may not depend on the total number of Min proteins in *E. coli*. The results from the use of this stochastic model are, at least qualitatively, consistent with that obtained by using our deterministic model (Modchang *et al.*, 2005). With respect to the fluctuation driven instability, it was

also found that in the case of low N the stochastically fluctuated data could be very far off from the average behavior or those results from the use of a deterministic model. The noise involved has shifted the correct trend of Min proteins behavior. However, as a consequence of the robustness of the dynamics, the oscillatory pattern of the proteins still exists even though the number of Min proteins is relatively low. However, considering the correlations between the local and global minimum (maximum) of MinD (MinE), our result suggests that using high enough Min protein concentration would reduce the local minimum (maximum) effect, which is related to the probability of polar division in each single oscillator cycle. This leads us to believe that too low a concentration of Min proteins can result in an unacceptable probability of polar division.

Though the studied model is simple and neglects some complex mechanisms concerning protein oscillation in correlation with cell division, it was demonstrated to be good enough for positioning the dividing site. Therefore, with regards to this problem, more experimental and theoretical works are needed. More realistic model (which would of course be more complicated), either deterministic or stochastic, needs to be developed.

Lastly, it is to be mentioned that this study may be of significant importance in the development of new technological processes in the fields of agriculture, food and medicine. Moreover, with the correct link to other compartments like signal transduction or even at the level of system biology, we believe it will contribute greatly to the health and wellbeing of mankind of our communities.

Acknowledgements

This work was supported by the National Center for Genetic Engineering and Biotechnology (BIOTEC), the Thailand Research Fund (TRF), the Third World Academy of Sciences (TWAS), and Institute of Science and Technology Development (ISTD).

References

10

20

30

35

- 5 Addinall, S. G., Holland, B., 2002. The tubulin ancester, FtsZ, draughsman, designer and driving force for bacterial cytokinesis. J. Mol. Biol. 318: 219–236.
 - Åkerlund, T., Bernander, R., Nordstro°m, K.,1992. Cell division in Escherichia coli minB mutants. Mol. Microbiol. 6:2073–2083.
 - Babcock, HP., Chen, C., Zhuang, X., 2004. Using Single-Particle Tracking to Study Nuclear Trafficking of Viral Genes. J. Biophys. 87 2749-2758.
 - Bawcom, DW., Thompson, LD., Miller, MF., Ramsey, CB., 1995. Reduction of microorganisms of beef surfaces utilizing electricity. J. Food Protection 58:35-38.
 - Borgens, RB., Roederer, E., J. CM., 1981. Enhanced spinal cord regeneration in lamprey by applied electric fields. Science (Wash. DC). 213:611-617.
- Borgens, RB., Vanable, JW., Jr., F, JL., 1977. Bioelectricity and regeneration. I. Initiation of frog limb regeneration by minute currents. J. Exp. Zool. 200:403-416.
 - Cucullo, L., Dini, G., Hallene, K,L., et al., 2005. Very low intensity alternating current decreases cell proliferation. GLIA. 51(1): 65-72.
 - Cooper, MS., Keller, R.E., 1984. Perpendicular orientation and directional migration of amphibian neural crest cells in dc electrical fields. Proc. Nati. Acad. Sci. U.S.A. 81:160-164.
 - Cooper, MS., Schliwa, M., 1985. Electrical and ionic controls of tissue cell locomotion in dc electric fields. J. Neurosci. Res. 13:223-244.
 - Coster, H., Zimmermann, U., 1975. Dielectricbreakdownin the membrane of Valonia utricularis. Biochim. Biophys. Acta. 382:410-418.
- de Boer, P.A.D., Crossley, R.E., Rothfield, L.I., 1989. A division inhibitor and a topological specificity factor coded for by the mini-cell locus determine proper placement of the division septum in E. coli. Cell. 56:641–649.
 - de Boer, P. A. J., Crossley, R. E., Rothfield. L. I., 1990. Central role for the *Escherichia coli minC* gene product in two different cell division-inhibi-tionsystems. Proc. Natl. Acad. Sci. U.S.A. 87:1129–1133.
 - de Boer, P.A.J., Crossley, R.E., Hand A.R., Rothfield, L.I.. 1991. The MinD protein is a membrane ATPase required for the correct placement of the Escherichia coli division site. J. EMBO 10:4371-4380.
 - de Boer, P. A. J., Crossley, R. E., Rothfield. L. I., 1992. Roles of MinC and MinD in the site-specific septation block mediated by the MinCDE system of *Escherichia coli*. J. Bacteriol. 174:63–70.
 - Denegre, J.M., Valles, J.M., Jr., Lin, K., Jordan, W.B., Mowry, K.L.. 1998. Cleavage planes in Frog eggs altered by strong magnetic fields. Proc. Natl. Acad. Sci. U.S.A. 95:14729-14732.
 - Drew, D. A., Osborn, M. J., Rothfield, L. I., 2005. A polymerization—depolymerization model that accurately generates the self-sustained oscillatory system involved in bacterial division site placement. Proc. Natl. Acad. Sci U.S.A. 102:6114–8.
 - Doubrovinski, K., Howard, M., 2005. Stochastic model for Soj relocation dynamics in *Bacillus subtilis* Proc. Natl. Acad. Sci. U.S.A. 102:9808–13.
 - Elf, J., Ehrenberg, M., 2004. Spontaneous separation of bi-stable biochemical systems into spatial domains of opposite phases. Syst. Biol. 2: 230–236.
- Endow, S.A., 2001. Green fluorescent protein as a tag for molecular motor proteins. 1: Methods Mol Biol.164:123-31.
 - Espachs-Barroso, A., Barbosa-Canovas, G.V., Martin-Belloso, O., 2003. Microbial and Enzymatic Changes in Fruit Juice Induced by High-Intensity Pulsed Electric Fields. Food Reviews International. 19:253-273.
- Fange, D., Elf, J., 2006. Noise-induced Min phenotypes in E-coli. PLOS COMPUTATIONAL BIOLOGY. 2(6): 637-648

- Fu, X., Shih, Y.L., Zhang, Y., LI, R., 2001. The MinE ring required for proper placement of the division site is a mobile structure that changes its cellular location during the Escherichia coli division cycle. Proc Natl. Acad. Sci. U.S.A. 98:980-985.
- Gascoyne, P.R.C., Pethig, R., Burt, J.P.H., Becker, F.F.,1993. Membrane changes accompanying the induced differentiation of Friend erythroleukemia cells studied by dielectrophoresis. Biochim. Biophys. Acta. 1149:119–126.
- Gascoyne, P.R.C., Noshari, J., Becker, F.F., Pethig, R.,1994. Use of dielectrophoretic collection spectra for characterizing differences between normal and cancerous cells. IEEE Trans. Ind.Appl.30:829–834.

25

- Gascoyne, P.R.C.,. Wang, X.B., Huang, Y., Becker, F.F., 1997. Dielectrophoretic separation of cancer cells from blood.IEEE Trans. Ind. Appl. 33 (3):670–678.
 - Gerhart, J., Danilchik, M., Doniach, T., Roberts, S., Rowning, B., Stewart, R., 1989. Cortical rotation of the Xenopus egg: consequences for the anteroposterior pattern of embryonic dorsal development. Development. Supplement:37-51.
- Gimsa, J., Marszalek, P., Loewe, U., Tsong, T.Y., 1991. Dielectrophoresis and electrorotation of neurospora slime and murine myeloma cells. J. Biophys. 60(4):749–760.
 - Giner, J., Gimeno, V., Palomes, M., Barbosa-Canovas, G.V., Martin, O., 2003. Lessening Polygalaturonase Activity in a Commercial Enzyme Preparation by Exposure to Pulsed Electric Fields. European Food Research Technology. 217:43-48.
- Goodman, R., Bassett, CAL., Henderson, AS., 1983. Pulsing Eelectromagnetic fields induce cellular transcription. . Science (Wash.DC). 220:1283-1285.
 - Hale, C.A., Meinhardt, H., P.A., d.B., 2001. Dynamic localization cycle of the cell division regulator MinE in Escherichia coli. J. EMBO 20:1563–1572.
 - Helmstetter, C.E., 1997. Gravity and the orientation of cell division. Proc. Nat. Acad. Sci. U.S.A. 94:10195-10198.
 - Henderson, D.C., Bisgrove, S.R., Hable, W.E., Alessa, L., Kropf, D.L., 1998. Division patterns in the thallus of Pelvetia compressa embryos and the effects of gravity. Protoplasma. 203:112-117.
 - Hernandez-Bule M.L., Trillo, M.A., Cid, M.A., *et al.*, 2007. In vitro exposure to 0.57-MHz electric currents exerts cytostatic effects in HepG2 human hepatocarcinoma cells. International Journal of Oncology. 30 (3): 583-592.
 - Hilsheger, H., Niemann, EG., 1980. Lethal effects of high-voltage pulses on E. coli K12. Radiat Environ Biophys 18:281-288.
 - Howard, M., Rutenberg, A.D., 2003. Pattern Formation inside Bacteria: Fluctuations due to the Low Copy Number of Proteins. Physical Review Letters, 90(12):128102.
- Howard, M., Rutenberg, A.D., de Vet, S., 2001. Dynamic Compartmentalization of Bacteria: Accurate Division in E. Coli. Physical Review Letters. 87(27):278102.
 - Hu Z, J. L., 1999. Topological regulation of cell division in Escherichia coli involves rapid pole to pole oscillation of the division inhibitor MinC under the control of MinD and MinE. Mol Microbiol 34: 82-90.
- Hu, Z., Mukherjee, A., Pichoff, S., Lutkenhaus, J., 1999. The MinC component of the division site selection system in Escherichia coli interacts with FtsZ to prevent polymerization. Proc. Natl. Acad. Sci. U.S.A. 96:14819-14824.
 - Hu, Z., Gogol, EP., Lutkenhaus, J., 2002. Dynamic assembly of MinD on phospholipid vesicles regulated by ATP and MinE. Proc. Natl Acad. Sci. U.S.A 99:6761-6766.
- Hu, Z., Lutkenhaus, J. 2000. Analysis of MinC reveals two independent domains involved in interaction with MinD and FtsZ. J. Bacteriol. 182: 3965–3971
 - Hu, Z., Lutkenhaus, J., 2001. Topological regulation of cell division in E. coli: spatiotemporal oscillation of MinD requires stimulation of its ATPase by MinE and phospholipid. Mol. Cell. 7:1337-1343.
- Huang, J., Cao, C., Lutkenhaus, J., 1996. Interaction between FtsZ and inhibitors of cell division. J. Bacteriol, 178(17):5080-5.

- Huang, Y., Ho'lzel, R., Pethig, R., Wang, X.B., 1992. Differences in the AC electrodynamics of viable and non-viable yeast cells determined through combined dielectrophores and electrorotation studies. Phys. Med. Biol. 37:1499–1517.
- Huang, Y., Wang, X.B., Becker, F.F., Gascoyne, P.R.C., Biochim. 1996. Biophys. Membrane changes associated with the temperaturesensitive P85gag-mos-dependent transformation of rat kidney cells as determined by dielectrophoresis and electrorotation. Acta. 1282: 76–84.

15

20

30

- Huang, Y., Wang, X.B., Gascoyne, P.R.C., Becker, F.F.,1999. Membrane dielectric responses of human T-lymphocytes following mitogenic stimulation. Biochim. Biophys. Acta. 1417 (1):51–62
- Huang, K., Meir, Y. C., Wingreen, N. S., 2003. Dynamic structures in *Escherichia coli*: spontaneous formation of MinE rings and MinD polar zones. Proc. Natl. Acad. Sci. U.S.A. 100:12724–8
 - Jaffe, L.F., 1979. Control of development by ionic currents. In Membrane Transduction Mechanisms. Raven, New York.:199-231.
 - Jaffe, L.F., M-m, P., 1979. Neurites grow faster towards the cathode than the anode in a steady field. J. Exp. Zool. 209:115-128.
 - Jaffe, L.F., Stern, C.D., 1979. Strong electrical currents leave the primitive streak of chick embryos. Science. 206:569-571.
 - Janigro, D., Perju, C., Fazio, V., et al., 2006. Alternating current electrical stimulation enhanced chemotherapy: a novel strategy to bypass multidrug resistance in tumor cells. BMC CANCER. 6: 72.
 - Kain, S.R., Kitts, P., 1997. Expression and detection of green fluorescent protein (GFP). 1: Methods Mol. Biol. 63:305-24.
 - Kenner, G.H., Gabrielson, E.W, Lovell, J.E., Marshall, H.E., S. W.W., 1975. Electrical modification of disuse osteoporosis. . Calcif. Tissue Res. 18:111-117.
- Kerr, R.A., Levine, H., Sejnowski, T.J., et al., 2006. Division accuracy in a stochastic model of Min oscillations in Escherichia coli. Proceedings of the National Academy of Sciences of the United States of America. 103 (2):347-352.
 - Kim, S.Y., Gitai, Z., Kinkhabwala, A., Shapiro, L., Moerner, W.E., 2006. Single molecules of the bacterial actin MreB undergo directed treadmilling motion in Caulobacter crescetus. Proc. Natl. Acad. Sci. U.S.A. 103:10929-10934.
 - Kinosita, K., Tsong, TY., 1979. Voltage-induced conductance in human erythrocyte membranes. Biochim. Biophys. Acta. 554:479-497.
 - Kirson, E.D., Gurvich, Z., Schneiderman, R., Dekel, E., Itzhaki, A., Wasserman, Y., Schatzberger, R., Palti, Y., 2004. Disruption of cancer cell replication by alternating electric fields. Cancer Rrsearch. 64(9):3288-3295.
 - Knight, D, F., Baker, BP., 1982. The chromaffin granule proton pump and calcium-dependent exocytosis in bovine adrenal medullary cells. J. Membr. Biol. 68:107-140.
 - Kruse, K., 2002. A dynamic model for determining the middle of *Escherichia coli*. J. Biophys. 82: 618–27
- 40 Labie, C., Bouche', F., Bouche'. J.-P.,1990. Minicell-forming mutants of *Escherichia coli*: suppression of both DicB- and MinD-dependent division inhibition by inactivation of the *minC* gene product. J. Bacteriol. 172:5852–5855.
 - Luther, P.W., Peng, H.B., J-C, LJ., 1983. Changes in cell shape and actin distribution induced by constant electric fields. Nature (Lond.) 303:61-64.
- Margolin, W., 2001. Bacterial cell division: a moving MinE sweeper boggles the MinD. Curr. Biol. 11, R.395–R398.
 - Margolin, W., 2001. Spatial regulation of cytokinesis in bacteria. Curr. Opin. Microbiol. 4: 647–652.
 - Meacci, G., Kruse, K., 2005. Min-oscillations in *Escherichia coli* induced by interactions of membrane-bound proteins. Phys. Biol. 2:89–97.
- Meinhardt, H., de Boer, P. A., 2001. Pattern formation in Escherichia coli:a model for the pole-to-pole oscillations of Min proteins and the localization of the division site. Proc. Natl. Acad. Sci. U. S. A. 98:14202–14207.

- Modchang, C., Kanthang, P., Triampo, W., Ngamsaad, W., Nuttawut, N., I.M., T., 2005. Modeling of the Dynamics Pole-to-pole Oscillations of the Min Proteins in Bacterial Cell Division: the Effect of an External Field. J. Korean Phys. Soc. 46(4):1031-1036.
- Ngamsaad, W., Triampo, W., Kanthang, P. Modchang, C., Nuttavut, N., Tang, I.M., Lenbury, Y., 2005. A lattice Boltzmann method for modeling the dynamic pole-to-pole oscillations of Min proteins for determining the position of the midcell division plane, J. Korean Phys. Soc., 46 (4): 1025-1030.
- Palaniappan, S., Sastry, S.K., Richter, E.R., 1990. Effects of electricity on microorganisms. A review. J. Food Processing and Preservation. 14:393-414.
- Palaniappan, S., Sastry, S.K., Richter, E.R., 1992. Effects of electroconductive heat treatment and electrical pretreatment on thermal death kinetics of selected microorganisms. Biotechnology and Bioengineering. 39:225-232.
 - Pathak, S., Fen, L., Tang, J., 2003. Finite Difference Time Domain Simulation of Single-Mode 915 MHz Cavities in Processing Pre-Packaged Foods. J. Microwave Power and Electromagnetic Energy. 38:37-48.
 - Paulson, J., 2004. Summing up the noise in gene networks. Nature. 427(6973): 415-418.

15

35

- Pavin, N., Paljetak, H.C., Krsti'c, V., 2005. Min oscillation in *Escherichia coli* with spontaneous formation of two stranded filaments in 3D stochastic reaction-diffusion model .Preprint q-bio.SC/0505051.
- 20 Pavin, N., Paljetak, H.C., Krstic V,. 2006. Min-protein oscillations in Escherichia coli with spontaneous formation of two-stranded filaments in a three-dimensional stochastic reactiondiffusion model. PHYSICAL REVIEW E. 73 (2): 021904
 - Pethig, R., Markx, G.H., 1997. Applications of dielectrophoresis in biotechnology. Trends Biotechnol. 15 (10): 426–432.
- Pierce, D.W., Hom-Booher, N., Vale, R.D., 1997. Imaging individual green fluorescent proteins. Nature. Jul. 24:388(6640):338.
 - Qian, H., Sheetz, M.P., Elson, E.l., 1991. Single particle tracking. Analysis of diffusion and flow in two-dimensional systems. J. Biophy. 60:910-21
- Rajnicek, A.M., McCaig, C.D., Gow, N.A.R., 1994. Electric fields induce curved growth of Ent. cloacae, E. coli and B. subtilis cells: implications for mechanisms of galvanotropism and bacterial growth. J. Bacteriology. 176:702-713.
 - Raskin, D., de Boer. P., 1997. The MinE ring: an FtsZ-independent cell structure required for selection of the correct division site in *E. coli*. Cell. 91:685–694.
 - Raskin, D., de Boer. P., 1999. Rapid pole-to-pole oscillation of a protein required for directing division to the middle of *Escherichia coli*. Proc. Natl. Acad. Sci. U.S.A. 96:4971–4976.
 - Raskin, D., de Boer, P.A.J., 1999a. Rapid pole-to-pole oscillation of a protein required for directing division to the middle of Escherichia coli. Proc. Natl Acad. Sci. U.S.A. 96:4971-4976.
 - Raskin, DM., de Boer, PA., 1999b. MinDE-dependent pole-to-pole oscillation of division inhibitor MinC in Escherichia coli. J. Bacteriol. 181(20):6419-24.
- 40 Robinson, KR., 1985. The responses of cells to electrical fields: a review. J. Cell Biol. 101:2023-2027. Rothfield, L., Justice, S., Garcia-Lara, J., 1999. Bacterial Cell Division. Annu. Rev. Genet. 33: 423–
 - 448
 Rothfield, L., Taghbalout, A., Shih, Y-L., 2005. Spatial control of bacterial division-site placement.
 Nat. Rev. Microbiol. 31:959-968.
- Rowland, S.L., Fu, X., Sayed, M.A., Zhang, Y., Cook, W.R., Rothfield, L.I., 2000. Membrane redistribution of the Escherichia coli MinD protein induced by MinE. J. Bacteriol. 182(3):613-9
 - Sage, D., Neumann, FR., Hediger, F., Gasser, SM., Unser, M., 2005. Automatic tracking of individual fluorescence particles: application to the study of chromosome dynamics. IEEE Trans Image Process. 14:1372-83.
 - Sakurauchi, Y., Kondo, E., 1980. Lethal effects of high electric fields on microorganisms. J. Agricult Chem. Soc. Jpn. 54:837-844.

- Sale, A., Hamilton, W.A., 1967. Effects of high electric fields on microorganisms I. and II. Biochim. Biophys. Acta. 148:781-800.
- Sale, A.J.H., Hamilton, W.A., 1968. Effects of high electric fields on microorganisms III. Biochim Biophys. Act. 163:37-43.
- 5 San Martin, M.F., Barbosa-Canovas, G.V., Swanson, B.G., 2003. Innovations in Food Processing. Chemical Engineering Progress. 99:54-60.
 - Sauer, H., Stanelle, R., Hescheler, J., Wartenberg, M., 2002. The DC electrical-field-induced Ca2+ response and growth stimulation of multicellular tumor spheroids are mediated by ATP release and purinergic receptor stimulation. J. Cell. Science .115(16):3265-3273.
- Saxton, M.J., Jacobson, K., 1997. SINGLE-PARTICLE TRACKING: Applications to Membrane Dynamics. Ann. Rev. Biophys. Biomol. Struct. 29:373-399.
 - Shih, Y.L., Fu, X.F., King, G., Le, T., Rothfield, L., 2002. Division site placement in *E. coli*: mutations that prevent formation of the MinE ring lead to loss of the normal midcell arrest of growth of polar MinD membrane domains. J. Embo. 21(13):3347-57.
- Shih, Y. L., Le, T., Rothfield, L. I., 2003. Division site selection in *Escherichia coli* involves dynamic redistribution of Min proteins within coiled structures that extend between the two cell poles Proc. Natl. Acad. Sci. U.S.A. 100:7865–70.
 - Simonson, T., 2003. Electrostatics and dynamics of proteins. Rep. Prog. Phys. 66: 737–787

- Song, B., Zhao, M., Forrester, J.V., McCaig, C.D., 2002. Electrical cues regulate the orientation and frequency of cell division and the rate of wound healing in vivo. Proc. Natl. Acad. Sci. U.S.A 99:13577-13582.
 - Suefuji, K., Valluzzi, R., RayChaudhuri, D., 2002. Dynamic assembly of MinD into filament bundles modulated by ATP, phospholipids, and MinE. Proc. Natl. Acad. Sci. U.S.A. 99:16776-16781.
 - Tessie, J., Knutson, V.P., Tsong, T.Y., D. LM., 1982. Electric pulse-induced fusion of 3T3 cells in monolayer culture. Science (Wash. DC). 216:537-538.
 - Togashi, Y., Kaneko, K., 2004. Molecular discreteness in reaction-diffusion systems yields steady states not seen in the continuum limit. Phys. Rev. E. Stat. Nonlin. Soft. Matter Phys. 70: 020901.
 - Tostevin, F., Howard, M., 2006. A stochastic model of Min oscillations in Escherichia coli and Min protein segregation during cell division. Phys. Biol. 3:1–12
 - Valles, J.M., 2002. Model of magnetic field-induced mitotic apparatus reorientation in frog eggs. J. Biophysical. 82(3):1260-1265. MAR.
 - Wang, E., Zhao, M., Forrester, J.V., McCaig, C.D., 2000. Reorientation and faster, directed migration of lens epithelial cells in a physiological electric field. Exp. Eye Res. 71:91-98.
- Weaver, J.C., Astumian, R.D., 1990. The response of living cells to very weak electric fields: the thermal noise limit. . Science (Wash.DC). 247:459-462.
 - Yang, J., Huang, Y., Wang, X.B., Becker, F.F., Gascoyne, P.R.C.,1999. Cell separation on microfabricated electrodes using dielectrophoretic/gravitational field flow fractionation. Anal. Chem. 71(5):911 918.
- 40 Yang, J. Huang, Y. Wang, X.J. Wang, X.B., Becker, F.F., Gascoyne, P.R.C., 1999. Dielectric properties of human leukocyte subpopulations determined by electrorotation as a cell separation criterion. J.Biophys. 76 (6):3307–3314.
 - Yang, J., Huang, Y., Wang, X.B., Becker, F.F., Gascoyne, P.R.C., 2000. Differential analysis of human leukocytes by dielectrophoretic field-flow fractionation. J. Biophys. 78: 2680–2689.
- Yokota, H., Neff, A.W., Malacinski, G.M., 1992. Altering the position of the first horizontal cleavage furrow of the amphibian (Xenopus) egg reduces embryonic survival. Int. J. Dev. Biol. 36:527-535
 - Young, S.H., M-m, P., 1983. Topographical rearrangement of acetylcholine receptors alters channel kinetics. Nature (Lond.). 304:161-163.
- Yu, X.C., Margolin, W.,1999. FtsZ ring clusters in min and partition mutants: role of both the min system and the nucleoid in regulating FtsZ ring localization. Mol. Microbiol. 32, 315-326.

- Zhao, M., Forrester, J.V., McCaig, CD., 1999. A small, physiological electric field orients cell division. Proc. Natl. Acad. Sci. U.S.A. 96:4942-4946.
- Zimmermann, U., Pilwat, G., Holzapfel, C., Rosenheck, K., 1976a. Electrical hemolysis of human and bovine re blood cells. J. Membrane Bio 130:135-152.
- 5 Zimmermann, U., Pilwat, G., Riemann, F., 1974. Dielectric breakdown of cell membranes. Biophys J 14:881-899.
 - Zimmermann, U., Pilwat, G., Riemann, F., 1976. Effects of external fields on cell membranes. Bioel Bioeng 3:58-83.
 - Zimmermann, U., Schulz, J., Pilwat, G., 1973. Transeellular ion flowin *Escherichia coli* and electrical sizing of bacterias. J. Biophys. 13:1005-1013.
 - Zimmermann, U., Vienken, J.,1982. Electric field-induced cell-to-cell fusion. J. Membr. Biol. 67:165-182.

10

20

25

30

FIGURES

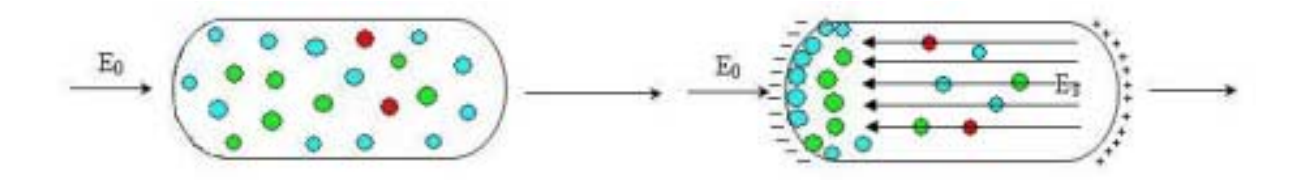


Figure 1. Dielectric like E. coli cell in a uniform field E_0 , showing the polarization on the left and the polarization charge with its associated, opposing, electric field on the right.

Fluorescence image sequences
(using InVivo software)

SPT
(using plugin of ImageJ software)

Positions of Molecule
(x,y)

Dynamics & Localization
Analysis
(using MATLAB software)

Figure 2: Fluorescence image analysis procedure.

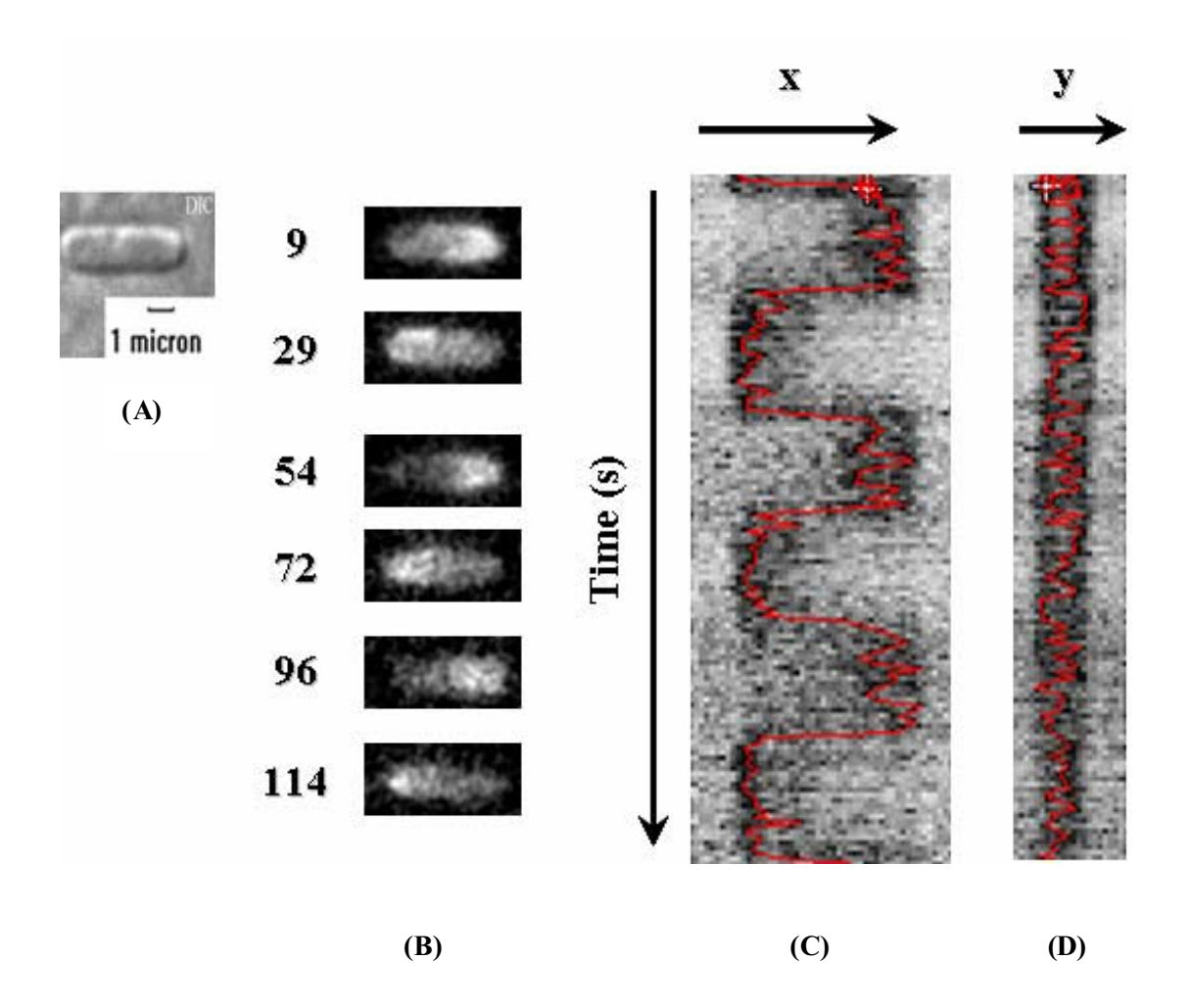


Fig.3: The GFP:MinD oscillations from pole to pole with the approximately 45 seconds of period. **(A)** The differential interference contrast (DIC) images showing cell length $\sim 4~\mu m$. **(B)** The 2D image sequence of pole-to-pole MinD oscillations at each successive time. Each fluorescence image represents the ensemble of GFP:MinD signal locating at polar zones. The time(s) labeled on the left side of column is the first time of GFP:MinD assembles after switching to new pole. **(C)** The results of SPT show the GFP signal time evolution trajectory of MinD oscillations on the x(t). The red line represents the ensemble of GFP:MinD trajectory. **(D)** Spot projection on y(t) GFP signal time evolution trajectory of MinD oscillations.

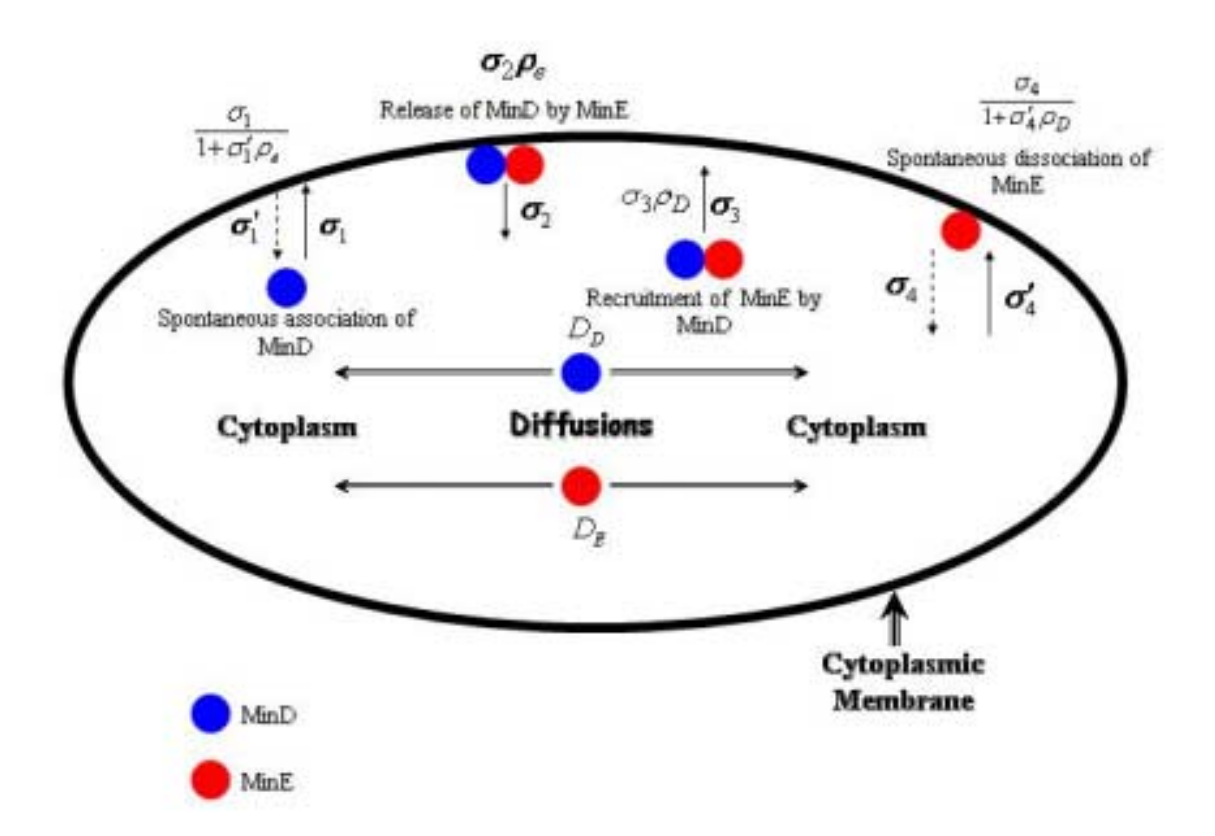


Figure 4. Schematic diagram of the MinCDE dynamics.

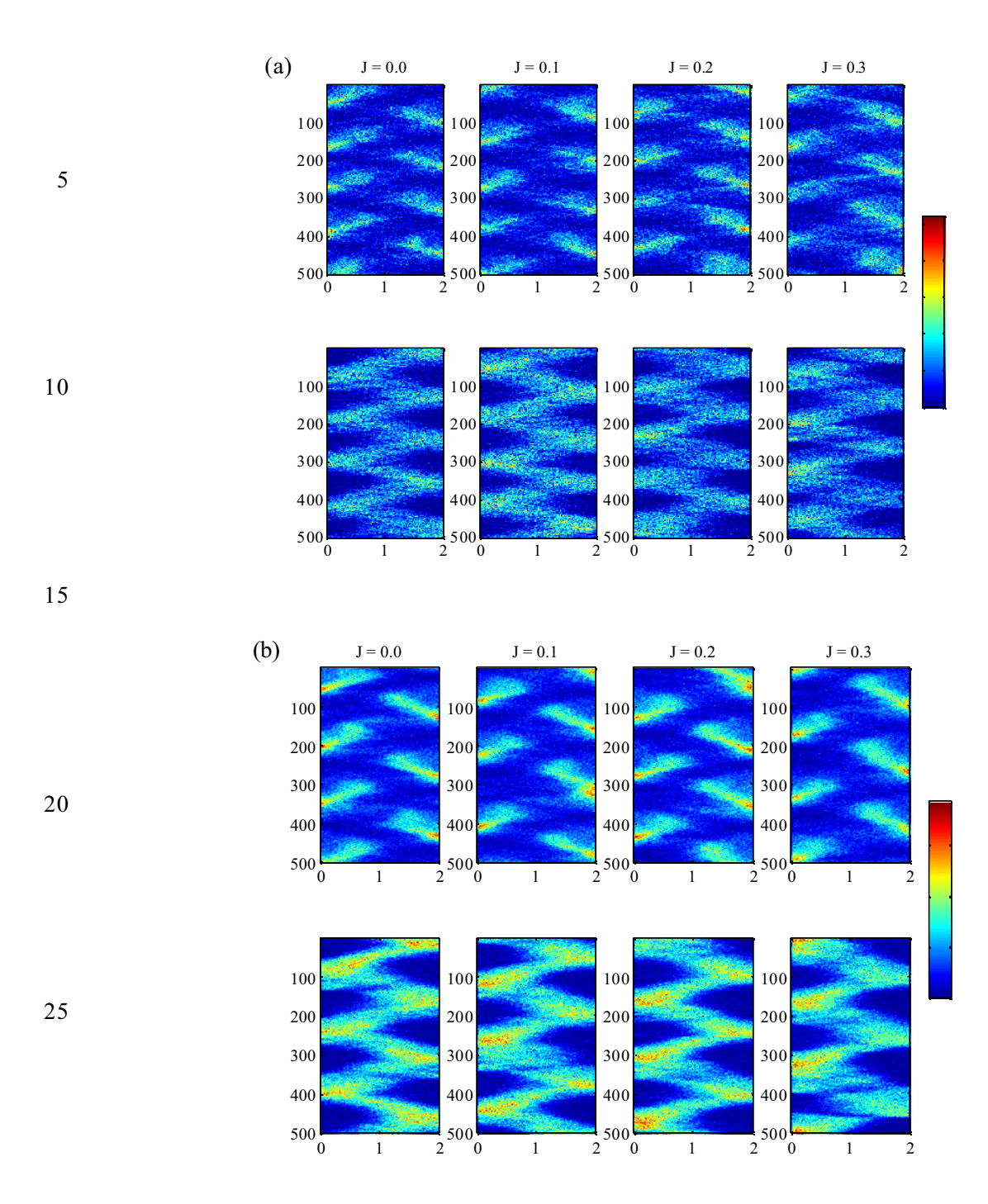


Figure 5. Space-time plots of the total $\left(n_D^k + n_d^k\right)$ MinD (above) and total $\left(n_E^k + n_e^k\right)$ MinE (below) concentrations for J = 0.0 m/s to J = 0.3 m/s where (a) N = 400 and (b) N = 1500. The color scale, running from blue to red, denotes an increase in the total numbers of Min proteins from the lowest to the highest. The vertical scale spans time for 500 s. The time increases from top to bottom. The horizontal scale spans the bacterial length $2 \mu m$. Note the increase in the MinD concentration at the right pole and MinE concentration at the left pole.

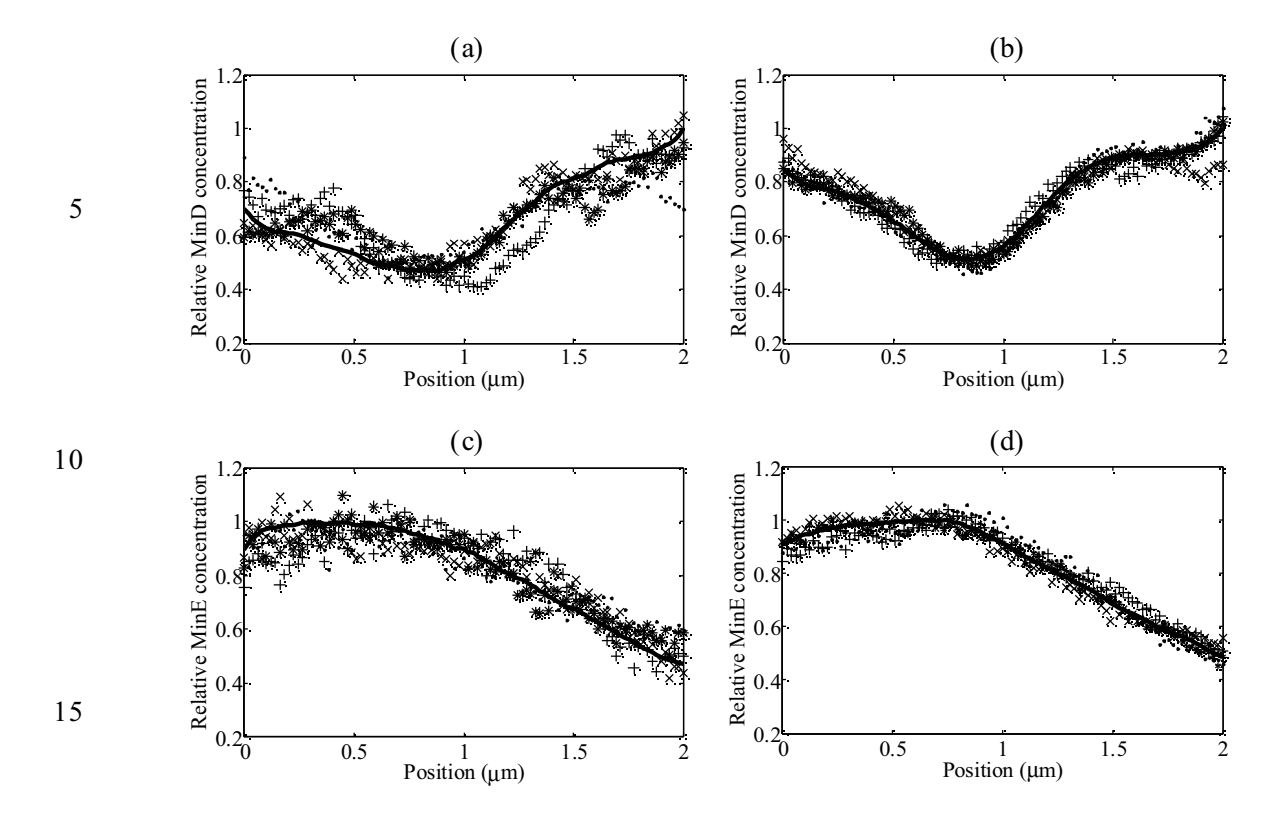


Figure 6. (a), (b) relative MinD concentrations and (c), (d) relative MinE concentrations as functions of x for J = 0.3 m/s. In (a), (c) N = 400 and (b), (d) N = 1500. Solid lines show averages over 15 successive cycles. Markers in the figures represent Min protein concentrations of four individual oscillation cycles.

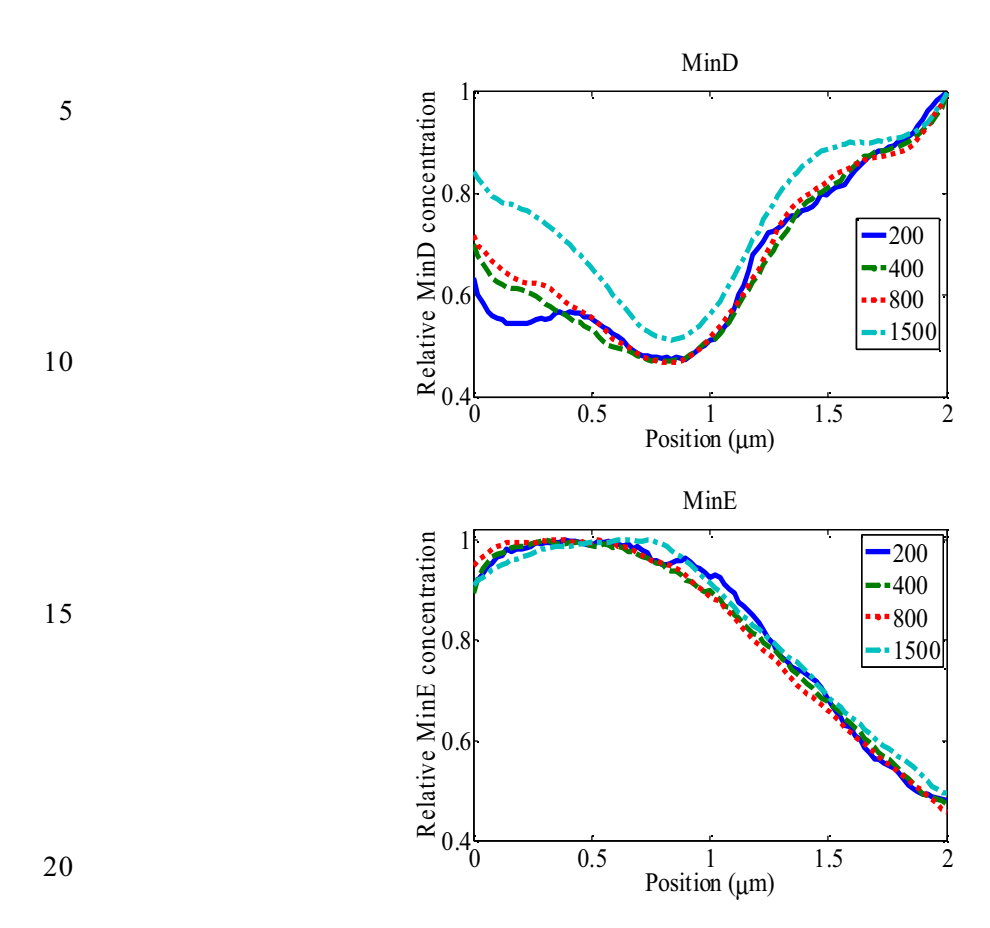


Figure 7. Relative concentrations of MinD (above) and MinE (below) as functions of position x along the bacterium length under the influence of an electric field with J = 0.3 m/s. The curves show that varying the total number of Min proteins does not change the MinD global minimum and MinE global maximum position.

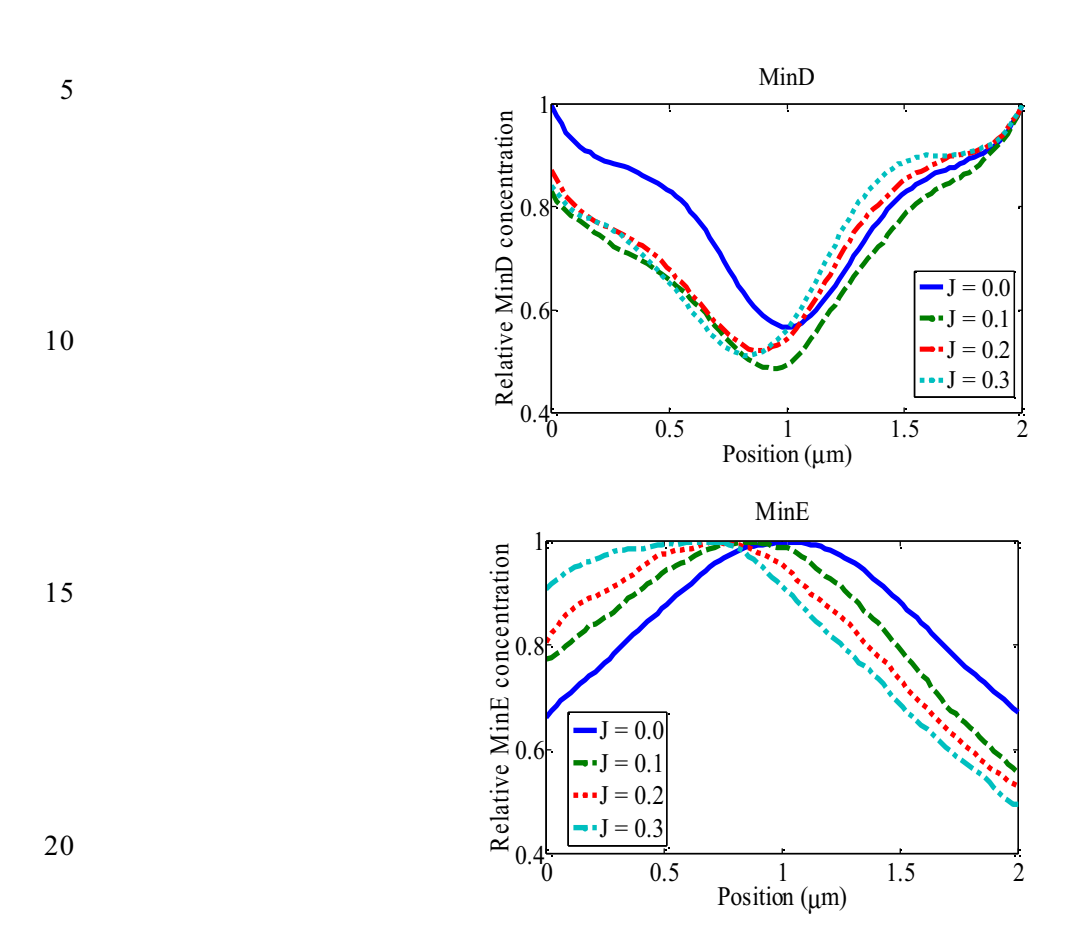


Figure 8. Relative concentrations of MinD (above) and MinE (below) as functions of position x along the bacterium length under the influence of an electric field for N=1500. The curve shows a shift, which depends on the strength of the field, in the local minima of the MinD and the local maxima of the MinE from the mid-cell